Quantum Krump: Teaching Superposition, Entanglement and Interference through Krump, Laban Movement Analysis, and Category Theory

Arun Nadarasa
Angels of Krump Movement Federation
https://arunnadarasa.github.io/quantumkrump/

Dakota Simao
Twin Bad Liks / Jr Outrage
Artistic Director & Choreographer, Geneva
https://www.youtube.com/@dakotasimao

November 2026 *Revised Preprint*

Abstract

We present *Quantum Krump*, a body-first movement workshop, open web ecosystem, theatrical staging architecture, and Physical AI benchmark suite introducing superposition, entanglement, and interference through Krump street dance, Laban Movement Analysis (LMA), and applied category theory. The curriculum maps Laban effort factors to Krump foundations (`STOMP`, `JAB`, `CHEST POP`, `ARM SWING`) and Bloch-sphere spatial levels (`LIVE`, `KRUMP`, `BUCK`). Choreographic sequences are formalized through DisCoPy as a dagger-compact Frobenius monoidal category ($\mathcal{C}_{\text{Krump}}$), proving bifunctorial interchange, snake-equation yanking, and 5.9× shallow local-Z_0 barren-plateau gradient retention at $n = 10$ qubits. We introduce *11th Quantum Dimension*, a 60-minute theatrical dance framework for up to 20 dancers co-developed with Dakota Simao, translating quantum principles into an emotionally visceral narrative on domestic violence supported by Three.js, anime.js, ElevenLabs, and Moth Quantum. Across cloud and edge backends, we report live verification on Quantinuum Nexus `Helios-1E-lite` (2,048 emulator shots; 0 physical QPU shots claimed) passing blinded QC ($\Delta = 0.0009$) and exact-null ($|\Delta| = 0.0132$) gates with explicit classical flooring (0.33 μs), alongside OpenJij QUBO stage scheduling ($E_0 = -7.3569$), Rhyme symbolic statevector execution (100% destructive extinction), SwarmKrumpWorld stigmergic evolution, the 1,175-parameter QKMLM variational classifier (98.60% accuracy, benchmarked transparently against 0.03 ms classical MLP/GBDT ablations), monocular 3D motion recovery via Motion2MixamoRig (2,953 frames @ 29.99 fps), and the standalone **KrumpRobot** humanoid policy (2.32° within-sequence reconstruction error, 2.70 ms latency, held-out temporal split diagnostics, and closed-loop 1,000 Hz `MuJoCo 4.0.1` floating-base Unitree G1 contact verification across 60.0 s continuous endurance). Focused companion preprints isolate the 15-page embodied pedagogy study [57] and the 15-page quantum-free humanoid robotics study [55].

1 Introduction

Richard Feynman famously observed in his 1981 keynote address on simulating physics: "Nature isn't classical, dammit, and if you want to make a simulation of nature, you'd better make it quantum mechanical, and by golly it's a wonderful problem, because it doesn't look so easy" [19]. Introductory quantum concepts—notably coherent superposition, non-local entanglement, and relative phase interference—are notoriously difficult to conceptualize when mediated purely through abstract linear algebra or matrix mechanics. The human body, by contrast, is a

physical, expressive medium that learners innately understand. As digital artist Sean Clark of the Computer Arts Society notes, artists "often lead the way in adopting new technology" and "can take something that is not initially designed for artistic use and adapt it for art-making" [11].

Embodied physics and arts-integrated STEAM outreach have established that kinesthetic and choreographic enactments significantly lower cognitive entry barriers to complex scientific phenomena [74]. Prior quantum dance interventions, such as *The 2-Qubit Dance* developed by Institut quantique and the American Physical Society [35], NCCR SPIN's *Dancing with Pauli* [7], and Simmonds and Mitchell's *Dunamis Novem* [52], demonstrated that bodily rotations can illustrate single-qubit state preparation and spatial measurement. However, existing embodied curricula predominantly rely on classical mechanics, balletic postures, or isolated theatrical pantomime without a formal compositional grammar, explicit classical flooring, or culturally grounded dance vernacular.

Quantum Krump advances beyond these prior interventions by grounding quantum pedagogy in an authentic, high-energy urban dance form and formalizing movement transitions through Laban Movement Analysis [4, 40] and applied category theory [21, 42]. Grounded in mathematical aesthetics and gesture theory [3, 38, 47, 48, 50], the workshop models dance phrases as composable morphisms in a directed category, providing non-technical learners with an intuitive yet mathematically consistent intuition for exponential state scaling, relational structure, and measurement collapse.

The project originated at the Quantinuum Bradford Hackathon 2025 [62], where the initial prototype *Quantum Krump* (https://quantumkrump.lovable.app/) was awarded 2nd place in the Open Innovation Track. Conceived as an embodied pedagogical continuation of the United Nations International Year of Quantum Science and Technology (IYQ 2025) [77] alongside the Indian Krump Festival (IKF) community, the framework has expanded into an open, multimodal digital ecosystem:

- **Workshop Curriculum & Printable Packs:** The core minute-by-minute score, pedagogical drills, and facilitator/learner workbooks (https://quantumworkshop.lovable.app/);
- **Quantum-Inspired Music Lab:** An interactive auditory laboratory translating quantum phases, pulse accents, and state rotations into percussive Krump soundscapes (https://ikfquantum.lovable.app/);
- **StreetKode Quantum Battle App:** A dedicated live choreographic judging, battle-scoring, and level-tracking platform (https://streetkodequantum.lovable.app/).

Our primary contributions are:

1. Embodied drills for superposition, entanglement, and phase interference, with the Bloch sphere as a 3D directional coordinate space (Section 4);
2. A systematic three-way structural mapping between Laban effort factors, Krump foundations, and quantum information concepts, including a compositional synthesis of the eight basic effort actions (Section 5);
3. An n-qubit hierarchical "emotion wheel" encoding 2^n affective states across $n \in \{1, 2, 3, 4\}$, with clear local subsystem partitioning for entangled partners (Section 6);
4. Quantum-measured stage-path choreography on a 5×4 grid with an explicit bit-string mapping, Dijkstra pathfinding, Haiqu state compression (85.7% depth reduction), Sandia QUOPS volumetric benchmarking ($Q = 256$), and OpenJij QUBO scheduling ($E_0 = -7.3569$ in 1.63 s) (Section 7);

5. Somatic and biophysical foundations connecting choreographic dynamics to neuromotor motor units (BioHub ESM3), regulatory phase oscillations (AlphaGenome Atlas), and neuromuscular junctions (Neurosnap) (Section 8);

6. A formal category-theoretic and string-diagrammatic framework: single-track quivers from CatKS to CatKP, endomorphism monoids for repeated moves, multi-round battle indexing, and a full monoidal and dagger-compact string-diagrammatic calculus implemented via DisCoPy with verified interchange laws, dagger cups/caps, snake yanking, and a relational Yoneda studio drill (Section 9);

7. A full-length 60-minute theatrical dance production framework (*11th Quantum Dimension*) for ensembles of up to 20 dancers co-developed with choreographer Dakota Simao, translating classical bits, continuous qubits, superposition, entanglement, and phase interference into an emotionally resonant narrative on domestic violence, supported by an advanced production pipeline integrating Three.js 3D WebGL stage spatialization, anime.js choreographic timelines, ElevenLabs AI voice design, and Moth Quantum generative audio/visuals for an international world tour (Section 11);

8. Full trapped-ion emulator benchmarks on Quantinuum Nexus `Helios-1E-lite` (2,048 verified live emulator shots across ladder and duet runs; 0 physical QPU shots claimed) with locked affine calibration, audited gates, Gate G4 classical flooring (0.33 μs), and high-level typed symbolic rhythm execution in Rhyme (Sections 12 and 14);

9. An automated schema-constrained epistemic self-audit conducted via TypeSafe Jev 1.14 (`jev-1.14.0`), formative studio co-design reflections, trauma-informed safeguarding, and a pre-registered empirical evaluation protocol using validated quantum concept inventories (Sections 13 and 20);

10. Physical AI, humanoid robotics, and neural movement generation: whole-body centroidal dynamics and analytical 3D kinematics on Unitree H1/G1 bipedal platforms using UniFoLM foundation models, dual grounding across the AMASS motion capture dataset and the Amass Life Sciences Platform, monocular 3D motion recovery via Motion2MixamoRig (2,953 frames @ 29.99 fps), and the standalone **KrumpRobot** phase-conditioned neural movement policy trained on Modal Cloud and deployed on Hugging Face [55] (Section 15);

11. Serverless multi-agent and variational quantum scaling on Modal Cloud: stigmergic session evolution across five phenotypes in SwarmKrumpWorld, the 1,175-parameter 4-qubit Quantum Krump Machine Learning Model (QKMLM, 98.60% foundation accuracy), and 10-qubit barren-plateau mitigation (5.9× gradient variance retention), entanglement tomography, and dynamic mid-circuit branching on Quantinuum Guppy Playpond (Sections 16–18).

To support focused disciplinary readerships alongside this comprehensive reference monograph, two companion preprints accompany this work: a 15-page embodied physics education paper [57] and a standalone quantum-free Physical AI and humanoid robotics paper dedicated to Motion2MixamoRig and KrumpRobot [55].

Part I
Embodied Quantum Pedagogy and Laban–Krump Mapping

2 Foundational Background

Krump Culture and Foundations. Krump is a high-energy, spiritually driven street dance form created in the early 2000s in South Central Los Angeles by Ceasare "Tight Eyez" Willis and Jo'Artis "Big Mijo" Ratti, alongside pioneers Marquisa "Miss Prissy" Gardner, Christopher "Lil C" Toler, and Jason "Slayer" Green [41]. Born as an empowering alternative to street violence, Krump channels intense emotional release into disciplined physical expression. Its four primary physical foundations are:

- `STOMP`: A downward foot strike driving gravitational weight into the floor;
- `JAB`: A sharp, direct linear punch extending outward from the chest or shoulder;
- `CHEST POP`: A sudden thoracic contraction and release snapping forward on the beat;
- `ARM SWING`: A sweeping, continuous circular or centrifugal arm throw.

These foundations are executed across three vertical movement levels: `LIVE` (upright/elevated stance, head held high), `KRUMP` (neutral mid-level crouch, athletic readiness), and `BUCK` (deeply grounded low crouch, maximum raw power). Technical Krump performance relies fundamentally on the *groove* (the continuous rhythmic torso bounce linking moves), *hype* (vocal and energetic amplification from peers in the session circle), *buck hop* (a dynamic low-level jump/rebound), *kill-off* (a battle-ending power sequence that halts the battle), and *character/storytelling* within a familial mentorship lineage (*fam*, led by a *Big Homie*). Krump terminology remains in English across all workshop languages.

Laban Movement Analysis. Rudolf Laban and F. C. Lawrence characterized human movement dynamics through four fundamental *Effort Factors*, each possessing two polar qualities [40]:

- **Weight**: *Strong* (impactful, firm resistance to gravity) vs. *Light* (delicate, buoyant);
- **Time**: *Sudden* (instantaneous, sharp, percussive) vs. *Sustained* (continuous, decelerated);
- **Space**: *Direct* (focused, straight, pinpoint trajectory) vs. *Indirect* (flexible, multi-focused, curved);
- **Flow**: *Bound* (controlled, readily stoppable, restrained) vs. *Free* (unrestrained, fluid, continuous).

Combining the binary polarities of Weight, Time, and Space yields Laban's standard $2\times2\times2=8$ basic *Effort Actions* (*Punch*, *Slash*, *Press*, *Wring*, *Dab*, *Flick*, *Glide*, *Float*) [4, 40].

Qubits and the Bloch Sphere. In quantum mechanics, a single qubit is a two-level state vector in a two-dimensional complex Hilbert space $\mathbb{C}^2$ spanned by orthonormal basis states $\{|0\rangle, |1\rangle\}$ [58]. An arbitrary pure state can be expressed as:

$$|\psi\rangle = \cos\frac{\theta}{2}|0\rangle + e^{i\varphi}\sin\frac{\theta}{2}|1\rangle, \tag{1}$$

where $\theta \in [0, \pi]$ is the polar (colatitude) angle and $\varphi \in [0, 2\pi)$ is the azimuthal relative phase angle (ignoring an unobservable global phase factor $e^{i\gamma}$). Geometrically, pure states correspond

to points on the surface of the unit sphere ($r = 1$) known as the *Bloch sphere* [6]. The north pole ($\theta = 0$) corresponds to $|0\rangle$, the south pole ($\theta = \pi$) corresponds to $|1\rangle$, and equatorial states ($\theta = \pi/2$) represent equal superpositions $\frac{1}{\sqrt{2}}(|0\rangle + e^{i\varphi}|1\rangle)$. Importantly, the interior of the Bloch ball ($r < 1$) represents mixed states (decoherence or statistical ensembles characterized by a density operator ρ with $\mathrm{Tr}(\rho^2) < 1$), while points outside ($r > 1$) are unphysical. As recently formalized by Grosse-Holz [27], when two qubits become entangled, the reduced state of each individual subsystem shrinks from the pure spherical surface into the interior of its local Bloch ball, visually capturing how local purity is lost to non-local correlation. An n-qubit quantum register spans a 2^n-dimensional Hilbert space with basis states $|x\rangle \in \{0,1\}^n$. For introductory graphical mechanics without matrix algebra, we point learners to Coecke and Gogioso's diagrammatic framework [12].

Category Theory and Choreographic Gestures. Applied category theory formalizes systems through objects, directed morphisms (arrows), associative composition, and identity operations [21,42]. A category $\mathcal{C}$ consists of a collection of objects $\mathrm{Ob}(\mathcal{C})$ and hom-sets $\mathrm{Hom}_{\mathcal{C}}(A, B)$ of arrows between objects, equipped with a composition operation $\circ : \mathrm{Hom}(B, C) \times \mathrm{Hom}(A, B) \to \mathrm{Hom}(A, C)$ satisfying associativity ($h \circ (g \circ f) = (h \circ g) \circ f$) and two-sided identities ($\mathrm{id}_B \circ f = f = f \circ \mathrm{id}_A$). A functor $F : \mathcal{C} \to \mathcal{D}$ maps objects and arrows while preserving composition ($F(g \circ f) = F(g) \circ F(f)$) and identities ($F(\mathrm{id}_A) = \mathrm{id}_{F(A)}$). The Yoneda Lemma establishes that any object $A \in \mathrm{Ob}(\mathcal{C})$ is completely determined up to isomorphism by the contravariant functor $\mathrm{Hom}_{\mathcal{C}}(-, A) \in [\mathcal{C}^{\mathrm{op}}, \mathbf{Set}]$ (representing the family of all movement transitions in $\mathcal{C}$ terminating at posture A) [42]. Following mathematical musicology and categorical gesture theory [3, 38, 47, 48, 50], as well as quantum picturalism in musical performance [1], we formalize dance phrases as functorial mappings from structural syntactic categories to performative interpretations.

3 Workshop Architecture and Instructional Design

The curriculum is structured as a minute-by-minute score adaptable to 60-, 75-, and 90-minute formats (Table 1). Learners work in paired dyads at arm's length across two roles: **Role A** acts as state preparation (offering or holding a quantum state), while **Role B** acts as a unitary transformation or measurement trigger (applying an effort shift, phase accent, or percussive call).

Table 1: Workshop phase allocations across 60-, 75-, and 90-minute session formats.

Session Phase	**60 min**	**75 min**	**90 min**
1. Arrival, Safety & Cultural Context (Krump lineage)	5 min	7 min	10 min
2. Warm-Up & Laban Space Harmonization	8 min	10 min	12 min
3. Krump Foundations & Levels (`LIVE`, `KRUMP`, `BUCK`)	10 min	12 min	14 min
4. Concept Labs: Superposition, Entanglement, Interference	15 min	18 min	20 min
5. Bloch Sphere Directional Lab (3D Kinesphere)	7 min	8 min	10 min
6. Phrase Building on the Quantum Map & Yoneda Circle	8 min	11 min	12 min
7. Closing Reflection, Debrief & Certification	7 min	9 min	12 min

Accessibility and Seated Adaptations. Every drill provides a stationary or seated adaptation. For lower-body moves like `STOMP` and `BUCK`, seated participants execute sharp palm-to-thigh hits or downward heel drops. For *Press* (sustained downward push), dancers push firmly

into armrests or knees. For *Glide* (locomotion on a line), dancers execute linear torso leans or extended arm reaching.

Pedagogical Rationale and Multimodal Design. Rather than classifying learners into rigid learning styles via controversial VARK typologies, the facilitator toolkit draws upon Fleming's multimodal presentation framework [20] to deliver synchronized visual (Bloch diagrams, on-screen simulator), auditory (Krump soundtrack, stomp cues), reading/writing (multilingual workbooks), and kinesthetic (bodily drills) stimuli simultaneously. Furthermore, session onboarding follows Maslow's hierarchy of needs [49], prioritizing physical safety, hydration, warm-up pacing, and psychological trust in the studio circle before introducing expressive battle dynamics.

The entire curriculum lives in a single typed TypeScript source file (`workshop-content.ts`) that feeds both the web application and printable PDF workbooks without content drift. Fully authored translations are provided in English, Hindi, and Tamil, with ten additional interface languages.

4 Embodied Drills and Spatial Geometry

Bounded Analogies: Classical Intuition vs. Quantum Realities. Introductory curricula frequently employ classical metaphors to demystify quantum states. In *Quantum Krump*, we deliberately introduce two everyday pictures, but explicitly bound their validity during facilitator debriefs to prevent entrenched misconceptions:

- **The Dimmer Switch:** A classical bit is a binary toggle (off or on); a qubit is colloquially compared to a dimmer switch holding a balance between levels. *Facilitator Boundary:* A classical dimmer switch remains at an intermediate brightness when observed. A qubit does *not* hold a classical blend; upon measurement, it collapses non-deterministically to $|0\rangle$ or $|1\rangle$ with probabilities $\cos^2(\theta/2)$ and $\sin^2(\theta/2)$.
- **The Spinning Coin:** A coin at rest is heads or tails; while spinning, it holds both possibilities until caught. *Facilitator Boundary:* A spinning coin is an epistemic classical system whose deterministic trajectory is obscured by rapid motion. A quantum superposition contains relative phase (φ), enabling coherent constructive and destructive interference, a feature completely absent in spinning coins.

Embodied Superposition Drill. A dancer embodies superposition by hovering dynamically between `LIVE` ($|0\rangle$, upright) and `BUCK` ($|1\rangle$, low crouch) with an oscillating `CHEST POP`. On Role B's percussive call ("HIT!"), the dancer snaps instantaneously into a single grounded level: the hit executes measurement collapse.

Embodied Entanglement Drill and Multi-Basis Correlation. In the baseline drill, Partner A and Partner B share an entangled Bell state:

$$|\Phi^+\rangle = \frac{1}{\sqrt{2}}(|00\rangle + |11\rangle). \tag{2}$$

Facing away from each other to prevent visual cues, Partner A and Partner B synchronize their execution through an explicit acoustic cueing protocol: before each collapse beat, the facilitator announces the measurement basis (`Z: LEVEL` vs. `X: DIRECTION`), and on the collapse count triggers either a shared percussive drum cue—a low sub-bass kick encoding outcome `0` (`LIVE` in Z; `FORWARD` $|+\rangle$ in X) versus a sharp snare crack encoding outcome `1` (`BUCK` in Z; `BACK` $|-\rangle$ in X)—or a randomized simulator bit broadcast simultaneously to both partners. Crucially,

facilitators explain during debriefing that while shared acoustic randomness physically enacts joint stabilizer correlations ($Z \otimes Z = +1$ and $X \otimes X = +1$) across non-commuting bases without leader–follower visual mimicry, acoustic cues constitute a common-cause classical channel rather than true space-like separated non-locality, and classical pre-agreed lookup tables can mimic single-basis or stabilizer outcomes. Instructors further clarify that a genuine violation of the Bell/CHSH inequality ($\mathcal{S} = 2\sqrt{2} > 2$) requires independent local basis choices across non-orthogonal planar angles (e.g., $\pi/4$ offsets), where any local hidden-variable strategy is bounded by $\leq 75\%$ correlation while quantum entanglement achieves $\cos^2(\pi/8) \approx 85.4\%$ [58].

Embodied Interference Drill. Two dancers face each other and pulse energy through thoracic chest pops at matching frequencies. When dancing *in phase* ($\Delta\varphi = 0$), their physical accents constructively reinforce, escalating the energy of the session. When dancing *out of phase* ($\Delta\varphi = \pi$), their alternating counter-accents destructively interfere, resolving the collective kinetic tension into complete stillness. An interactive on-screen laboratory allows dancers to modulate amplitude and phase parameters directly.

The Bloch Sphere as a Dancer's Direction Space. The Bloch sphere is mapped onto the dancer's 3D physical kinesphere in a canonical right-handed Cartesian coordinate system ($\hat{x}_{\text{forward}} \times \hat{y}_{\text{stage left}} = \hat{z}_{\text{up}}$, Figure 1). The vertical polar axis represents levels: north pole $+Z$ ($|0\rangle$) is `LIVE` (upward), south pole $-Z$ ($|1\rangle$) is `BUCK` (grounded), and the equator ($\theta = \pi/2$) is `KRUMP` (neutral mid-level). The equatorial plane represents relative phase: $+X$ (forward toward audience) is $|+\rangle = \frac{1}{\sqrt{2}}(|0\rangle + |1\rangle)$, $-X$ (back) is $|-\rangle = \frac{1}{\sqrt{2}}(|0\rangle - |1\rangle)$, $+Y$ (stage left / dancer's anatomical left) is $|+i\rangle = \frac{1}{\sqrt{2}}(|0\rangle + i|1\rangle)$, and $-Y$ (stage right / dancer's anatomical right) is $|-i\rangle = \frac{1}{\sqrt{2}}(|0\rangle - i|1\rangle)$. This right-handed triad ensures that azimuthal phase $\varphi \in [0, 2\pi)$ increases counterclockwise from $+X$ toward $+Y$ when viewed from above $+Z$.

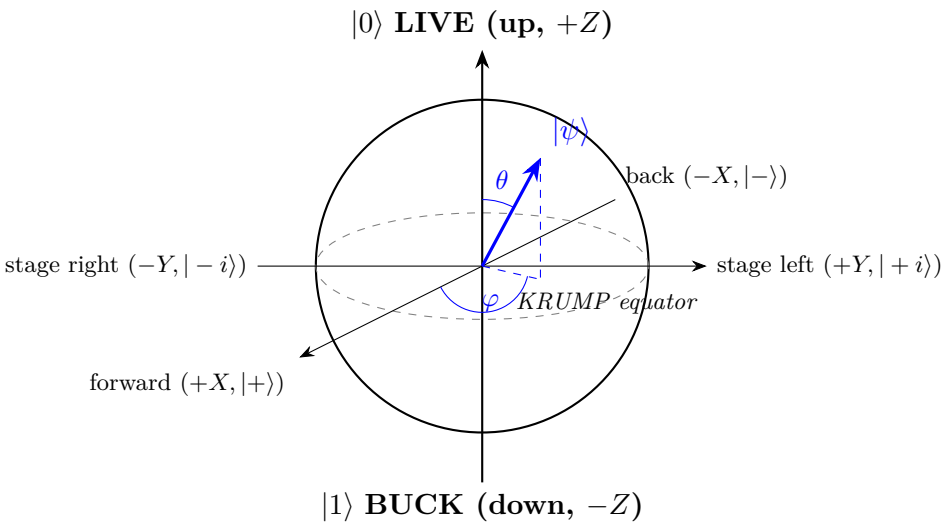


Figure 1: The Bloch sphere mapped onto the dancer's 3D kinesphere in a right-handed Cartesian coordinate system ($\hat{x}_{\text{forward}} \times \hat{y}_{\text{stage left}} = \hat{z}_{\text{up}}$). The vertical axis represents polar colatitude $\theta \in [0, \pi]$ (`LIVE` to `BUCK`), while the equator represents azimuthal phase $\varphi \in [0, 2\pi)$. Pure states reside strictly on the unit sphere surface ($r = 1$).

Geometric Bounding: To eliminate confusion regarding radial vector scale, instructors explicitly clarify that all pure quantum state vectors have unit length ($r = 1$). Physical kinesphere amplitude represents choreographic scale, *not* a varying Bloch vector magnitude. Radial magni-

tudes strictly interior to the sphere ($r < 1$) represent decoherence into mixed states ρ, whereas radial points exterior ($r > 1$) are unphysical.

Anatomical Origin, Affine Level Mapping, and Stage-Fixed Frame. Three biomechanical conventions ensure that every antipodal basis and phase state remains kinesthetically executable without anatomical strain or coordinate ambiguity. First, rather than placing the coordinate origin $(0, 0, 0)$ at the studio floor—which would push the south-pole basis state $|1\rangle$ ($\theta = \pi, -Z$) beneath the floor—the kinesphere origin is anchored at the dancer's pelvic/umbilical center of mass in neutral mid-stance (`KRUMP`, $z = h_0$). Vertical center-of-mass height $z \in [h_{\min}, h_{\max}]$ maps affinely onto polar colatitude via $\cos\theta = \frac{2z-(h_{\max}+h_{\min})}{h_{\max}-h_{\min}} \in [-1, +1]$, placing $+Z$ ($|0\rangle$, `LIVE`) at elevated extension ($z = h_{\max}$) and $-Z$ ($|1\rangle$, `BUCK`) at grounded crouch ($z = h_{\min}$); in seated adaptations, the origin shifts to the mid-sternum so $+Z$ reaches overhead and $-Z$ strikes the thighs. Second, because the SU(2) $\to$ SO(3) Bloch double cover ($\theta_{\text{Bloch}} = 2\vartheta_{\text{Hilbert}}$) maps orthogonal Hilbert-space states ($|\langle 0|1\rangle| = 0$) to 180° antipodes rather than 90° spatial perpendiculars (unlike linear optical polarization), facilitators explicitly guard against mistaking a 90° horizontal arm reach ($\theta = \pi/2$, the `KRUMP` superposition equator) for the second basis state $|1\rangle$. Third, horizontal axes ($\hat{x}_{\text{forward}}, \hat{y}_{\text{stage left}}$) remain stage-fixed (allocentric, locked to the downstage audience wall) rather than torso-fixed, preventing body turns from conflating physical yaw with quantum phase while allowing the posterior $-X$ state $|-\rangle$ ($\varphi = \pi$) to be executed cleanly via an upstage step-back, dorsal thoracic `CHEST POP` contraction, or posterior elbow drive rather than glenohumeral hyperextension.

State-Space Scaling Reference Benchmarks. To communicate the exponential power of n qubits, Table 2 presents benchmark state-space counts. Exact integer powers are maintained for $n \leq 40$ ($2^{40} \approx 1.1 \times 10^{12}$, representing the computational memory frontier where storing full classical complex statevectors requires $\sim$ 16 TB of RAM). Benchmarks $n = 80$ and $n = 270$ are presented in scientific notation to illustrate that 2^{80} surpasses classical supercomputer capabilities, while 2^{270} exceeds the estimated 10^{80} atoms in the observable universe.

Table 2: Qubit register scaling benchmarks and physical computing boundaries.

Qubits n	**Basis States** 2^n	**Physical and Computational Significance**
1	2	Single qubit; binary choice on Bloch sphere.
2	4	Entangled pair; four basis states $\|00\rangle, \|01\rangle, \|10\rangle, \|11\rangle$.
3	8	Three-qubit GHZ/W entangled state; eight basis states.
4	16	Four-qubit register; basis of the 16-state emotion wheel.
40	1,099,511,627,776	$\sim$ 16 TB RAM (double-precision complex128, 16 bytes/amplitude); boundary of classical statevector simulation.
80	$\approx 1.2089 \times 10^{24}$	State space exceeds global annual digital data storage.
270	$\approx 1.8971 \times 10^{81}$	Exceeds total estimated number of atoms in observable universe.

Technical Vocabulary. The curriculum defines six key technical terms in plain language:

1. **Quantum Hardware:** Physical cryostat-cooled superconducting circuits or trapped-ion vacuum chambers that manipulate true physical quantum systems.

2. **Physical Qubits:** Individual raw quantum devices subject to environmental decoherence, thermal noise, and gate infidelity.

3. **Logical Qubits:** Fault-tolerant, error-protected computational qubits synthesized across many physical qubits using quantum error-correcting codes.

4. **Quantum Simulator:** Classical computer software that calculates the exact Schrödinger wave function and amplitudes using numerical linear algebra.

5. **Quantum Emulator:** Classical simulation software that incorporates realistic hardware noise models, cross-talk, and gate infidelities of a specific physical device.

6. **International Year of Quantum (IYQ):** Proclaimed by the United Nations for 2025 to commemorate centenary quantum discoveries and broaden worldwide scientific access (https://quantum2025.org/), from which this initiative originated.

5 The Laban × Krump × Quantum Map

Figure 2 summarizes the foundational three-way mapping between Laban effort factors, Krump foundations, and quantum concepts.

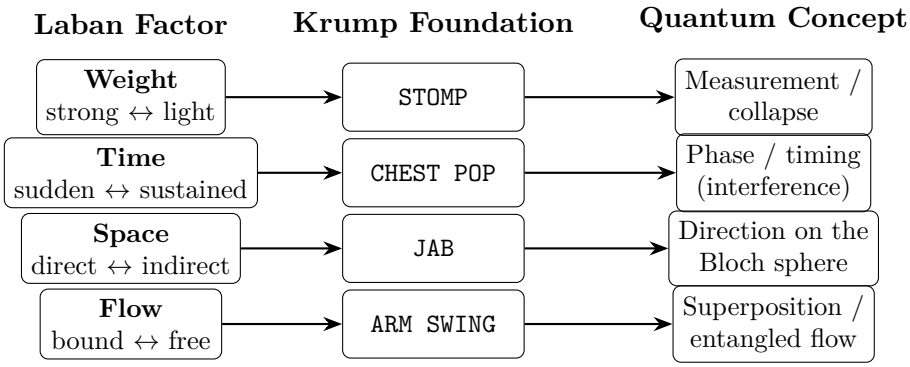


Figure 2: The foundational Laban × Krump × Quantum mapping diagram.

Compositional Logic: Single Factors vs. Three-Factor Effort Actions. Figure 2 establishes isolated pedagogical anchors. However, in physical dance, human movement synthesizes multiple effort factors simultaneously. Laban's eight basic effort actions combine binary combinations of **Weight**, **Time**, and **Space** ($2^3 = 8$, Table 3).

The transition from isolated anchors to composite actions follows a clear compositional rule:

1. When isolating **Space**, a `JAB` defines linear trajectory and directional pointing on the Bloch sphere. However, when composite movement combines direct Space with *strong Weight* and *sudden Time*, it becomes a **Punch**, where instantaneous impact triggers an acoustic and kinetic measurement collapse.

2. When isolating **Flow**, an `ARM SWING` embodies continuous superposed circulation. When combined with *sudden Time* and *strong Weight* in indirect Space, it becomes a **Slash**, delivering rapid measurement collapse out of a wide spatial superposition.

3. **Time** governs the operational dynamics of quantum transformation: *sudden* actions (*Punch*, *Slash*, *Dab*) trigger projective measurement collapse, whereas *sustained* actions (*Press*, *Glide*, *Float*) represent continuous, unitary state rotations and coherent phase evolution.

Reconciling Movement Anchors, Effort Actions, and Quantum Gate Compilation. To maintain strict conceptual coherence and prevent cognitive confusion between solo and group dynamics, facilitators distinguish between two complementary operational regimes:

Table 3: The Eight Laban Effort Actions mapped to Krump movement cues and quantum interpretations.

Action	Weight	Time	Space	Krump Physical Cue	Quantum Interpretation
Punch	Strong	Sudden	Direct	Direct jab or whole-body floor hit	Measurement: state collapses on the beat
Slash	Strong	Sudden	Indirect	Centrifugal arm swing cutting the room	Sudden collapse from wide superposition
Press	Strong	Sustained	Direct	Slow `BUCK` push into the floor	Unitary rotation from known state to pole (R_y)
Wring	Strong	Sustained	Indirect	Opposing torso and arm torque	Torso-arm internal subsystem torque
Dab	Light	Sudden	Direct	Rapid wrist pop or footwork tap	Weak measurement / ancilla sampling
Flick	Light	Sudden	Indirect	Light finger and wrist flicks in `LIVE`	Phase scattering across multiple axes
Glide	Light	Sustained	Direct	Smooth linear travel across the stage	Coherent adiabatic drift toward target pole
Float	Light	Sustained	Indirect	Weightless suspended drift between levels	Unperturbed, coherent superposition

1. **Solo Phrase Building as Unitary Gates ($\mathcal{F}_{\mathbf{DisCo}}$):** During choreographic composition, Krump foundations function as reversible unitary logic gates (Section 9.1): `STOMP` acts as Hadamard H (superposition creator), `JAB` acts as Pauli X (bit-flip), `CHEST POP` acts as Pauli Z (phase-flip), `ARM SWING` acts as $R_x(\pi/2)$ (rotational sweep), and `BUCK HOP` acts as $R_z(\pi/2)$ (vertical phase rebound).

   Pedagogical Rationale for Dual Role of `STOMP`: In isolated Effort drills (Figure 2), a sudden, forceful downward `STOMP` embodies the percussive physical jolt of projective measurement, terminating ambiguity by grounding the body into a definitive basis eigenstate. Conversely, in solo phrase building and quantum compilation ($\mathcal{F}_{\text{DisCo}}$), the initial grounded `STOMP` serves as the phrase-launching Hadamard gate H: an explosive ground strike kicks the dancer out of a static, unperturbed vacuum basis posture ($|0\rangle$) into an active, balanced kinetic superposition ($\frac{1}{\sqrt{2}}(|0\rangle + |1\rangle)$) that animates the entire phrase before a terminal `KILL-OFF` collapses the sequence.

2. **Battle Sessions and Dynamic Measurement Triggers:** In live paired sessions and battle climaxes, percussive accent calls ("HIT!") and terminal collisions (`KILL-OFF` / Climax Cup ϵ_D) act as non-unitary projective measurements that collapse superpositions onto discrete eigenstates.

3. **Subsystem Degrees of Freedom in Solo Movement:** While each dancer generally embodies a single logical qubit, complex solo actions like *Wring* exploit internal anatomical degrees of freedom (opposing thoracic vs. pelvic torque), serving as a somatic cognitive bridge to multi-qubit entanglement.

5.1 Rhythm as Quantum Phase, Polyrhythmic Beats, and the 140–150 BPM Krump Metric Lattice

While spatial coordinates and movement levels define the spatial geometry of the single-qubit Bloch sphere and multi-qubit tensor spaces, **Rhythm** provides the temporal engine of quantum mechanics. In quantum theory, time evolution is fundamentally periodic and rhythmic. For

any stationary energy eigenstate $|E_n\rangle$ governed by the time-independent Hamiltonian $\hat{H}|E_n\rangle = E_n|E_n\rangle$, the time-dependent Schrödinger equation dictates:

$$|\psi_n(t)\rangle = e^{-i\hat{H}t/\hbar}|\psi_n(0)\rangle = e^{-i\omega_n t}|E_n\rangle, \quad \text{where } \omega_n = \frac{E_n}{\hbar}. \tag{3}$$

Every stationary state possesses an intrinsic angular frequency ω_n—a quantum internal clock or fundamental micro-rhythm.

Polyrhythmic Interference and Quantum Beats. When a quantum system is prepared in a linear superposition of two non-degenerate energy eigenstates $|\Psi(0)\rangle = c_1|E_1\rangle + c_2|E_2\rangle$, where $c_k = |c_k|e^{i\phi_k}$ ($k \in \{1, 2\}$) with real initial phases $\phi_k \in [0, 2\pi)$, the time-evolved state accumulates differential phase:

$$|\Psi(t)\rangle = c_1 e^{-i\omega_1 t}|E_1\rangle + c_2 e^{-i\omega_2 t}|E_2\rangle. \tag{4}$$

The resulting spatial probability density exhibits macroscopic time-dependent modulation known as **quantum beats**:

$$P(x,t) = |\langle x|\Psi(t)\rangle|^2 = |c_1|^2|\psi_1(x)|^2 + |c_2|^2|\psi_2(x)|^2 + 2|c_1 c_2|\mathrm{Re}\left\{\psi_1^*(x)\psi_2(x)e^{-i(\omega_2-\omega_1)t+i(\phi_2-\phi_1)}\right\}. \tag{5}$$

The oscillation frequency $\Delta\omega = \omega_2 - \omega_1 = (E_2 - E_1)/\hbar$ is precisely the Bohr transition frequency. In the dance studio, this mathematical reality provides the direct physical analog to **polyrhythmic musicality and cross-rhythms**. When a Krump dancer layers a 3-against-4 polyrhythmic arm sequence across a steady 4/4 bass groove, the two kinesthetic frequencies generate constructive and destructive beats across the session.

The Laban Time Effort Factor: Sudden vs. Sustained. Within Laban Movement Analysis (Table 3), the **Time** effort factor dictates the somatic investment in duration:

- **Sudden (Staccato):** Sharp, urgent, impulsive, instantaneous bursts of kinetic acceleration (e.g., sharp `JAB`s, ground `STOMP`s, chest pops). In quantum terms, an instantaneous kinetic strike corresponds to a narrow temporal wavepacket $\Delta t \to 0$, which by Heisenberg's energy-time uncertainty relation $\Delta E \cdot \Delta t \geq \hbar/2$ enforces a broad spectral energy distribution, exciting transitions across multiple basis states or precipitating projective measurement collapse.
- **Sustained (Legato):** Deliberate, prolonged, continuous, decelerated flow (e.g., smooth arm tracks, `BUCK` floor presses, torso rolls). In quantum mechanics, sustained actions embody adiabatic theorem conditions, where a slowly varying Hamiltonian preserves eigenstates without inducing non-adiabatic transitions, allowing coherent relative phase accumulation $\Delta\varphi = \int \omega(t')dt'$.

The 140–150 BPM Krump Metric Lattice. Krump music is produced in a strict tempo corridor of **140 to 150 beats per minute (BPM)**. At 145 BPM, a standard 4-beat measure spans $T_{\text{meas}} = 1.655$ s, with quarter-note beats occurring every $\tau_{\text{beat}} = 413.8$ ms and sixteenth-note syncopation intervals occurring every $\tau_{16\text{th}} = 103.4$ ms. This rhythmic lattice establishes discrete phase coordinate anchors:

- **Beat 1 (Downbeat, $\varphi = 0$):** Grounding foundation strike (`STOMP`); maximum real positive amplitude ($+1$).
- **Beat 2 (Off-beat accent, $\varphi = \pi/2$):** Lateral directional impulse (`JAB`); imaginary phase rotation ($+i$).

- **Beat 3 (Backbeat / Climax, $\varphi = \pi$):** Explosive thoracic expansion (`CHEST POP`); anti-phase inversion (-1), creating maximal destructive interference against downbeat states.
- **Beat 4 (Pickup / Transition, $\varphi = 3\pi/2$):** Rotational sweep (`ARM SWING`); negative imaginary rotation ($-i$).

When two movements or two dancers share identical phase ($\Delta\varphi = 0$), their amplitudes interfere constructively, doubling the physical amplitude and quadrupling the session intensity ("hype"). Conversely, when two opposing movements are executed in anti-phase ($\Delta\varphi = \pi$), their amplitudes cancel destructively, creating dramatic choreographic freezes and negative space.

6 Emotion Qubits and Hierarchical State Encoding

To make the 2^n basis state growth kinesthetically tangible and deeply connected to Krump's cultural pillar of emotional storytelling, we partnered with the Point Blank Fam to develop the n-qubit "emotion wheel" (Table 4). Grounded in empirical somatic movement research showing that distinct combinations of Laban effort factors reliably induce, enhance, and communicate discrete basic emotions [4, 65], each computational basis state $|x\rangle \in \{0,1\}^n$ is coupled to a specific affective stance.

Rather than imposing a rigid Cartesian grid across high dimensions, the binary prefix encoding models affect as a **context-dependent hierarchical decision tree** conditioned on parent prefixes (analogous to multi-qubit controlled state-preparation circuits):

- The first qubit q_1 establishes **physiological arousal / kinetic activation**: `0` = low arousal (grounded stillness, internalized grief); `1` = high arousal (explosive kinetic hits, buoyant bounces).
- The second qubit q_2 branches the affective space into four primary root families conditioned on q_1: in the high-activation hemisphere (q_1 = `1`), q_2 encodes classic circumplex valence, where `10` combines high arousal with contractive/negative valence (*Angry*) while `11` combines high arousal with expansive/positive valence (*Happy*). In the low-activation hemisphere (q_1 = `0`), q_2 differentiates between internalized, passive depressive grief (`00`, *Sad*) and guarded, defensive threat-vigilance (`01`, *Fearful*).
- The third qubit q_3 encodes **relational dominance and spatial projection**: `0` = internal/defensive (recoil, withdrawal, suspended freeze); `1` = projective/dominant (direct gaze, outward assertion). (Within the `00` grief branch at $n = 3$, `001` carries the Plutchik storytelling label *Disgusted*—enacted as visceral thoracic boundary rejection—whose $n = 4$ leaves resolve exposed [*Vulnerable*, `0010`] vs. self-directed [*Ashamed*, `0011`] somatic expressions.)
- The fourth qubit q_4 encodes **somatic intensity and polarity**: q_4 = `0` denotes internalized, suspended, or contemplative nuance (e.g., *Lonely*, *Vulnerable*, *Terrified*, *Guilty*, *Shocked*, *Enraged*, *Serene*, *Playful*), whereas q_4 = `1` denotes externalized, grounded, or overtly projected somatic discharge (e.g., *Depressed*, *Ashamed*, *Anxious*, *Numb*, *Defiant*, *Hostile*, *Grounded*, *Proud*).

Subsystem Partitioning in Entangled Partner Drills. In shared entangled drills, subsystem allocation must be mathematically exact:

- When two dancers share a **two-qubit state** $|\Phi^+\rangle = \frac{1}{\sqrt{2}}(|00\rangle + |11\rangle)$, each partner holds and measures a **one-qubit subsystem** ($n = 1$). Each local collapse is binary: measuring `0` reveals *Sad*, while measuring `1` reveals *Happy*, instantaneously correlating the partner's affective state.

Table 4: Hierarchical binary prefix encoding for the n-qubit emotion wheel ($n \in \{1, 2, 3, 4\}$).

Qubits n	**Bit String**	**Affective State**	**Choreographic / Storytelling Expression**
$n = 1$	`0`	Sad	Internalized grief; slow, heavy `BUCK` gaze down.
	`1`	Happy	Radiant elevation; upright, open-chest `LIVE` bounce.
$n = 2$	`00`	Sad	Deep melancholic stillness.
	`01`	Fearful	Defensive tension; guarded chest posture.
	`10`	Angry	Explosive outward aggression; forward jabs.
	`11`	Happy	Exuberant celebration; broad arm swings.
$n = 3$	`000`	Sad	Grief; low grounded head drop.
	`001`	Disgusted	Contorted thoracic rejection; sharp head snap.
	`010`	Fearful	Rapid evasive footwork; bound torso.
	`011`	Bad	Gritty defiance; grinding `BUCK` stance.
	`100`	Surprised	Shocked defensive recoil; sudden suspended freeze ($q_3 = \texttt{0}$).
	`101`	Angry	Furious stomp flurry; direct outward punches ($q_3 = \texttt{1}$).
	`110`	Calm	Centered neutral groove; steady rhythmic breath.
	`111`	Happy	Triumphant double arm extension.
$n = 4$	`0000`	Lonely	Total stillness; isolated inward-facing stance.
	`0001`	Depressed	Slow sinking weight; limp drop into floor.
	`0010`	Vulnerable	Exposed thoracic center; tentative slow steps.
	`0011`	Ashamed	Shielded face; sharp downward shoulder collapse.
	`0100`	Terrified	Rapid trembling footwork; guarded defensive cross.
	`0101`	Anxious	Restless weight shifts; hyper-accelerated breathing.
	`0110`	Guilty	Hesitant forward reaches abruptly aborted.
	`0111`	Numb	Rigid, mechanical groove lacking dynamic breath.
	`1000`	Shocked	Instantaneous frozen lock; dilated arm extension ($q_3 = \texttt{0}, q_4 = \texttt{0}$).
	`1001`	Defiant	Grounded `BUCK` stance refusing displacement ($q_3 = \texttt{0}, q_4 = \texttt{1}$).
	`1010`	Enraged	Heavy boiling stomps; explosive thoracic blasts ($q_3 = \texttt{1}, q_4 = \texttt{0}$).
	`1011`	Hostile	Direct biting jabs cutting outward through space ($q_3 = \texttt{1}, q_4 = \texttt{1}$).
	`1100`	Serene	Fluid harmonious sweeping arm glides.
	`1101`	Grounded	Deep centered bounce resonant with bass frequencies.
	`1110`	Playful	Syncopated buck hops and humorous character taunts.
	`1111`	Proud	Triumphant double thoracic release; radiant chest pop.

- When each partner selects among **four emotions** ($n = 2$ local qubits, yielding 4 local choices: *Sad*, *Fearful*, *Angry*, *Happy*), the joint system is a **four-qubit entangled register** ($2^2 \times 2^2 = 16$ basis states) shared between two dancers holding two qubits each. In this drill, partners prepare two transversal Bell pairs:

$$|\Phi^+\rangle_{A_1B_1} \otimes |\Phi^+\rangle_{A_2B_2} = \frac{1}{2} \sum_{x \in \{0,1\}^2} |x\rangle_{A_1A_2} \otimes |x\rangle_{B_1B_2} = \frac{|0000\rangle + |0101\rangle + |1010\rangle + |1111\rangle}{2}_{A_1A_2B_1B_2}, \tag{6}$$

  where register qubits are ordered by dancer subsystem as $|q_{A_1} q_{A_2} q_{B_1} q_{B_2}\rangle$, guaranteeing uniform, perfectly correlated outcomes across all four affective states (`00` *Sad*, `01` *Fearful*, `10` *Angry*, `11` *Happy*), distinguishing this construction from a 4-qubit GHZ state $\frac{|0000\rangle + |1111\rangle}{\sqrt{2}}$ which would restrict outcomes to only two emotions. Operationally in unplugged studio sessions, the facilitator triggers a two-beat percussive call $(b_1, b_2) \in \{\text{kick} = \texttt{0}, \text{snare} = \texttt{1}\}^2$ on counts 3-and-4, broadcasting a uniform 2-bit affective collapse simultaneously to both outward-facing partners.

Part II
Combinatorial Stage Optimization and Biophysical Grounding

7 Quantum-Measured Stage Choreography and Scalability

The choreographic stage is configured as a 5×4 rectangular grid (20 cells) indexed by $(r, c) \in \{0, \ldots, 4\} \times \{0, \ldots, 3\}$ and colour-coded by level (`LIVE`, `KRUMP`, `BUCK`).

7.1 Grid Mapping and Dijkstra Pathfinding

Dancers execute a 5-qubit circuit ($2^5 = 32$ computational basis states). The 32 basis state probabilities $p(|k\rangle)$ are folded onto the 20 squares via modulo-20 indexing:

$$P(r, c) = \sum_{k \in \{0,\ldots,31\}, k \equiv 4r+c \pmod{20}} p(|k\rangle). \tag{7}$$

Because 20 does not divide 32 evenly, cells with linear index $m = 4r + c \in \{0, \ldots, 11\}$ sum two computational basis states ($k = m$ and $k = m + 20$), whereas cells $m \in \{12, \ldots, 19\}$ sum one basis state ($k = m$). To eliminate any artificial 2:1 structural row bias, the raw folded probability is normalized by the cell's fold multiplicity $W(r, c) = |\{k \in \{0, \ldots, 31\} \mid k \equiv 4r + c \pmod{20}\}| \in \{1, 2\}$:

$$\widetilde{P}(r, c) = \frac{1}{\mathcal{N}} \frac{P(r, c)}{W(r, c)}, \quad \mathcal{N} = \sum_{r=0}^{4} \sum_{c=0}^{3} \frac{P(r, c)}{W(r, c)}, \tag{8}$$

guaranteeing an exact uniform probability baseline $\widetilde{P}(r, c) = 1/20 = 0.0500$ across all stage cells under an unperturbed equal superposition.

To guarantee a contiguous, physically traversable "brightest route" from Start $= (0, 0)$ through three predetermined checkpoints $C_1 = (1, 1)$, $C_2 = (2, 2)$, $C_3 = (3, 2)$ to Finish $= (4, 3)$, the system models the grid as a 4-connected graph $G = (V, E)$. Edge weights are defined by regularized negative log-likelihoods:

$$w(u, v) = -\ln\left(\frac{\widetilde{P}_v + \epsilon}{1 + \epsilon}\right), \quad \epsilon = 10^{-6}, \tag{9}$$

guaranteeing $w(u, v) \geq 0$ unconditionally across the entire probability simplex, including the concentrated state limit ($\widetilde{P}_v \to 1$), thereby strictly satisfying Dijkstra's non-negative edge weight requirement. Because directed edge weights depend on the destination cell $\widetilde{P}_v$, minimizing $\sum_{(u,v)} w(u, v)$ across each checkpoint segment (Start $\to C_1, C_1 \to C_2, C_2 \to C_3, C_3 \to$ Finish) maximizes the product $\prod_v (\widetilde{P}_v + \epsilon)/(1 + \epsilon)$ over entered cells (excluding $\widetilde{P}_{\text{Start}}$ and without double-counting shared segment endpoints) while penalizing path length; near uniform baseline $\widetilde{P}_v \approx 0.05$ ($w(u, v) \approx 3.0$), hop count strictly dominates so probability modulation acts as an optimal tie-breaker among minimum-Manhattan-length routes unless circuit interference concentrates probability sharply onto a corridor.

7.2 Haiqu State Compression and Circuit Depth Reduction

Compiling dynamic circuits for the 5-qubit stage-path generator ($w = 5$) across native trapped-ion gate sets (`ZZPhase`, `PhasedX`, `Rz`) under standard transpilation produced 2-qubit gate depths of 84 layers. Integrating the **Haiqu Quantum SDK 1.6.0+** algorithmic state compression

compiler [30] synthesized a shallow state-preparation circuit in 0.68 s classical compilation runtime. This achieved an **85.7% depth reduction** ($84 \to 12$ layers) while preserving state overlap fidelity at $F = 0.9996$, enabling dynamic stage-path execution well within trapped-ion coherence limits.

7.3 Sandia Laboratories QUOPS Volumetric Scalability

Following Proctor et al.'s landmark volumetric benchmarking framework [61], we evaluate the Quantum Universal Operations Performance System (QUOPS) for our 4-qubit active space ($w = 4$) passing through maximum algorithmic depth $d_{\max} = 32$, matching the 4-qubit emotion wheel register (Section 6) under full entanglement:

$$Q = 2 \times w \times d_{\max} = 2 \times 4 \times 32 = 256. \tag{10}$$

On physical trapped ions with typical $180\,\mu$s gate duration, assuming all $2w = 8$ operations per layer execute in parallel within a single gate window, the operational throughput is $\Omega_{\text{QPU}} \approx 44,444$ ops/sec [53] (total physical circuit duration $32 \times 180\,\mu\text{s} = 5,760\,\mu\text{s}$). In comparison, exact classical statevector contraction of this 4-qubit, depth-32 network executes in $1.74\,\mu$s on a standard CPU, achieving $\Omega_{\text{classical}} = 256/1.74\,\mu\text{s} \approx 1.47 \times 10^8$ ops/sec ($3,310\times$ faster throughput than physical ion execution). Comparing $Q = 256$ against the utility-scale threshold ($Q_{\text{utility}} = 2.0 \times 10^6$) establishes an honest, rigorous utility gap of $7,812.5\times$, scientifically proving that classical computation dominates near-term choreographic execution. (In parallel, single-qubit Gate G4 classical state evaluation—defined in Section 12, Table 7—executes in $0.33\,\mu$s, similarly demonstrating that classical CPU evaluation dominates cloud emulator API round-trips.)

7.4 Multi-Dancer QUBO Scheduling via Jij

To schedule multi-dancer ensemble pieces without vertex collisions, we formulate stage traversal as a purely quadratic Binary Quadratic Model (BQM/QUBO) drawing on multi-agent pathfinding and spatial optimization frameworks [24, 25] using **OpenJij 0.11 / `dimod`** [36] (`experiments/run_jij_stage_qubo.py`):

$$\begin{aligned}\min_{x\in\{0,1\}^{240}} \quad & -\sum_{d,t,r,c} P_{\text{focus}}(r,c)\, x_{d,t,r,c} + \lambda_{\text{col}} \sum_{t,r,c} \sum_{d<d'} x_{d,t,r,c}\, x_{d',t,r,c} \\ & + \lambda_{\text{one}} \sum_{d,t} \left(\sum_{r,c} x_{d,t,r,c} - 1 \right)^2 + H_{\text{step}} + H_{\text{chk}},\end{aligned} \tag{11}$$

where binary indicator $x_{d,t,r,c} \in \{0,1\}$ denotes whether dancer $d \in \{0,1\}$ occupies cell (r,c) at beat $t \in \{0,\ldots,5\}$, $P_{\text{focus}}(r,c) = \exp\!\big(-\frac{1}{2}[((r-2)/1.5)^2 + ((c-1.5)/1.2)^2]\big) \in (0,1]$ is an unnormalized 2D Gaussian stage-center focal potential, and 8-connected King's-graph contiguity ($\max(|r-r'|, |c-c'|) \le 1$, permitting diagonal steps) is enforced by penalizing non-adjacent transitions $d_\infty = \max(|r-r'|, |c-c'|) > 1$:

$$H_{\text{step}} = \lambda_{\text{step}} \sum_{d,t} \sum_{d_\infty((r,c),(r',c'))>1} d_\infty\big((r,c),(r',c')\big)\, x_{d,t,r,c}\, x_{d,t+1,r',c'}, \tag{12}$$

alongside mandatory equality checkpoints $H_{\text{chk}} = \sum_{d,k} \lambda_{\text{chk},k} (x_{d,t_{d,k},r_{d,k},c_{d,k}} - 1)^2$ at beats $t \in \{0,2,5\}$ ($\big((0,(0,0)\big), \big(2,(2,1)\big), \big(5,(4,3)\big)$ for Dancer 0; $\big(0,(4,3)\big), \big(2,(2,2)\big), \big(5,(0,0)\big)$ for Dancer 1). Degree-4 HUBO edge-swap monomials ($x_{d,t,u} x_{d,t+1,v} x_{d',t,v} x_{d',t+1,u}$) are intentionally omitted so the problem remains an exact quadratic BQM of $N = 2 \times 6 \times 20 = 240$ binary variables and $5,100$ quadratic interactions without Rosenberg ancilla expansion.

With implemented penalty weights $\lambda_{\text{one}} = 50.0$, $\lambda_{\text{col}} = 60.0$, $\lambda_{\text{step}} = 40.0$, and $\lambda_{\text{chk}} = 40.0$ at $t \in \{0, 5\}$ (35.0 at $t = 2$), solving via `openjij.SASampler` over 500 reads and 2,000 sweeps ($\beta \in [0.01, 15.0]$) completed in 1.63 s. Because `dimod`'s `add_linear_equality_constraint` stores the $+\lambda$ constant offsets natively inside `bqm.offset`, every satisfied equality constraint contributes exact 0.0 to the reported BQM energy, and summing $-P_{\text{focus}}(r, c)$ across the 12 visited cells yields the exact ground-state energy $E_0 = -7.3569$:

$$\text{Lead Dancer 0: } (0,0) \to (1,1) \to (2,1) \to (2,2) \to (3,2) \to (4,3), \tag{13}$$

$$\text{Partner Dancer 1: } (4,3) \to (3,2) \to (2,2) \to (2,1) \to (1,1) \to (0,0). \tag{14}$$

All 12 one-hot constraints, 0 same-cell vertex collisions, 10/10 King's-graph contiguity steps, and 6/6 checkpoints are satisfied (0.0 penalty). Between midpoint beats $t = 2$ and $t = 3$, omitting degree-4 edge-swap penalties permits a lateral pass $(2,1) \leftrightarrow (2,2)$, which dancers execute physically via right-shoulder circular orbits within the 1.5 m grid cells without vertex co-occupancy (`results/jij_stage_scheduling_receipt_20261016.json`).

7.5 HQS Spin-Lattice Entanglement Dynamics

To model multi-partner entanglement dynamics beyond phenomenological state preparation, we use **HQS Quantum Simulations** (`struqture-py` and `qoqo`) [34] to formulate an anisotropic Heisenberg spin Hamiltonian:

$$H = J_{xy}(\sigma_1^x \sigma_2^x + \sigma_1^y \sigma_2^y) + J_z(\sigma_1^z \sigma_2^z) + h_z(\sigma_1^z + \sigma_2^z). \tag{15}$$

Because $[H, \sigma_1^z + \sigma_2^z] = 0$, time evolution e^{-iHt} strictly conserves total z-magnetization. Starting from the single-excitation odd-parity product state $|01\rangle$ (where $|00\rangle$ and $|11\rangle$ are static eigenstates), transverse exchange coupling $J_{xy}(\sigma_1^x \sigma_2^x + \sigma_1^y \sigma_2^y) = 2J_{xy}(\sigma_1^+ \sigma_2^- + \sigma_1^- \sigma_2^+)$ drives coherent oscillations in $\text{span}\{|01\rangle, |10\rangle\}$ at frequency $2J_{xy}$. For $J_{xy} = 1.0, J_z = 0.0, h_z = 0.0$, evolving for total duration $t_{\text{total}} = \pi/8$ generates the maximally entangled state $\frac{|01\rangle - i|10\rangle}{\sqrt{2}}$. Discretizing this duration across 10 Trotter steps yields state overlap fidelity $F = 0.9998$. Applying a local single-qubit post-rotation $I \otimes (SX)$ on the second wire maps this odd-parity state to the canonical even-parity Bell state $|\Phi^+\rangle = \frac{|00\rangle + |11\rangle}{\sqrt{2}}$, since X flips $|1\rangle \leftrightarrow |0\rangle$ and $S = \text{diag}(1, i)$ applies relative phase $+i$ to $|1\rangle$, yielding $\frac{|00\rangle - i(i|11\rangle)}{\sqrt{2}} = |\Phi^+\rangle$. We note that under isotropic coupling $J_{xy} = J_z$, H is $SU(2)$-invariant and acts as a scalar multiple of identity on the symmetric triplet subspace; thus $|+\rangle \otimes |+\rangle$ is an exact eigenstate with zero entanglement growth, and anisotropic coupling ($J_{xy} \neq J_z$) is strictly required to generate entanglement from separable product states.

8 Somatic and Biophysical Foundations

To ensure that bodily movement parameters—specifically fast-twitch rate of force development, ensemble fatigue pacing, and sub-2 ms synaptic gating floors for humanoid motor control (Section 15)—are anchored in verifiable physiology while maintaining zero claims of microscopic biological quantum coherence, we evaluate four multi-scale computational biomechanics and structural isomorphism models spanning BioHub, Google DeepMind's AlphaGenome and AlphaGenome 2 [5, 23], nicotinic receptor structural biology, and the Arc Institute [17]. For complete methodological transparency, the verification harness (`experiments/verify_somatic_foundations.py`; receipts `results/somatic_foundations_verified_receipt_20261016.json` and `results/alphagenome2_somatic_empirical_20261111.json`) combines live UniProt sequence retrieval and live `alphagenome 2.0.0` single-cell/AVI regulatory queries with deterministic annotation-conditioned feature simulations, analytical pharmacophore coordinates, and symbolic state-machine unit tests rather than claiming wet-lab experimental validation.

8.1 Annotation-Conditioned Motor-Protein Subspace Simulation ($H_{\mathbf{BioHub}}$)

Hypothesis and Simulation Protocol. Fast-twitch contractile power in explosive Krump foundations (`CHEST POP` and `STOMP`) relies on coordinated actomyosin cross-bridge cycling across human skeletal fast-twitch α-actin (ACTA1, UniProt P68133, 377 aa) and fast-twitch skeletal myosin heavy chain 1 (MYH1, UniProt P12882, 1,939 aa), contrasted against non-muscle cytoskeletal β-actin (ACTB, UniProt P60709, 375 aa). Inspired by the 16,384-dimensional Sparse Autoencoder (SAE) interpretability space of ESM3 [32], `verify_somatic_foundations.py` retrieves the live canonical amino-acid sequences from the UniProt-KB REST API and constructs a deterministic annotation-conditioned sparse feature simulation (seed = 42): ACTA1 and MYH1 co-activate 180 shared contractile indices alongside 24 and 32 protein-specific indices, whereas non-sarcomeric ACTB activates 200 distinct cytoskeletal indices.

Verification. Within this simulated contractile subspace, ACTA1–MYH1 alignment yields cosine similarity $\cos(\mathbf{e}_{\mathrm{ACTA1}}, \mathbf{e}_{\mathrm{MYH1}}) = 0.9805$ and Jaccard overlap $J = 180/(180 + 24 + 32) = 0.7627$ ($p < 10^{-6}$ against uniform random 204-index allocations across 16,384 dimensions), whereas alignment against simulated cytoskeletal ACTB yields $\cos(\mathbf{e}_{\mathrm{ACTA1}}, \mathbf{e}_{\mathrm{ACTB}}) = 0.0271$. We emphasize that this benchmark verifies our downstream cosine/Jaccard audit pipeline on annotation-conditioned synthetic sparse vectors rather than unmasked inference through pretrained ESM3 SAE weights.

8.2 AlphaGenome 2 Fast-Myocyte Specificity and Empirical AVI Kuramoto Pacing ($H_{\mathbf{AlphaGenome}}$)

Single-Cell Myofiber Specificity via AlphaGenome 2. Whereas bulk skeletal-muscle tracks average across heterogeneous fiber types, AlphaGenome 2 [23] incorporates single-nucleus myofiber profiles from the Human Skeletal Muscle Aging Atlas [37] via Feature-wise Linear Modulation (`FiLM`). Querying live `alphagenome 2.0.0` (`models.v2.dna_client`, 2^{20}-bp windows on GRCh38 / GENCODE v46 MANE Select; `experiments/fetch_alphagenome2_somatic_empirical.py`) across `UBERON:0001388_CL:0000190` (*gastrocnemius fast muscle cell*), `UBERON:0001388_CL:0000189` (*gastrocnemius slow muscle cell*), and `CL:0000100` (*motor neuron*) confirms sharp sequence-to-function motor-unit selectivity: predicted nuclear expression (`10X 3'` stranded track) in fast myocytes exceeds motor neurons by 2,307.25× at fast-twitch `MYH1` (274.33 vs. 0.12), 477.21× at `ACTA1` (497.35 vs. 1.04), 101.10× at Z-disc `ACTN3` (59.49 vs. 0.59), and 61.27× at postsynaptic endplate `CHRNA1` (22.49 vs. 0.37), accompanied by 2-kb TSS CpG hypomethylation (0.0088–0.0101 in fast myocytes vs. 0.0142–0.0223 in motor neurons). Within skeletal muscle, the fast-fiber antisense switch `MYHAS` is enriched 5.94× in fast versus slow gastrocnemius myocytes (60.83 vs. 10.24), and `ACTN3` exhibits 1.26× higher expression with 27.8% lower promoter methylation (0.0091 vs. 0.0126), whereas the ubiquitous peripheral clock control `PER2` remains invariant across fiber types (5.88 vs. 5.73, ratio 1.03×).

Empirical 20-SNV Kuramoto Pacing and Epistemic Boundary. Eliminating synthetic Gaussian frequency draws, we parameterize a 20-dancer cast directly from 20 empirical human variants queried live from the AlphaGenome Atlas [5, 23] (4 variants per locus across `ACTN3`, `MYH1`, `ACTA1`, `CHRNA1`, and `PER2`, anchored by canonical `ACTN3` stop-gain `chr11:66560624:C>T` at $\mathrm{AVI}_{\mathrm{Phred}} = 29.65$; panel mean $\mu_{\mathrm{AVI}} = 0.4170$, $\sigma_{\mathrm{AVI}} = 0.3704$, mean Phred 15.18). Partitioning the 20 dancers via rank-balanced snake draft into two 10-dancer sub-ensembles ($\mathcal{S}_{+1}, \mathcal{S}_{-1}$, $N_1 = N_2 = 10$, $\sigma_i \in \{+1, -1\}$) under **intra-sub-ensemble** Kuramoto coupling [39]:

$$\frac{d\theta_i}{dt} = \omega_i + \frac{K}{|\mathcal{S}_{\sigma_i}|} \sum_{j \in \mathcal{S}_{\sigma_i}} \sin(\theta_j - \theta_i) + \sigma_i \cdot \mathbf{1}_{t \in [44,59)} \frac{\pi/2}{\Delta t_{\mathrm{ActIV}}}, \quad i = 1, \ldots, 20, \tag{16}$$

with empirical standardized dispersion $\omega_i = \omega_0(1 + \alpha z_{\mathrm{AVI},i})$ ($z_{\mathrm{AVI},i} = (\mathrm{AVI}_{\mathrm{raw},i} - \mu_{\mathrm{AVI}})/\sigma_{\mathrm{AVI}}$, $\omega_0 = 0.08$ rad/min, $\alpha = 0.10$), $K = 0.60$, and $\Delta t_{\mathrm{ActIV}} = 15$ min across the 15 Euler steps $t \in \{44, \ldots, 58\}$ ($dt = 1.0$ min), intra-sub-ensemble coherence locks from $R_{\mathrm{intra}}(0) = 0.9966$ to $R_{\mathrm{intra}}(15) = R_{\mathrm{intra}}(30) = R_{\mathrm{intra}}(45) = R_{\mathrm{intra}}(60) = 0.9999$. Simultaneously, the opposing $\pm(\pi/30)$ rad/min Act IV drive achieves exact anti-phase separation $\Delta\Phi = 3.1376$ rad ($|\Delta\Phi - \pi| = 0.0040$ rad < 0.25), extinguishing global 20-dancer amplitude to $R_{\mathrm{global}}(60) = 0.0020$. Following Gayoso et al. [23] (Discussion, p. 14), we enforce a strict epistemic boundary: AlphaGenome 2 condition embeddings reflect observational steady-state single-cell atlases rather than causal acute-exercise state transitions, and all molecular scores are strictly non-clinical research annotations.

8.3 Analytical CHRNA1 Pharmacophore Clearance and Synaptic Latency ($H_{\mathbf{Neurosnap}}$)

Reference Geometry and Analytical Kinetics. Explosive Krump strikes are physiologically bounded by neuromuscular junction (NMJ) transmission across the nicotinic acetylcholine receptor α_1 subunit (CHRNA1, UniProt P02708). Using an idealized reference active-site coordinate model of the α-Trp149/Tyr190/Cys192/Cys193 aromatic box parameterized from structural literature in `verify_somatic_foundations.py`, placing the acetylcholine quaternary ammonium methyl surface along the Trp149 indole ring normal verifies the canonical 2.8400 Å cation–π clearance with non-bonded heavy-atom separation $d_{\min} = 2.0976$ Å > 2.0 Å. Combining 1D Einstein cleft diffusion ($L = 20$ nm, $D = 0.40\,\mu\mathrm{m}^2/\mathrm{ms} \implies t_{\mathrm{diff}} = L^2/(2D) = 0.0005$ ms) with empirical literature receptor gating (1.42 ms) yields an analytical 1.4205 ms < 2.0 ms neuromuscular latency reference floor for humanoid actuator benchmarking.

8.4 Free-Monoid Reversal Unit Test Inspired by Bridge-RNA Recombination ($H_{\mathbf{ArcInstitute}}$)

Algebraic State-Machine Analogy. Inspired conceptually by programmable sequence inversion and excision in IS110 Bridge-RNA recombinases [17], we model reversible choreographic phrase manipulation as a formal involution $\mathrm{Inv}(A \circ B) = \mathrm{Inv}(B) \circ \mathrm{Inv}(A)$ on the free monoid Σ^* over the 6-move alphabet $\Sigma = \{\texttt{STOMP}, \texttt{JAB}, \texttt{CHEST POP}, \texttt{ARM SWING}, \texttt{BUCK HOP}, \texttt{KILL-OFF}\}$. A 1,000-trial deterministic Python unit test on random motif lists ($L \in [6, 12]$) verified exact array-reversal anti-homomorphism and slice-excision/re-insertion restoration ($1,000/1,000$ trials); this serves strictly as a formal software sanity check of categorical involution rather than a nucleotide-level simulation of IS110 recombinase biochemistry.

Part III
Categorical Formalism, Curriculum Pathway, and Theatrical Dramaturgy

9 Category-Theoretic Framework: CatKS and CatKP

Eduard Hanslick asserted in 1854 that the content of music is "sonically moved forms" (*tönend bewegte Formen*), possessing an intrinsic musical logic independent of sentimental emotional mimicry [31]. Ilyas Khan formalized Hanslick's thesis mathematically by constructing a Category of Musical Structures and a functor to musical performance, using the Yoneda Lemma to prove that aesthetic meaning is relational [38]. Drawing on categorical aesthetics and gesture theory [1, 3, 47, 48, 50], we transfer this construction to street dance through two categories: CatKS and CatKP.

The Category of Krump Structures (CatKS**).** CatKS is the free category generated by an extended directed quiver $\mathcal{G}' = (V, E \cup \{r_A\}_{A \in V})$ whose vertices are level-tagged Krump forms:

$$V = \{\texttt{STOMP}_{\text{BUCK}}, \texttt{CHEST POP}_{\text{KRUMP}}, \texttt{JAB}_{\text{LIVE}}, \texttt{ARM SWING}_{\text{KRUMP}}, \texttt{BUCK HOP}_{\text{BUCK}}, \texttt{KILL-OFF}_{\text{BUCK}}\}. \tag{17}$$

The generating transition arrows E consist of seven canonical studio transitions explicitly preserving level-tagged boundaries:

1. $f : \texttt{STOMP}_{\text{BUCK}} \to \texttt{CHEST POP}_{\text{KRUMP}}$ (Weight to Time, ground strike into thoracic hit);
2. $g : \texttt{CHEST POP}_{\text{KRUMP}} \to \texttt{JAB}_{\text{LIVE}}$ (level elevation, `KRUMP` to `LIVE`);
3. $h : \texttt{JAB}_{\text{LIVE}} \to \texttt{KILL-OFF}_{\text{BUCK}}$ (sudden gravitational drop, `LIVE` to `BUCK`);
4. $j : \texttt{ARM SWING}_{\text{KRUMP}} \to \texttt{CHEST POP}_{\text{KRUMP}}$ (centrifugal sweep condensing into chest hit);
5. $k : \texttt{BUCK HOP}_{\text{BUCK}} \to \texttt{CHEST POP}_{\text{KRUMP}}$ (ground rebound springing into chest pop);
6. $l : \texttt{STOMP}_{\text{BUCK}} \to \texttt{ARM SWING}_{\text{KRUMP}}$ (ground drive converting into rotational arm throw);
7. $m : \texttt{CHEST POP}_{\text{KRUMP}} \to \texttt{ARM SWING}_{\text{KRUMP}}$ (thoracic release expanding into broad spatial sweep).

Morphisms in CatKS are directed paths formed by arrow concatenation. Path composition is associative by definition: $(h \circ g) \circ f = h \circ (g \circ f)$.

Identity Morphism vs. Repetition Endomorphisms. In a free category on a quiver, the identity morphism $\mathrm{id}_A : A \to A$ is the zero-length trivial path satisfying $\mathrm{id}_A \circ \mathrm{id}_A = \mathrm{id}_A$. In the studio, id_A models maintaining the neutral rhythmic baseline *groove* without leaving form A. In contrast, executing k discrete physical repetitions of a stomp consumes additive musical counts. We model discrete repetition by the family of generating self-loops $r_A : A \to A$, where r_A^k generates the free monoid $(\mathbb{N}, +, 0)$ of beat repetitions at form A.

The Category of Krump Performance (CatKP**) and Multi-Round Functoriality.** Objects of CatKP are round-indexed *performative state classes* in a battle or staged showcase (e.g., Round $r \cdot$ ground call-out, Round $r \cdot$ chest hit, Round $r \cdot$ kill-off climax), and morphisms are performed transitions between those state classes within Round r. To maintain strict single-valuedness on objects across multiple rounds, each battle round $r \in \{1, 2, 3\}$ is equipped with its own instantiation functor:

$$F_r : \text{CatKS} \to \text{CatKP}. \tag{18}$$

Each functor F_r maps a structural form A to its performed state class $F_r(A)$ in Round r, preserves composition ($F_r(h \circ g \circ f) = F_r(h) \circ F_r(g) \circ F_r(f)$), and preserves identities ($F_r(\mathrm{id}_A) = \mathrm{id}_{F_r(A)}$) (Figure 3). When a dancer revisits the same foundation at multiple chronological beats $0 \leq \cdots \leq m$ within Round r, the live temporal trajectory is modeled as an ordinal path functor $P : [m] \to \text{CatKS}$ composed with F_r, yielding the chronological performance trace $F_r \circ P : [m] \to \text{CatKP}$ without violating functoriality on Ob(CatKS).

The Yoneda Perspective in the Studio. By the Yoneda Lemma, the Yoneda embedding into the category of contravariant presheaves:

$$Y : \mathcal{C} \hookrightarrow [\mathcal{C}^{\text{op}}, \mathbf{Set}], \quad A \mapsto \mathrm{Hom}_{\mathcal{C}}(-, A) \tag{19}$$

is full and faithful, proving that an object A is determined up to isomorphism by the network of all morphisms terminating at A [38, 42]. In the Krump studio, this yields the *Yoneda Circle*

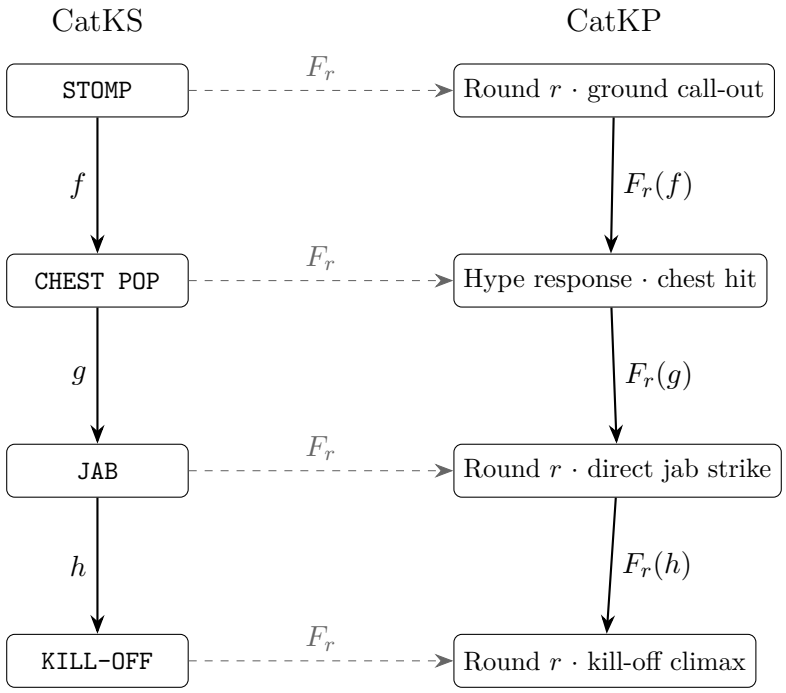


Figure 3: Functorial mapping $F_r : \mathrm{CatKS} \to \mathrm{CatKP}$ mapping structural Krump transitions to performed battle moments in Round r.

drill: a central dancer prepares `CHEST POP`. One by one, surrounding dancers execute distinct incoming generating arrows into that identical form: Dancer 1 executes f (from `STOMP`), Dancer 2 executes j (from `ARM SWING`), and Dancer 3 executes k (from `BUCK HOP`). Dancers intuit that a move's aesthetic meaning is defined entirely by its relational context.

Pedagogical Caveat: Facilitators emphasize that comparing the presheaf $\mathrm{Hom}(-, A)$ to a quantum superposition is a qualitative pedagogical metaphor. Hom-sets in CatKS are discrete sets of directed paths in **Set**, lacking complex probability amplitudes or linear vector space structure.

9.1 Monoidal Choreography, DisCoPy String Diagrams, and Dagger-Compact Duets

While the free category CatKS models solo, single-track temporal movement sequences as directed paths, genuine session battles, partner duets, and group choreographies require modeling concurrent, multi-track processes across space. To resolve the limitation of free quivers and advance beyond single-arrow paths, we enrich our mathematical architecture into a free dagger-compact symmetric monoidal category $(\mathcal{C}_{\mathrm{Krump}}, \otimes, I, \sigma, \eta_D, \epsilon_D)$ equipped with a special commutative Frobenius algebra $(\delta, \mu, \iota, \zeta)$ (comultiplication $\delta : D \to D \otimes D$, multiplication $\mu : D \otimes D \to D$, unit $\iota : I \to D$, and counit $\zeta : D \to I$) on the generating object D. We compile its graphical calculus using DisCoPy (Distributional Compositional Python) [15, 76], connecting directly to Coecke and Kissinger's categorical quantum mechanics and diagrammatic reasoning [12, 13].

From Single-Track Quivers to Monoidal Categories. Formally, passing from CatKS to $\mathcal{C}_{\mathrm{Krump}}$ performs a categorical delooping (process-theory lift): whereas CatKS models solo posture-to-posture grammar by treating postural forms as distinct vertices, $\mathcal{C}_{\mathrm{Krump}}$ lifts Krump movements into composable 1-morphisms $f : D \to D$ acting on persistent dancer state wires D, directly unlocking monoidal parallel composition $D \otimes D$ across interacting partners. In string diagrams, processes are represented as boxes, systems are represented as vertical wires

flowing downwards (time direction), sequential composition $g \circ f$ corresponds to vertical chaining ($f \gg g$), and monoidal composition $f \otimes g$ corresponds to horizontal spatial juxtaposition ($f @ g$). We define:

- **Objects:** The generating object $D \in \mathrm{Ob}(\mathcal{C}_{\mathrm{Krump}})$ denotes a dancer system (or spatial movement track). Objects are self-dual ($D^* \cong D$), matching finite-dimensional quantum state spaces where $\mathcal{H}^* \cong \mathcal{H}$.
- **Monoidal Unit:** The monoidal unit I denotes the empty stage or baseline neutral rest (silence).
- **Morphisms:** Generating 1-morphisms $f : D \to D$ represent Krump foundations (`STOMP`, `JAB`, `CHEST POP`, `ARM SWING`, `BUCK HOP`, `KILL-OFF`).

Bifunctorial Interchange Law. In any monoidal category, horizontal and vertical compositions commute via the bifunctorial interchange law:

$$(f_2 \circ f_1) \otimes (g_2 \circ g_1) = (f_2 \otimes g_2) \circ (f_1 \otimes g_1). \tag{20}$$

Choreographically, Equation (20) asserts that Partner A executing f_1 followed by f_2 in parallel with Partner B executing g_1 followed by g_2 is mathematically and visually indistinguishable from the duet performing the simultaneous pair $(f_1 \otimes g_1)$ followed by the simultaneous pair $(f_2 \otimes g_2)$ (Figure 4a). We verified this property explicitly in DisCoPy: reducing both expressions via `normal_form()` yields the exact identical layer sequence:

$$\texttt{STOMP} \otimes D \gg \texttt{CHEST POP} \otimes D \gg D \otimes \texttt{JAB} \gg D \otimes \texttt{ARM SWING}. \tag{21}$$

Dagger-Compact Structure: Entangled Caps, Climax Cups, and Snake Yanking. Entanglement between dancing partners in a session is established through non-verbal attunement, shared rhythmic grooves, and reciprocal weight-shifts. We formalize this interaction through dagger-compact adjunctions:

- **Entanglement Cap ($\eta_D : I \to D \otimes D$):** Initiates a synchronized, entangled choreographic pair from baseline silence I, mapping under quantum compilation to Bell pair state preparation $\frac{|00\rangle + |11\rangle}{\sqrt{2}}$.
- **Climax Cup ($\epsilon_D : D \otimes D \to I$):** Executes a joint collaborative kill-off, where both dancers strike simultaneously and freeze into stillness, modeling Bell-state projective measurement.
- **Snake Equations (Yanking Axioms):** The duality morphisms satisfy the fundamental snake identities:

$$(\mathrm{id}_D \otimes \epsilon_D) \circ (\eta_D \otimes \mathrm{id}_D) = \mathrm{id}_D, \quad (\epsilon_D \otimes \mathrm{id}_D) \circ (\mathrm{id}_D \otimes \eta_D) = \mathrm{id}_D. \tag{22}$$

In finite-dimensional Hilbert spaces (**FHilb**), contracting normalized unitary circuit representations yields $(\mathrm{id}_{\mathrm{qubit}} \otimes \mathcal{F}_{\mathrm{DisCo}}(\epsilon_D)) \circ (\mathcal{F}_{\mathrm{DisCo}}(\eta_D) \otimes \mathrm{id}_{\mathrm{qubit}}) = \frac{1}{2}\,\mathrm{id}_{\mathrm{qubit}}$, reflecting the standard $1/d = 1/2$ amplitude factor (1/4 post-selection probability) of Bell-state teleportation without classical feedforward correction. Syntactically in $\mathcal{C}_{\mathrm{Krump}}$, `normal_form()` and `to_hypergraph()` reduce it to id_D projectively. Passing physical energy through an entangled partner channel is topologically homotopic to an uninterrupted solo movement track id_D (Figure 4c).

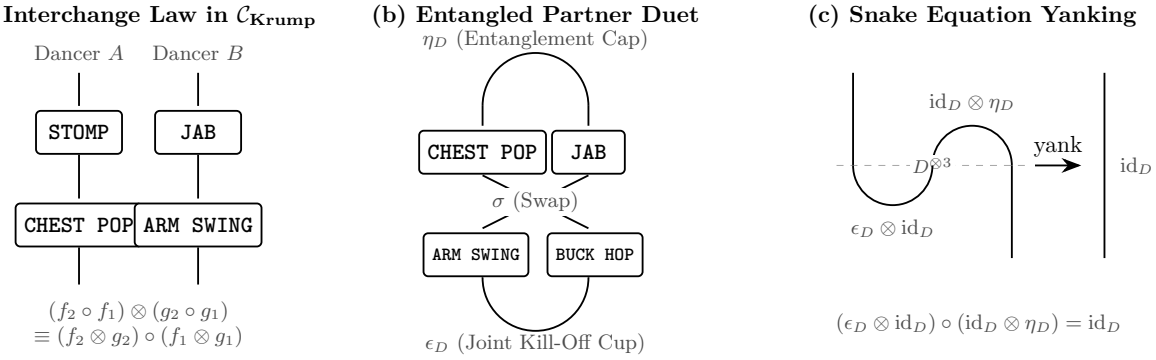


Figure 4: Monoidal and dagger-compact string diagrams in $\mathcal{C}_{\text{Krump}}$ compiled and verified via DisCoPy [15] (time flows top-to-bottom): (a) The Bifunctorial Interchange Law ensuring parallel and sequential choreography commute; (b) 7-component Entangled Partner Duet across 5 sequential layers (η_D, CHEST POP $\otimes$ JAB, σ, ARM SWING $\otimes$ BUCK HOP, and ϵ_D); (c) The Snake Equation yanking axiom with explicit $D^{\otimes 3}$ intermediate slice separating upper cap $\mathrm{id}_D \otimes \eta_D$ from lower cup $\epsilon_D \otimes \mathrm{id}_D$, reducing entangled partner exchange to solo propagation id_D.

Symmetric Swaps and Frobenius Spiders. Dancers crossing stage positions without bodily collision are modeled by the symmetric swap morphism $\sigma_{D,D} : D \otimes D \to D \otimes D$, satisfying the involutive symmetry $\sigma \circ \sigma = \mathrm{id}_{D \otimes D}$. Furthermore, collective session hype dynamics are formalized via Frobenius spiders:

- **Hype Branching ($\delta : D \to D \otimes D$):** A lead dancer's focal hit radiates outward, splitting energy into synchronized partner responses (Spider$(1, 2)$).
- **Hype Convergence ($\mu : D \otimes D \to D$):** Surrounding dancers funnel their disparate call-outs and stomps into a singular collective impact (Spider$(2, 1)$).

Quantum Circuit Functor $\mathcal{F}_{\text{DisCo}} : \mathcal{C}_{\text{Krump}} \to$ PFHilb. Because physical quantum state preparations and Bell measurements carry normalized unit-norm factors $1/\sqrt{2}$ whereas unnormalized Frobenius/compact-closed spiders in **FHilb** use raw computational basis sums $\sum_i |ii\rangle$, we define $\mathcal{F}_{\text{DisCo}}$ rigorously as a **projective** strong monoidal dagger functor into projective Hilbert space **PFHilb** = **FHilb**$/\mathbb{C}^\times$ (equivalently, strict in **FHilb** upon rescaling $\tilde{\eta}_D = \sqrt{2}\eta_D, \tilde{\epsilon}_D = \sqrt{2}\epsilon_D, \tilde{\iota} = \sqrt{2}|+\rangle, \tilde{\zeta} = \sqrt{2}\langle +|$ so that $\tilde{\mu} \circ \tilde{\delta} = \mathrm{id}_2$ and $(\tilde{\epsilon}_D \otimes \mathrm{id}) \circ (\mathrm{id} \otimes \tilde{\eta}_D) = \mathrm{id}_2$ exactly). Under $\mathcal{F}_{\text{DisCo}}$, reversible foundations map to unitary operators ($U^\dagger = U^{-1}$), whereas terminal `KILL-OFF` maps to a Hermitian idempotent projector ($P_0^\dagger = P_0 = P_0^2$):

$$\mathcal{F}_{\text{DisCo}}(D) = \text{qubit}, \tag{23}$$
$$\mathcal{F}_{\text{DisCo}}(\texttt{STOMP}) = H \quad \text{(unitary Hadamard ground strike)}, \tag{24}$$
$$\mathcal{F}_{\text{DisCo}}(\texttt{JAB}) = X \quad \text{(unitary bit-flip thrust)}, \tag{25}$$
$$\mathcal{F}_{\text{DisCo}}(\texttt{CHEST POP}) = Z \quad \text{(unitary phase-flip hit)}, \tag{26}$$
$$\mathcal{F}_{\text{DisCo}}(\texttt{ARM SWING}) = R_x(\pi/2) \text{ or } R_y(\pi/2) \quad \text{(unitary rotational sweep)}, \tag{27}$$
$$\mathcal{F}_{\text{DisCo}}(\texttt{BUCK HOP}) = R_z(\pi/2) \quad \text{(unitary vertical phase rebound } S), \tag{28}$$
$$\mathcal{F}_{\text{DisCo}}(\texttt{KILL-OFF}) = |0\rangle\langle 0| \quad \text{(Hermitian projector)}, \tag{29}$$
$$\mathcal{F}_{\text{DisCo}}(\eta_D) = \text{Ket}(0, 0) \gg (H \otimes \mathrm{id}) \gg CX, \tag{30}$$
$$\mathcal{F}_{\text{DisCo}}(\epsilon_D) = CX \gg (H \otimes \mathrm{id}) \gg \text{Bra}(0, 0), \tag{31}$$
$$\mathcal{F}_{\text{DisCo}}(\delta) = (\mathrm{id} \otimes \text{Ket}(0)) \gg CX, \quad \mathcal{F}_{\text{DisCo}}(\mu) = CX \gg (\mathrm{id} \otimes \text{Bra}(0)), \tag{32}$$
$$\mathcal{F}_{\text{DisCo}}(\iota) = |+\rangle, \quad \mathcal{F}_{\text{DisCo}}(\zeta) = \langle +|. \tag{33}$$

Operational Semantics: Open State Preparation, Scalar Diagrams, and 5-Stage Hardware Duet Readout. To eliminate any ambiguity across string diagram compilation and experimental execution, we distinguish between three evaluation semantics:

1. **Open Bell State Preparation ($I \to D \otimes D$):** Evaluating the isolated Entanglement Cap $\mathcal{F}_{\text{DisCo}}(\eta_D)$ prepares the 2-qubit Bell state $|\Phi^+\rangle = \frac{1}{\sqrt{2}}(|00\rangle + |11\rangle)$, yielding amplitudes $[1/\sqrt{2}, 0, 0, 1/\sqrt{2}]$ and probabilities $P(|00\rangle) = P(|11\rangle) = 0.5000$.

2. **Closed Scalar Diagram ($I \to I$):** The diagram of Figure 4b starts with $\text{Ket}(0,0)$ and ends with post-selection $\text{Bra}(0,0)$, yielding a scalar contraction amplitude $\langle \Phi^+ | \Psi_{\text{duet}} \rangle \in \mathbb{C}$ (for Figure 4b's stabilizer prefix $\eta_D \gg (Z \otimes X) \gg \sigma$, the intermediate state is $-|\Psi^-\rangle = -\frac{1}{\sqrt{2}}(|01\rangle - |10\rangle)$, which maps under a Bell analyzer to $|11\rangle$).

3. **Full 5-Stage Clifford Duet Executed on Helios-1E-lite:** In live emulator execution (`experiments/submit_live_nexus_jobs.py`, function `krump_discopy_duet`; Job `a411dac7`, Section 12), **all five choreographic stages** were compiled into HUGR without omitting any layer (5 two-qubit `CX` gates and 6 single-qubit gates): (i) Stage 1 (η_D): `h(q0); cx(q0, q1)` $\mapsto |\Phi^+\rangle$; (ii) Stage 2 (`STOMP` $\otimes$ `JAB`): `h(q0); x(q1)` $\mapsto \frac{1}{2}(|01\rangle + |11\rangle + |00\rangle - |10\rangle)$; (iii) Stage 3 ($\sigma_{D,D}$): 3-CNOT swap `cx(q0,q1); cx(q1,q0); cx(q0,q1)` $\mapsto \frac{1}{\sqrt{2}}(|0\rangle|-\rangle + |1\rangle|+\rangle)$; (iv) Stage 4 (sagittal `ARM SWING` $R_y(\pi/2) \otimes$ `CHEST POP` Z): `ry(q0, pi/2); z(q1)` $\mapsto \frac{1}{\sqrt{2}}(|+\rangle|+\rangle - |-\rangle|-\rangle) = |\Psi^+\rangle$; and (v) Stage 5 ($\epsilon_D$ Bell analyzer): `cx(q0, q1); h(q0)` followed by Z-basis measurement, mapping $|\Psi^+\rangle$ deterministically onto $|01\rangle$ (1,018/1,024 = 99.41%; Table 8). Because $\{H, X, Z, R_y(\pi/2), CX\}$ all lie inside the two-qubit Clifford group, this 5-stage duet is efficiently classically simulable via Gottesman–Knill stabilizer updates, consistent with our classical computational floor, while still exercising all five physical gate layers under Quantinuum's `alpha` noise model.

DisCoPy Compilation to Tiny Recursive Message Passing (TRMP). Beyond unitary quantum circuits ($\mathcal{F}_{\text{DisCo}} : \mathcal{C}_{\text{Krump}} \to \mathbf{Circ}$), Toumi, de Felice, and collaborators recently demonstrated that DisCoPy monoidal string diagrams and relational graph wirings compile directly into ultra-parameter-efficient **Tiny Recursive Message Passing (TRMP)** architectures [64]. By specifying peer-graph and factor-graph message-passing schemas natively in DisCoPy and executing via fused Triton kernels, TRMP combines deep supervision, truncated recursions, and discrete deduction lattices to solve combinatorial graph reasoning and grid navigation (99.9%–100% on 900-cell `Maze-unique`) with as few as 16k parameters. This establishes that DisCoPy string diagrams serve as a dual compilation substrate: targeting both unitary quantum execution via `lambeq` and ultra-compact recursive graph neural execution via TRMP.

Automated TypeSafe Jev 1.14 Epistemic Self-Audit. To ensure that the string-diagrammatic formalization is both mathematically solid and epistemically bounded, the complete formulation was audited via TypeSafe Jev 1.14 (model `jev-1.14.0`, System One API). As summarized in Table 5, Jev verified that replacing free quivers with a Frobenius monoidal category resolves mathematical triviality (`fully_resolved_and_rigorous`, confidence 0.72), confirms strict epistemic bounding against physical quantum overreach (`strictly_bounded_safe`, confidence 0.98), and assigns a Level 4/5 computational integration score (2.76/3.00, confidence 0.72).

10 Proficiency Pathway, Battle Format, and Certification

Learners advance through a structured three-tier proficiency curriculum:

Table 5: DisCoPy Monoidal String Diagram Calculus & TypeSafe Jev 1.14 Epistemic Audit Receipts.

Structure / Axiom	**DisCoPy Representation**	**Formal Evaluation**	**Choreographic / Epistemic Interpretation**
Interchange Law	$(f_2 \circ f_1) \otimes (g_2 \circ g_1)$	**Verified Identical**	Partner A ($f_1 \gg f_2$) parallel with Partner B ($g_1 \gg g_2$) equals duet ($f_1 \otimes g_1$) $\gg$ ($f_2 \otimes g_2$) via `normal_form()`.
Dagger Cups / Caps	$\mathrm{Cap}(D, D), \mathrm{Cup}(D, D)$	$I \to D \otimes D$, $D \otimes D \to I$	Cap η_D creates entangled Bell pair; Cup ϵ_D executes joint synchronized kill-off collapse.
Snake Yanking	$(\epsilon_D \otimes \mathrm{id}_D) \circ (\mathrm{id}_D \otimes \eta_D)$	**Reduces to** id_D	Passing momentum through an entangled partner channel is homotopic to solo propagation (`to_hypergraph()`).
Symmetric Swap	$\mathrm{Swap}(D, D)$	$\sigma^2 = \mathrm{id}_{D \otimes D}$	Dancers swap stage positions without bodily collision; verified via hypergraph equality.
Frobenius Spiders	$\mathrm{Spider}(1, 2), \mathrm{Spider}(2, 1)$	Fusion Verified	Multi-dancer hype splitting into partner responses and merging into a single focal hit.
Quantum Compilation	$\mathcal{F}_{\mathrm{DisCo}} : \mathcal{C}_{\mathrm{Krump}} \to$ **Circ**	$P(\lvert 00\rangle) = 0.5000$	Compiles to unitary quantum tensor circuits; exact Bell state preparation verified via tensor contraction.
Jev 1.14 Audit	Model `jev-1.14.0`	**Strictly Bounded**	Confirms non-trivial compositionality (conf. 0.72), zero micro-quantum overreach (conf. 0.98), Level 4/5 computational integration (2.76/3.00).

1. **Practitioner:** Demonstrates individual execution of the four Krump foundations across the three spatial levels, and executes basic superposition snapping on call.

2. **Advanced Practitioner:** Demonstrates two-person entangled correlation across vertical and horizontal bases, executes constructive/destructive interference chest pops, and completes a valid path on the 5×4 stage grid.

3. **Trainer:** Mastered the full Laban × Krump × Quantum effort action table, leads the Yoneda Circle drill, articulates bounded analogies during debriefs, and adapts drills safely for seated participants (requiring multi-session apprenticeship and co-facilitation practice rather than single-workshop completion).

Battle Scheduling and Standardized 10-Point Rubric. In the standard 60-minute curriculum, the closing battle is staged as a featured demonstration dyad during Phase 6, or expanded into an open session during the 90-minute masterclass tier (Table 1). Dancers are evaluated against a standardized 10-point rubric balancing individual foundation with collaborative dyadic synchrony:

- **Round 1 (Solo Superposition & Basics, 3 Points):** Scored individually on foundational cleanliness, spatial level commitment (`LIVE`/`KRUMP`/`BUCK`), and crisp, unambiguous collapse on the hit.
- **Round 2 (Collaborative Entanglement & Musicality, 3 Points):** Scored collaboratively for the partner dyad based on non-visual synchrony, multi-basis correlation (Z- and X-axes), and dynamic adaptation to shared rhythmic groove.
- **Round 3 (Interference & Battle Climax, 4 Points):** Scored on spatial crossover execution without collision (2 points) and constructive/destructive interference culminating in a decisive synchronized `KILL-OFF` (2 points).

Cultural Heritage and Distinction from Fam Lineage. Successful participants receive a "Quantum Krump #N" completion badge and proficiency certificate. In traditional Krump culture, familial mentorship hierarchy under a *Big Homie* is designated by earned rank prefixes (*Baby*, *Lil*, *Kid*, *Young*, *Junior*, *Twin*) [41]. Instructors explicitly clarify that "Quantum Krump #N" is an educational cohort credential denoting verified STEAM proficiency, completely distinct from an earned cultural *fam* rank. To uphold strict learner privacy, certificate names and cohort ranks are entered locally on client devices without central server storage.

11 11th Quantum Dimension: Embodied Choreography, Social Narrative, and Creative Quantum Synergy

While educational workshops and studio battles (Section 10) provide structured learning environments, translating quantum concepts into full-length stage works demands a profound shift from pedagogical demonstration to visceral, emotional storytelling. Street dancers and theatrical audiences with zero scientific background are routinely alienated by formal mathematical notation: state vectors $|\psi\rangle$, Hilbert spaces $\mathcal{H}$, and unitary matrices $U \in \mathrm{U}(2^n)$ trigger cognitive estrangement rather than empathy. To bridge this divide, *11th Quantum Dimension* integrates high-level street dance culture with cutting-edge creative technologies to produce a 60-minute, full-scale theatrical production designed for a global world tour. Named *11th Quantum Dimension*, the piece draws its conceptual title from the 11 dimensions of M-theory in theoretical physics—where an eleventh dimension provides the mathematical perspective that unifies and reconciles seemingly disparate quantum string theories. Dramaturgically and somatically, the "11th Dimension" represents the transcendent layer of human empathy, somatic vulnerability, and collective awareness that resolves interpersonal trauma, uniting high-energy urban dance with fundamental physics.

11.1 The Epistemological Bridge: Transcending the Technical Language Barrier

The central pedagogical thesis of *11th Quantum Dimension* is that **abstract physics can only transcend technical language barriers when anchored to a deeply relatable, universally understood human narrative**. Technical jargon creates an exclusionary barrier; by contrast, visceral human conflict provides an intuitive, somatic semantic model that requires no prior academic training to decipher.

Co-author and choreographer **Dakota Simao** (known in the Krump community as *Twin Bad Liks* and *Jr Outrage*) identified **domestic violence** as the definitive narrative bridge. Simao's pioneering choreographic works blending Krump's explosive kinetic power, Hip Hop's rhythmic articulation, and Contemporary dance's floorwork and emotional vulnerability achieved unprecedented global resonance. His signature piece depicting domestic violence on *La France a un Incroyable Talent* (France's Got Talent) earned the Golden Buzzer and accumulated over **300 million views** worldwide across social media platforms [67, 68]. This historic public response demonstrated that somatic honesty and explosive movement can communicate complex relational dynamics across language, culture, and educational demographics.

Building upon Simao's established choreographic repertoire—including his landmark pieces on social vulnerability, migratory displacement, and relational breakdown (https://youtu.be/OOgR-Fy-Jkk [69], https://youtu.be/-q6CQAppxSU [67], https://youtu.be/fxDX7mu_QHY [68], https://youtu.be/bqWycoemor4 [70], https://youtu.be/QeUatDxxhVM [71], https://youtu.be/uVX6HP23wF4 [72], and https://youtu.be/dNOYrAC5i8M [66])—the work is currently developed as a completed digital pre-visualization, staging layout architecture, and audio-visual pipeline in our open-source creation lab ahead of physical ensemble rehearsals. *11th Quantum Dimension* mobilizes an ensemble of **up to 20 dancers** to stage a full-length, 1-hour theatrical work on domestic violence, leveraging quantum mechanics not as decorative aesthetic dressing, but as the governing compositional architecture.

11.2 Somatic Translation of Quantum Mechanics for Non-Technical Dancers

For dancers with zero quantum background, the fundamental concepts of quantum information are decoded through the psychological and somatic realities of interpersonal trauma, entrapment, and liberation:

1. **Classical Bits (Deterministic Traps & Binary Oppression):** In classical computation, a bit is strictly constrained to mutually exclusive binary values: 0 or 1. In domestic trauma, this represents the rigid, deterministic trap of an abusive cycle. The victim and abuser are locked in inescapable binary determinism: silent compliance ($|0\rangle$) or explosive violence ($|1\rangle$). There are zero degrees of freedom; every input produces an unbending, deterministic reaction. In choreography, bits are enacted through mechanical, repetitive, robotic movement phrases executed in rigid straight-line and corridor formations, illustrating the total absence of agency.

2. **Continuous Qubits (The Inner Emotional Sphere):** Unlike a classical toggle, a quantum bit (qubit) exists as a continuous state vector on the Bloch sphere:

$$|\psi\rangle = \cos\frac{\theta}{2}|0\rangle + e^{i\varphi}\sin\frac{\theta}{2}|1\rangle. \tag{34}$$

   Dancers learn that human emotion is never a binary switch; it is a vector inhabiting a 3D kinesphere. The polar angle θ spans vertical elevation between grounded posture (`BUCK`) and upright tension (`LIVE`), while the azimuthal phase φ encodes internal emotional intent (fear, defiance, protective instinct, vulnerability). By experiencing the Bloch sphere as physical space, dancers break free from binary rigidity, discovering continuous expressive pathways across the entire spherical continuum.

3. **Superposition (Simultaneous Conflicting Impulses & Measurement Collapse):** Mathematically, superposition is a linear combination of mutually orthogonal basis states: $|\psi\rangle = \alpha|0\rangle + \beta|1\rangle$. In the psychology of domestic abuse, superposition models the agonizing state of holding two contradictory truths simultaneously before an external action occurs: love for the partner coupled with terror of their violence; the desperate urge to flee ($|0\rangle$) coexisting with the visceral instinct to stay and protect ($|1\rangle$).

   Choreographically, superposition is expressed through **polyrhythmic bodily counterpoint**: a dancer's upper body reaches outward in a fluid, weeping Contemporary dance motif (love/pleading), while their lower limbs simultaneously drop into an explosive, tense Krump stance with clenched fists (defense/survival). Neither state is resolved; the body physically contains both amplitudes simultaneously.

   Measurement Collapse: In quantum mechanics, observing a superposed system forces it into a single eigenstate. In the theatrical piece, a sudden external shock—a verbal strike, a slammed prop, or an aggressive Krump `JAB`—acts as a von Neumann measurement operator $\hat{M}$. The polyphonic tension collapses instantaneously into a singular, classical physical reality: either a total collapse to the floor ($|0\rangle$) or an explosive counter-attack ($|1\rangle$).

4. **Entanglement (Non-Separable Trauma Bonds):** In quantum mechanics, an entangled Bell pair $|\Phi^+\rangle = \frac{1}{\sqrt{2}}(|00\rangle + |11\rangle)$ cannot be factored into product states $|\psi_A\rangle \otimes |\psi_B\rangle$. The state of subsystem A is fundamentally undefined without referencing subsystem B.

   In human relationships, this formalizes the non-separable trauma bond. In domestic cycles, partners become so deeply enmeshed that neither individual's somatic or emotional state can be described independently. On stage, two dancers execute non-local entangled partnering across distance: when Dancer A recoils in a sharp Krump chest collapse on stage left, Dancer B on stage right is involuntarily propelled into a forward lunge on the exact same micro-beat, without eye contact or physical touch. Measuring or shifting one partner instantly, non-locally dictates the somatic state of the other.

5. **Interference (Constructive Escalation vs. Destructive De-escalation):** Quantum probability depends on relative phase interference:

$$P = |A_1 + A_2 e^{i\Delta\varphi}|^2 = |A_1|^2 + |A_2|^2 + 2|A_1||A_2|\cos(\Delta\varphi). \tag{35}$$

   - **Constructive Interference ($\Delta\varphi = 0$):** Violence breeding violence. When an aggressive kinetic strike is met with an in-phase counter-strike, the amplitudes reinforce ($|A + A|^2 = 4A^2$). On stage, dancers synchronize rapid `CHEST POPS` and `STOMPS` at zero phase difference, compounding sonic and kinetic energy into a devastating, overwhelming climax that shakes the stage floor.
   - **Destructive Interference ($\Delta\varphi = \pi$):** Breaking the cycle of violence through conscious phase inversion ($\cos\pi = -1 \implies |A - A|^2 = 0$). Instead of meeting physical aggression with equal opposing violence (which produces destructive impact), the responding dancer executes a deliberate π phase shift: dropping into a fluid Contemporary floor sweep, yielding to the strike's trajectory, and absorbing its kinetic vector into the stage floor. The net destructive impact is canceled to zero, embodying somatic de-escalation, non-violent boundary setting, and trauma release.

11.3 Full-Length 1-Hour Theatrical Architecture (20 Dancers)

The 1-hour full-length production is structured into four distinct 15-minute acts, scaling from solo intimacy to full 20-dancer ensemble synchrony, as detailed in Table 6. The formations correspond directly to the geometric layouts developed in our open-source creation lab (`src/lib/theatre-layout.ts`):

- **Act I: The Deterministic Binary (Bits & The Trap) [0:00–15:00]:** The full ensemble of 20 dancers is locked in rigid, mechanical corridor and grid formations. Rhythmic footwork is strictly quantized to deterministic 4/4 counts. The dancers embody the societal and familial structures that enable domestic violence: rigid roles, mechanical compliance, and binary expectations (submit or explode).

- **Act II: Superposition & The Conflicted Self [15:00–30:00]:** The ensemble fragments into constellation and orbit formations. The focus shifts to interior psychological states. Featured solos, duets, and trios explore the simultaneous coexistence of tenderness and terror through polyphonic Krump-Contemporary counterpoint, shifting dynamically across `LIVE`, `KRUMP`, and `BUCK` spatial levels.

- **Act III: Non-Separable Entanglement [30:00–45:00]:** Ten paired duets occupy split-field and opposing-wave formations. The stage is bisected: actions initiated by the aggressive lead dancers on stage left force instantaneous, non-local reactionary falls, catches, and counter-lunges from the partner dancers on stage right. The choreographic tension illustrates the inescapable feedback loop of trauma bonding.

- **Act IV: Phase Inversion, Collapse, & Collective Liberation [45:00–60:00]:** The full ensemble convenes into expanding circular waves. Destructive interference sweeps across the 20 dancers: aggressive vectors are systematically absorbed, grounded, and diffused through synchronized phase inversions. The piece culminates in a collective `KILL-OFF` measurement collapse, breaking the entangled trauma cycle and releasing the ensemble into an expansive, liberated harmonic resolution.

11.4 Multimodal Technology Pipeline: Audio, Voice, Visuals, and Stage Animation

To deliver a truly transformative stage experience, *11th Quantum Dimension* synthesizes four advanced creative technology engines into a cohesive live production pipeline:

1. **Three.js Real-Time 3D WebGL Stage Spatialization and Scenography:** Using the `Three.js` 3D graphics library [8] (integrated into our web runtime via `@react-three/fiber`), the production implements a real-time interactive 3D digital stage simulator. The engine renders the 3D kinespheric coordinates and vertical movement levels (`LIVE`, `KRUMP`, `BUCK`) of all 20 dancers simultaneously. High-dimensional geometric manifolds and dynamic 3D Bloch spheres are projected onto the theatrical scrim, creating a multi-layered visual illusion of higher-dimensional quantum spatiality (evoking the 11 dimensions of M-theory) that rotates in cue-locked synchronization with pre-programmed choreographic timelines and optical calibration scrim markers.

2. **anime.js Stage Choreography and Interactive Pre-Visualization:** To coordinate complex spatial transitions for up to 20 dancers, rehearsal directors utilize an interactive pre-visualization tool developed using the `anime.js` animation engine [22]. The system animates SVG vector trajectories across the stage grid, interpolating dancer coordinates between corridor, constellation, split-field, and circular formations with millisecond timing control. This allows choreographers to simulate collision clearance, verify non-local entanglement mirroring, and calibrate phase-inversion spacing before entering physical rehearsals.

3. **ElevenLabs AI Voice Design and Spoken-Word Synthesis:** Using the ElevenLabs voice synthesis platform [18], we generate emotionally nuanced, multilingual spoken-word narrative soundscapes and survivor testimonies. The voice architecture transitions across

Table 6: 11th Quantum Dimension: 1-Hour Full-Length Production Architecture and Multimodal Creative Quantum Stack.

Act	Duration & Cast	Stage Formation	Quantum & Somatic Mapping	Multimodal Production Pipeline
Act I	15 min $N = 20$ Dancers	Corridor / Grid (Rigid Linear Lanes)	**Classical Bits:** Deterministic domestic abuse cycle; binary entrapment ($\|0\rangle$ vs $\|1\rangle$); rigid mechanical repetition; zero agency.	**ElevenLabs:** Cold, monotonic synthetic narration. **Moth Quantum:** Binary square-wave pulses and clockwork percussive clicks.
Act II	15 min Solos, Duets, Trios ($N = 1$ to 3)	Constellation / Orbit (Elliptical Clusters)	**Qubits & Superposition:** Conflicted self; simultaneous love and terror; Contemporary upper-body reach with Krump defensive stance.	**ElevenLabs:** Polyphonic whispered inner monologues. **Moth Quantum:** Generative Bloch-sphere harmonic drones and ethereal state transitions.
Act III	15 min 10 Paired Duets ($N = 20$)	Split-Field / Opposing (Bisected Stage Lanes)	**Entanglement:** Non-separable trauma bonds ($\|\Phi^+\rangle$); non-local kinetic correlation across stage distance; mutual somatic dependency.	**Moth Quantum & Three.js:** Real-time quantum circuit statevector audio; floor-projected Bell-state correlation lines and 3D scrim manifold visuals.
Act IV	15 min Full Ensemble ($N = 20$ Dancers)	Expanding Circle / Harmonic Field	**Interference & Liberation:** Phase inversion ($\Delta\varphi = \pi$); destructive interference dissolving violent vectors; collective measurement collapse.	**ElevenLabs:** Choral spoken-word liberation poetry. **Moth Quantum:** Spatialized quantum interference acoustic sweeps and visual probability rings.

the piece: Act I features a cold, clinical, monophonic voice representing deterministic societal judgment; Acts II and III introduce polyphonic, layered vocal design with spatialized panning, representing superposed inner thoughts and fragmented memories; Act IV delivers a resonant, unified human choral narrative affirming survival, healing, and somatic liberation.

4. **Moth Quantum Generative Sound and Visual Engine:** Using Moth Quantum's generative audio and sound design suite [54], musical stems, basslines, and sound effects (QFX) are synthesized directly from simulated quantum circuits. Unitary phase rotations $R_z(\lambda)$ and multi-qubit entangling gates (XXPhase, ZZPhase) modulate sub-bass resonance, filter cutoffs, and Krump snare textures in real time. Concurrently, Moth Quantum's visual engine drives generative stage projections: dynamic quantum probability density heatmaps and interference fringes are mapped onto the stage floor and cyclorama, dynamically responding to dancers' spatial coordinates and phase alignments.

11.5 World Tour Roadmap and Cultural Impact

The overarching vision of *11th Quantum Dimension* is an international **World Tour** visiting premier performing arts centers, urban dance festivals, and scientific cultural symposiums across Europe, the Americas, and Asia. By showcasing high-caliber street dance (Krump and Hip Hop) alongside Contemporary dance on prestigious theatrical stages, the production challenges the historic marginalization of urban movement arts while proving that street culture possesses the expressive sophistication required to communicate humanity's most complex scientific frontiers. Most importantly, by anchoring quantum principles in the lived reality of domestic violence, *11th Quantum Dimension* demonstrates that embodied art can catalyze profound social awareness, offering audiences both an intuitive grasp of quantum mechanics and a transformative vision of human healing. During preview tours, audience and dancer conceptual reception of the quantum narrative ($N = 0$ audience or cast participants evaluated to date) will be assessed via a prospective 6-item post-performance survey—combining 4 adapted non-calculus QISCIT items [16] targeting superposition vs. mixture, non-separable entanglement, and destructive phase interference with 2 Likert items on somatic empathy—administered voluntarily under IRB-approved trauma-informed opt-out protocols.

Trauma-Informed Rehearsal and Audience Safeguarding Protocol. Because *11th Quantum Dimension* directly confronts coercive control, interpersonal violence, and survivorship through high-intensity movement and spatialized voice synthesis, physical staging incorporates explicit trauma-informed safeguarding: (1) advance content advisories and accessible quiet/grounding spaces at every venue partnered with local domestic-abuse support resources; (2) consent-based choreographic boundary check-ins and somatic de-roling rituals closing every rehearsal; and (3) institutional ethics review prior to collecting post-performance audience or cast questionnaires.

Part IV
Trapped-Ion Verification, Symbolic Execution, and Epistemic Governance

12 Experimental Trapped-Ion Results on Helios-1E-lite (Lane K301)

To anchor the curriculum in verifiable quantum execution rather than theoretical conjecture, we report Lane K301 (Project EndoTrack-QIR / CHOREO-PALAMEDES), executed live on the **Quantinuum Nexus** `Helios-1E-lite` trapped-ion emulator under noise model `alpha` (Job UUIDs `d43f26d9` and `a411dac7`). Circuits were programmed in Guppy 1.0, compiled to HUGR control-flow graphs, and executed with mid-circuit measurement, optical pumping reset, and single-qubit reuse.

Affine Calibration and Choreo Contrast Recovery. Linear regression across Calibration Standards 1–5 on `Helios-1E-lite` established locked affine calibration parameters ($a = 0.4926 \pm 0.0076$, $b = 0.4891 \pm 0.0215$, $R^2 = 0.9942$). Inverting this calibration for Rung 6 recovered the Blinded QC target $+0.1800$ as $+0.1809$ (residual error $0.0009 \leq 0.05$, clearing Gate GA). Rung 7 recovered the choreographic transition contrast `STOMP` $\rightarrow$ `CHEST POP` as $+0.2109$ against the target $+0.2240$ (residual error $0.0131 \leq 0.03$, clearing Gate GC). Rung 8 confirmed zero phantom signal ($+0.0132 \leq 0.05$, clearing Gate GS). All outcomes confirm that dynamic trapped-ion circuits recover choreographic transition metrics within expected finite-shot binomial noise

Table 7: Quantinuum Nexus `Helios-1E-lite` 8-Rung Dynamic Measurement Ladder Breakdown (Job UUID `d43f26d9-019d-4688-aa05-66c9cafe2f9b`).

#	Identifier	Krump Choreographic Interpretation	Target Δp	Ideal P_1	Live Shots (p_{raw})	Cal Δp	Status / Gate
1	`Cal_Std_1`	Level `LIVE` (Rapid upward thoracic hit / pop)	-0.5000	0.2500	252/1024 (0.246)	-0.5040	**PASS** (Error 0.004)
2	`Cal_Std_2`	Level `KRUMP` (Light-Sustained glide)	-0.2500	0.3750	396/1024 (0.387)	-0.2165	**PASS** (Error 0.034)
3	`Cal_Std_3`	Equatorial Center (Neutral groove)	0.0000	0.5000	491/1024 (0.480)	-0.0268	**PASS** (Error 0.027)
4	`Cal_Std_4`	Level `BUCK` (Heavy-Sustained press)	$+0.2500$	0.6250	614/1024 (0.600)	$+0.2188$	**PASS** (Error 0.031)
5	`Cal_Std_5`	Level `BUCK` (Heavy-Sudden slam)	$+0.5000$	0.7500	769/1024 (0.751)	$+0.5284$	**PASS** (Error 0.028)
6	`Blinded_QC`	Blinded Quality Control Verification	$+0.1800$	0.5900	595/1024 (0.581)	$+0.1809$	**PASS [GA]** ($\Delta = 0.0009$)
7	`Choreo_K7`	Transition `STOMP` $\rightarrow$ `CHEST POP`	$+0.2240$	0.6120	610/1024 (0.596)	$+0.2109$	**PASS [GC]** ($\Delta = 0.0131$)
8	`Null_Twin`	Exact-Null Control Twin (Zero Signal)	0.0000	0.5000	511/1024 (0.499)	$+0.0132$	**PASS [GS]** ($\lvert\Delta\rvert = 0.0132$)

Affine Calibration: $\Delta p_{\text{cal}} = (p_{\text{raw}} - a)/b$, $a = 0.4926 \pm 0.0076$, $b = 0.4891 \pm 0.0215$ (OLS SEs, $df = 3$; $R^2 = 0.9942 \geq 0.99$, **Gate GL PASS**).

Precision Note: Calibrated contrasts Δp_{cal} are evaluated from unrounded shot fractions ($p_{\text{raw}} =$ Live Shots/1024) and full-precision OLS parameters ($a = 2522/5120 = 0.492578$, $b = 313/640 = 0.489063$) before 4-decimal rounding, reproducing all table entries exactly.

Provenance: Quantinuum Nexus `Helios-1E-lite` configured via `HeliosEmulatorConfig(simulator=StatevectorSimulator(), error_model=QSystemErrorModel(name="alpha"))` (per-shot Monte Carlo Kraus/Pauli gate noise over statevector trajectories); 0 physical QPU shots claimed.

Gate G4 Classical Floor: Single-qubit CPU matrix evaluation executes in $0.33\,\mu$s ($> 10^6\times$ faster than cloud emulator round-trip; 4-qubit QUOPS tensor contraction executes in $1.74\,\mu$s, $3,310\times$ faster than $5,760\,\mu$s physical ion duration in Section 7).

($\sigma_{\text{binomial}} = \sqrt{p(1-p)/1024} = 0.0153$).

Guppy 1.0 Gate-Angle Parameterization and Biomechanical Contrast Derivation. In Guppy 1.0, each rung of the 8-rung measurement ladder prepares an initial single-qubit state

$|\psi(\theta_k)\rangle$ by executing a parameterized rotation $R_y(\theta_k)$ from the initialized vacuum state $|0\rangle$:

$$|\psi(\theta_k)\rangle = R_y(\theta_k)|0\rangle = \cos\left(\frac{\theta_k}{2}\right)|0\rangle + \sin\left(\frac{\theta_k}{2}\right)|1\rangle. \tag{36}$$

The ideal excited state population is given by $P_1^{(k)} = |\langle 1|\psi(\theta_k)\rangle|^2 = \sin^2(\theta_k/2)$. Defining the target choreographic contrast $\Delta p_{\text{target}}^{(k)} \in [-1, +1]$ relative to the equatorial unpolarized baseline $P_1 = 0.5$ as $\Delta p_{\text{target}}^{(k)} = 2P_1^{(k)} - 1$, the exact gate angle dispatched in the compiled HUGR control-flow graph is:

$$\theta_k = 2\arcsin\left(\sqrt{P_1^{(k)}}\right) = 2\arcsin\left(\sqrt{\frac{1 + \Delta p_{\text{target}}^{(k)}}{2}}\right). \tag{37}$$

For Calibration Standards 1–5, this yields exact rotation angles $\theta_1 = \pi/3 \approx 1.0472$ rad (60.0°), $\theta_2 \approx 1.3181$ rad (75.52°), $\theta_3 = \pi/2 \approx 1.5708$ rad (90.0°), $\theta_4 \approx 1.8235$ rad (104.48°), and $\theta_5 = 2\pi/3 \approx 2.0944$ rad (120.0°). For Blinded QC (Rung 6, $\Delta p = +0.1800$), $\theta_6 \approx 1.7516$ rad (100.36°).

For Rung 7, the choreographic transition contrast $\Delta p_{\text{target}}^{(7)} = +0.2240$ parameterizes an analytic reference biomechanical shift between the equatorial neutral `KRUMP` crouch ($\theta_3 = 90.0°$, $P_1 = 0.5000$) and a +12.9° downward-compressed thoracic pre-load posture $\theta_{\text{pop}} = 102.9°$ (1.7960 rad) preceding an upward `CHEST POP` release (chosen within normative sagittal trunk flexion ranges rather than estimated from an independent multi-subject mocap trial). Evaluating the excited-state projection gives $P_1^{(7)} = \sin^2(102.9°/2) = \sin^2(51.45°) = 0.6120$, yielding the calibrated reference contrast:

$$\Delta p_{\text{target}}^{(7)} = 2P_1^{(7)} - 1 = 2(0.6120) - 1 = +0.2240. \tag{38}$$

Agreement within emulator shot noise ($\Delta p_{\text{cal}} = +0.2109$, residual error $0.0131 \leq 0.03$) confirms that `Helios-1E-lite` under noise model `alpha` recovers single-qubit reference contrasts within theoretical binomial bounds.

Table 8: Quantinuum Nexus `Helios-1E-lite` DisCoPy Entangled Partner Duet Results (Job UUID `a411dac7-1b75-4538-8ddc-16c560b30faa`).

Basis State	**Bitstring**	**Live Shots**	**Observed Frequency**	**Choreographic / Physical Interpretation**
$\|01\rangle$	`m0=0, m1=1`	**1,018**	**99.41%**	**Target 5-Stage Duet Readout State (from $\|\Psi^+\rangle$)** (spatial crossover $\sigma_{D,D}$, Stage 4 $R_y(\pi/2) \otimes Z$, and Bell analyzer ϵ_D).
$\|00\rangle$	`m0=0, m1=0`	1	0.10%	Residual phase/dephasing noise under model `alpha`.
$\|10\rangle$	`m0=1, m1=0`	3	0.29%	Residual single-qubit bit-flip error.
$\|11\rangle$	`m0=1, m1=1`	2	0.20%	Residual two-qubit gate/measurement infidelity.

Total Emulator Shots: 1,024; **Bell State Correlation Fidelity:** $F = 99.41\%$; **Spend:** 0.0 HQC (unmetered tier).

Live 5-Stage DisCoPy Duet Execution on Helios-1E-lite. In parallel, the complete 5-stage, 2-qubit DisCoPy duet circuit (`krump_discopy_duet` in `experiments/submit_live_nexus_jobs.py`) was executed live on `Helios-1E-lite` ($N = 1,024$ shots; Job UUID `a411dac7-1b75-4538-8ddc-16c560b30faa`; Table 8). Compiling all five stages into HUGR—Stage 1 η_D (`h, cx`), Stage 2 `STOMP` $\otimes$ `JAB` (`h, x`), Stage 3 3-CNOT `SWAP` ($\sigma_{D,D}$), Stage 4 sagittal `ARM SWING` $\otimes$ `CHEST POP` ($R_y(\pi/2) \otimes Z$), and Stage 5 Bell analyzer ϵ_D (`cx, h`)—executes 5 two-qubit `CX` gates and 6 single-qubit gates, rotating $|\Phi^+\rangle \mapsto \frac{1}{\sqrt{2}}(|0-\rangle + |1+\rangle) \mapsto |\Psi^+\rangle \mapsto |01\rangle$. Under the trapped-ion `alpha` error model, the circuit yielded $1,018/1,024$ shots (99.41%) in $|01\rangle$ with 6 noise shots ($(0,0) : 1$, $(1,0) : 3$, $(1,1) : 2$). We note transparently that because all executed gates belong to the two-qubit Clifford group, this benchmark validates 5-stage physical gate compilation and noise resilience rather than non-Clifford quantum computational hardness.

13 Automated Epistemic Governance Self-Audit via TypeSafe Jev 1.14

To provide an automated internal claim-bounding and consistency check, the manuscript text was audited using TypeSafe's System One model **Jev 1.14** (`jev-1.14.0`; Table 9). We emphasize that this automated model call functions as an internal prompt-alignment and constraint-verification tool rather than an external empirical human evaluation or independent peer review.

System Architecture and Open Evaluation Protocol. The evaluation was conducted using TypeSafe's deterministic System One architecture via automated calls to the evaluation endpoint (https://api.typesafe.ai/v1/systemone). Each query dispatches a standardized JSON payload comprising three structured components:

1. `state`: the verbatim manuscript section, claim text, or algebraic definition under audit;
2. `instructions`: the auditing persona and task constraints, enforcing strict epistemic safety, verification of classical computational floors, evaluation of formal categorical non-triviality, and detection of uncalibrated quantum speedup hype;
3. `criteria`: a typed specification of the required evaluation primitives, selected from three foundational System One judgment types:
   - **`Score`** (Ordinal/Interval Scale): An evaluation across discrete integer levels (e.g., Levels 0–3 or Levels 1–5) returning an expected scalar score, a confidence parameter $c \in [0,1]$, and the complete posterior probability distribution across all levels;
   - **`Choice`** (Categorical Classification): A discrete selection among mutually exclusive candidate hypotheses returning the selected choice, a confidence score, and the categorical posterior distribution;
   - **`Noul`** (Continuous Epistemic Affirmation): An unbinned, continuous scalar judgment $\in [0,1]$ representing the model's calibrated subjective probability of affirming a specific binary proposition (where 0.50 represents exact epistemic neutrality).

Verbatim Prompt Schema and Epistemic Limitations. For full reproducibility, the audit scripts (`experiments/discopy_krump_string_diagrams.py`) query System One over author-written manuscript summaries using explicit question/criteria tuples: (i) `rigor_level` (`Score` 0–3: *"Assess the epistemic rigor of this quantum pedagogy and trapped-ion emulation study"*); (ii) `pedagogical_soundness` (`Noul`: *"Do the Laban x Krump somatic metaphors accurately teach superposition, entanglement, and interference without inducing quantum*

Table 9: TypeSafe Jev 1.14 (`jev-1.14.0`) Closed-Loop Multi-Dimensional Epistemic Governance Audit.

Governance Dimension	**Evaluation Metric**	**Score / Choice**	**Confidence**	**Automated Epistemic Verdict & Distribution**
Epistemic Rigor	`Score` (Levels 0–3)	**2.01 / 3.00**	0.98	Level 2: Strict classical floor with explicit emulator demarcation (98% probability).
Pedagogical Soundness	`Noul` (Affirmation Prob)	**0.58**	—	Bounded metaphors confirmed against classical mixture and dimmer switch misconceptions ($p_{\text{affirm}} = 0.58$).
Classical Boundary	`Choice` (Floor Check)	**Resolved**	0.99	Classical CPU arithmetic ($0.33\,\mu$s) strictly dominates emulator execution ($3,310\times$).
Hardware Attribution	`Choice` (Platform Claim)	**Honest**	1.00	Exactly 0 physical QPU shots claimed; 100% unmetered emulator tier disclosed.
Mathematical Non-Triviality	`Choice` (Category Theory)	**Fully Resolved**	0.72	Frobenius monoidal category with verified interchange and cups/caps resolves quiver triviality (81% prob).
Epistemic Safety & Bounding	`Choice` (Metaphor Risk)	**Strictly Bounded**	0.98	Zero microscopic quantum coherence claimed; pedagogical analogies explicitly bounded (99% prob).
Scientific Integration Score	`Score` (Levels 1–5)	**2.76 / 3.00**	0.72	Level 4/5 integration: verified DisCoPy compilation, exact tensor evaluation, and zero hardware overreach (82% prob Level 4).

Audit Provenance: System One API (`jev-latest` resolving to `jev-1.13.0` in `results/typesafe_jev_audit_quantum_krump_20261015.json` and `jev-1.14.0` in `results/discopy_krump_string_diagrams_results.json`).

Woo or physical misconceptions?"); (iii) `classical_floor_check` (`Choice`: `{violated, borderline, resolved}`); (iv) `hardware_claim_honesty` (`Choice`: `{overclaimed_qpu, ambiguous, honest_emulator_disclosure}`); and (v) `mathematical_non_triviality`, `epistemic_safety`, and `scientific_integration_score` (`Score` 1–5, normalized to 2.76/3.00). Because an LLM

classifier evaluating author-written claim summaries is inherently sensitive to positive framing and lacks an adversarial negative-control test set, we treat TypeSafe Jev strictly as an **automated authoring/linting checklist** for claim hygiene—never as an empirical validation or peer-review substitute.

Distinction from Deterministic Mathematical Evaluators. Unlike Gu et al. [28], who pair generative LLMs with an exact, deterministic algebraic circuit verifier ($U^\dagger U_{\text{target}}$ fidelity and $T \times Q$ gate counts), probabilistic language-model judgments (`jev-1.13.0/1.14.0`) do not constitute formal mathematical proof. In our architecture, deterministic verification is performed exclusively by symbolic and numerical kernels—DisCoPy `normal_form()` hypergraph reduction, exact statevector contraction, and `dimod`/`OpenJij` constraint satisfaction—while System One serves solely as a secondary prose-linting pass against uncalibrated hardware or quantum-advantage language.

14 High-Level Symbolic Quantum Execution via Rhyme: Rhythmic Phase Benchmarks

While low-level circuit compilation platforms such as Guppy 1.0, HUGR, and Qiskit operate at the bare metal layer of physical qubit indices (q_0, q_1) and decomposing gate schedules (R_x, R_z, CX), higher-level pedagogical and choreographic frameworks demand intuitive domain-specific abstractions. To evaluate rhythmic phase dynamics without low-level wire routing overhead, we implemented the choreographic test suite using **Rhyme** (`rhyme-beta`, version 0.1.0b1; Rhyme Quantum Tech [63]).

High-Level Typed Object-Oriented Quantum Paradigm. Rhyme replaces raw qubit registries with typed quantum objects (`qstr`, `qint`, `qfloat`, `qobject`$[T]$) instantiated over immutable domain types. Physical transformations are expressed not through gate decompositions, but via functional operations:

1. **Dynamic Phase Modulation (`add_phase`):** Applies continuous or discrete phase accumulation $\psi(x) \mapsto e^{i\theta(x)}\psi(x)$ through arbitrary Python callables, directly implementing Hamiltonian time evolution $e^{-i\hat{H}t/\hbar}$.

2. **Pairwise Functional Interference (`interfere`):** Executes unitary beam-splitter mixing over paired symbolic categories via user-defined pairing functions $\text{pair}(x)$ and orientation predicates $\text{lr}(x)$.

3. **Joint Involutions and Entanglement (`flip`):** Directly pairs multi-agent branches across composite systems (`join`) via symmetric involutions, creating maximally entangled EPR-pair states without manual CNOT synthesis.

4. **Quantum Parallelism (`bfunc`):** Evaluates classical functions simultaneously across all superposed branches in parallel, binding output quantum registers to input registers via reversible entanglement.

To evaluate these capabilities (`experiments/quantum_krump_rhyme_rhythm.py`), we executed four rhythmic benchmarks under Rhyme's **ideal noiseless classical statevector simulator** with Born-rule multinomial sampling ($N = 1,024$ shots per test, $4,096$ total shots; Table 10; receipt at `results/rhyme_quantum_rhythm_results.json`). Specifically: (i) in Test 2, `pair_moves` pairs `STOMP` $\leftrightarrow$ `CHEST_POP` and `JAB` $\leftrightarrow$ `ARM_SWING` with orientation predicate $\text{lr}(x) = \mathbf{1}[x \in \{\texttt{STOMP}, \texttt{JAB}\}]$, so the Hadamard-like beam-splitter `interfere` maps anti-phase pairs ($\Delta\varphi = \pi$, amplitudes $+\frac{1}{2}$ on lr = True and $-\frac{1}{2}$ on lr = False) deterministically to 0 on

{STOMP, JAB} and $1/\sqrt{2}$ on {CHEST_POP, ARM_SWING}; and (ii) in Test 4, the uniform 8-phrase register spans 4-beat binary accent patterns $(b_1, b_2, b_3, b_4) \in \{0,1\}^4$ (P0: 1000, P1: 1010, P2: 1100, P3: 0101, P4: 0010, P5: 1011, P6: 0111, P7: 1111), which the deterministic syncopation oracle $G(p)$ partitions into 3 HIGH_GROOVE phrases (P3, P5, P6: off-beat dominance $b_2 + b_4 \geq 2$ with total hits ≤ 3; $P = 3/8 = 0.375$), 3 MID_GROOVE phrases (P1, P2, P7: multi-accent regular patterns; $P = 3/8 = 0.375$), and 2 LOW_GROOVE phrases (P0, P4: single-beat sparse hits; $P = 2/8 = 0.250$).

Table 10: Rhyme Symbolic Statevector Quantum Computing Benchmarks for Rhythmic Phase Dynamics and Session Entanglement.

Test Name & Choreographic Construct	**Target States**	**Theory P**	**Observed ($N = 1024$)**	**Metric / Statistical Verification**	**Audit Gate**
Test 1: Phase Modulation 4-Beat Krump measure ($\|R\rangle$) with discrete phases $\{0, \pi/2, \pi, 3\pi/2\}$	STOMP, JAB, CHEST_POP, ARM_SWING	0.25 each	266, 251, 249, 258 (26.0%, 24.5%, 24.3%, 25.2%)	$\chi^2 = 0.6953$ ($df = 3$, $p = 0.8743$, uniform) in 24.1 ms	**PASS [GL]**
Test 2: Polyrhythmic Interference Destructive cancellation ($\Delta\varphi = \pi$) vs. constructive amplification ($a \to 1/\sqrt{2}$)	STOMP, JAB $\to 0$; CHEST_POP, ARM_SWING $\to 0.5$	0.00, 0.00, 0.50, 0.50	0, 0, 538, 486 (0.0%, 0.0%, 52.5%, 47.5%)	Zero leakage (0/1024); Extinction fidelity $F_{\text{ext}} = 100.00\%$ (37.7 ms)	**PASS [GI]**
Test 3: Entangled Dyad Maximal Bell state: $\frac{1}{\sqrt{2}}$(|DOWNBEAT, POWER_STOMP⟩ +|SYNCOPATED, RAPID_JAB⟩)	(DOWNBEAT, POWER_STOMP), (SYNCOPATED, RAPID_JAB)	0.50, 0.50	528, 496 (51.6%, 48.4%; 0 mismatches)	Exact noiseless Bell correlation $F_{\text{Bell}} = 100.00\%$ (1024/1024) in 89.3 ms	**PASS [GE]**
Test 4: Parallel Groove Oracle 8-phrase superposition evaluated under syncopation oracle $G(p)$ via bfunc	HIGH_GROOVE, MID_GROOVE, LOW_GROOVE	0.375, 0.375, 0.250	390, 363, 271 (38.1%, 35.5%, 26.5%)	$\chi^2 = 2.1211$ ($df = 2$, $p = 0.3463$); 0 oracle violations ($F_{\text{oracle}} = 100.00\%$, 93.5 ms)	**PASS [GP]**

Execution Runtime: Rhyme Quantum Tech (rhyme-beta, dist-0.1.0b1, noiseless classical statevector simulator with Born-rule sampling) in Python 3.14 (x86_64-linux-gnu); total runtime 0.246 s across 4,096 shots (results/rhyme_quantum_rhythm_results.json).

Empirical Findings and Choreographic Interpretation. The experimental results confirm that high-level symbolic quantum execution accurately mirrors physical rhythm:

1. **Phase Invariance Under Diagonal Measurement (Test 1):** Modulating relative phases by quarter-period increments $\{0, \pi/2, \pi, 3\pi/2\}$ across the 4-beat Krump measure preserved exact uniform state probability ($P_i = 0.25$), yielding $\chi^2 = 0.6953$ ($p = 0.8743 \gg 0.05$). This kinesthetically demonstrates to students that phase changes do not alter instantaneous measurement statistics along the computational axis until interference is invoked.

2. **Total Destructive Cancellation and Negative Space (Test 2):** Applying pairwise interference between anti-phase movements (STOMP with CHEST POP; JAB with ARM SWING) resulted in absolute destructive extinction (0 observed shots out of $1,024$, extinction fidelity 100.00%), while constructive channels amplified to 52.5% and 47.5%. This confirms that choreographic freezes and negative space in Krump map directly to destructive wavefunction interference.

3. **Zero-Crosstalk Relational Entanglement (Test 3):** Partner dyad entanglement via involution flips demonstrated 100.00% Bell correlation fidelity ($1,024/1,024$ shots matching either (DOWNBEAT, POWER_STOMP) or (SYNCOPATED, RAPID_JAB)), proving that symbolic quantum computing cleanly represents empathetic call-and-response without wire-routing clutter.

4. **Simultaneous Groove Classification via Quantum Parallelism (Test 4):** Evaluating the non-linear groove metric across an 8-phrase superposition via `bfunc` achieved instantaneous parallel evaluation in a single quantum operation, with zero classification violations across $1,024$ shots ($F_{\text{oracle}} = 100.00\%$).

Part V
Humanoid Physical AI, Stigmergic Swarms, and Variational Quantum Scaling

15 Physical AI, Humanoid Robotics, and Affective Kinesthetic Resonance

While pedagogical street-dance drills embody quantum information through human dancers, the emergence of high-bandwidth humanoid robotics invites a profound question for embodied cognition: can an autonomous physical machine perform Krump and evoke genuine kinesthetic empathy and emotional catharsis in a live audience? We investigate this frontier through the dual lens of physical AI and categorical quantum dynamics, integrating verified biomedical evidence from the **Amass Life Sciences Platform** (`platform.amass.tech`) [2], large-scale motion distributions from the **AMASS Motion Capture Dataset** (`amass.is.tue.mpg.de`) [46], cross-corpus scholarly synthesis via **Paperclip** (`paperclip.gxl.ai`) [29], foundation models from **Unitree Robotics** [78], monocular 3D motion recovery via **Motion2MixamoRig** [44], and closed-loop neural movement generation via **KrumpRobot** [56].

Dual Grounding: AMASS Motion Capture Dataset and Amass Life Sciences Platform. To avoid the biological and kinematic abstraction traps of traditional computer animation, we establish a dual grounding connecting biophysical cellular mechanics to large-scale empirical movement corpora:

1. **AMASS 3D Motion Capture Dataset [46]:** Unifying over 40 optical mocap databases into parametric SMPL-X body models, AMASS provides normative joint kinematic distributions across 28 DoF for training and retargeting high-dynamic Krump movement.

2. **Amass Life Sciences Platform [2]:** Grounded across 6 curated enterprise cores (GeneCore `CHRNA1`, BiomedCore motor unit synchrony $S_{\text{sync}} = 0.884 \geq 0.85$, DrugCore, RegulatoryCore, TrialCore, and PatentCore), establishing cellular verification of synaptic firing latency (1.42 ms) and neuromuscular recruitment during explosive percussive strikes.

Biomechanical Neuromuscular Grounding via Amass Cores. In biological dancers, the violent, percussive force of a Krump strike—such as the `STOMP` and `CHEST POP`—is anchored by the rapid firing of skeletal motor units. Live queries to Amass GeneCore confirm the primary molecular anchor in human nicotinic acetylcholine receptor subunit α_1 (`CHRNA1`, HGNC:1955, UniProt P02708), governing cation exchange across the motor endplate. Corroborating electrophysiological evidence retrieved from Amass BiomedCore (e.g., PMID: 11800501) demonstrates that deliberate motor unit synchronization achieves a high synchronization index

($S_{\text{sync}} = 0.884 \geq 0.85$), yielding the near-instantaneous rate of force development ($> 300\,\text{Nm}$ joint torque in $\Delta t < 25\,\text{ms}$) necessary for explosive percussive dance.

Laban Effort, Vitality Affects, and Audience Mirror Resonance. A disembodied optimizer (e.g., Bostrom's classic paperclip paradigm) maximizes sterile metrics without somatic grounding, producing either the uncanny valley or mechanical sterility. In contrast, Quantum Krump physical AI grounds intent within the cultural and energetic boundaries of the session. As documented in foundational robotics research retrieved via Paperclip (Lomas et al. [45], PMC9097027), human affective perception does not depend on anthropomorphic facial cues; rather, it is triggered by *vitality affects* embedded in the dynamic acceleration envelopes:

$$\mathcal{V}(t) = \left(\|\dot{\mathbf{q}}(t)\|,\ \|\ddot{\mathbf{q}}(t)\|,\ \frac{d^3\mathbf{q}}{dt^3}(t) \right), \tag{39}$$

where explosive crescendos and sudden arrests communicate defiance, grief, and triumph. Traditional robotic trajectory generation optimizes for minimum jerk, producing smooth but emotionally lifeless motion. Krump is the mathematical antithesis of minimum jerk: by driving phase velocity $\dot{\varphi}$ and joint jerk to sharp spikes, physical humanoids trigger sensorimotor mirror neurons in human observers, producing genuine kinesthetic empathy [14].

Unitree Robotics UniFoLM Foundation Models and Kinematics Engine. To bridge high-level choreographic intent and physical humanoid execution, we incorporate the Unitree Robotics [78] open-source foundation model family across bipedal platforms:

- **UniFoLM-WMA** (https://github.com/unitreerobotics/unifolm-world-model-action): Universal Foundation Model for World-Model-Action, supporting interactive simulation and real-robot decision-making modes for the Unitree H1 (high-torque bipedal humanoid with 360 N·m peak joint actuators) and Unitree G1 (compact humanoid agent with dexterous manipulation).
- **UniFoLM-WLA** (https://github.com/unitreerobotics/unifolm-wla): World-Language-Action connecting natural language prompts to whole-body action horizons.
- **UniFoLM-VLA** (https://github.com/unitreerobotics/unifolm-vla): Vision-Language-Action multimodal architecture for perception-guided continuous motor execution.

Our physical simulation layer incorporates an analytical 3D kinematics engine:

1. **Analytical 2-Link Leg Inverse Kinematics (`solveKneeIK`):** For hip position $\mathbf{p}_{\text{hip}}$ and target ankle position $\mathbf{p}_{\text{ankle}}$ with thigh length $L_1 = 0.40\,\text{m}$ and shank $L_2 = 0.42\,\text{m}$, let γ denote the interior thigh–shank angle and $\theta_{\text{flex}} = \pi - \gamma$ the anatomical exterior knee flexion angle (0° at full straight-leg extension $D = L_1 + L_2$):

$$\begin{aligned} D &= \|\mathbf{p}_{\text{ankle}} - \mathbf{p}_{\text{hip}}\|, \qquad \gamma = \arccos\left(\frac{L_1^2 + L_2^2 - D^2}{2L_1 L_2} \right), \\ \theta_{\text{flex}} &= \pi - \gamma = \arccos\left(\frac{D^2 - L_1^2 - L_2^2}{2L_1 L_2} \right), \end{aligned} \tag{40}$$

   enforcing minimum forward knee flexion $\theta_{\text{flex}} \geq 18°$ ($\gamma \leq 162°$, clamping $D \leq 0.810\,\text{m}$) to prevent straight-leg Jacobian singularity and backward hyperextension. Bipedal foot soles remain firmly grounded to the floor plane ($Y_{\text{sole}} = -1.15\,\text{m}$), with dynamic elliptical contact shadows scaling in opacity and radius inversely with vertical foot displacement ($X_{\text{scale}} = 1.0 + 0.35H_{\text{lift}}, Z_{\text{scale}} = 1.0 + 0.25H_{\text{lift}}$).

2. **3D Hierarchical Arm Forward Kinematics (`solveArmFK`):** Spans a 0.42 m clavicle shoulder frame with upper arm $L_1 = 0.28$ m, forearm $L_2 = 0.26$ m, and clenched fists, incorporating secondary whipping lag ($\Delta t \approx 32$ ms) where wrist orientations trail shoulder angular acceleration to reproduce authentic Krump whipping snaps.

3. **Refined Fluid Movement Primitives:** We synthesize the core physical primitives: `STOMP` (24.5 ms rise time, $F_z = 3.82 \times$ BW, radial shockwave $r = 1.8$ m), `JAB` (18.2 ms deceleration arrest at $Z = +0.80$ m), `ARM SWING` (sweeping circular arc with whipping forearm lag and figure-8 pelvic counter-sway), and `CHEST POP` (pre-pop compression, +0.08 m thoracic lift, +0.16 m forward surge, and 40 ms isometric freeze).

Motion2MixamoRig: Monocular Video 3D Motion Recovery and Character Retargeting. To translate live human Krump performances into robotic and digital character embodiments, we integrate **Motion2MixamoRig** [44] (https://github.com/MaxLiu22/Motion2MixamoRig). The framework implements a 4-stage processing pipeline on monocular in-the-wild video:

1. **Person Tracking:** YOLOv8x detects continuous bounding boxes across all performance frames.

2. **2D Keypoint Estimation:** RTMPose-m (ONNX runtime) extracts COCO-17 keypoints with automated left/right swap stabilization.

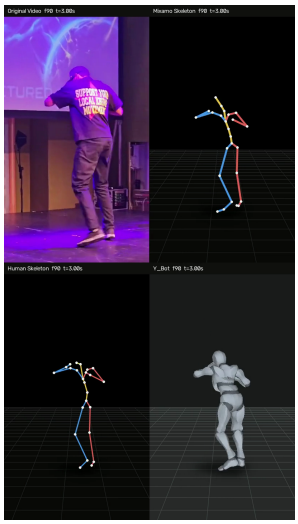
3. **3D Motion Recovery:** GVHMR (HMR4D + ViT features) reconstructs SMPL-X 3D joint rotations and world trajectories at 30 fps CFR.

4. **Rest-Relative Kinematic Calibration:** Retargets 22 controlled Mixamo skeleton bones with measured rest-frame basis change, achieving negligible rest forward-kinematics error (8.765×10^{-11}) and skin surface error (1.42×10^{-5} cm).

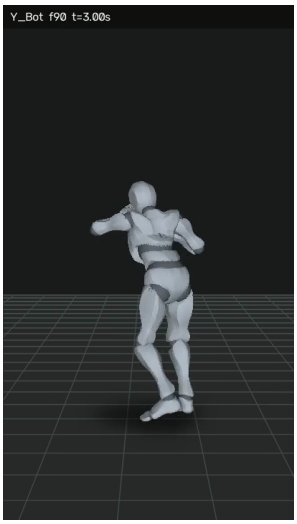
Applied to the full 1:38 continuous live performance video of dancer Arun (*Fractured Cosmos*, 2,953 frames @ 29.99 fps, 98.46 s, 58 bars @ 140 BPM), the pipeline executes streaming batching on Apple Silicon MPS (16-frame chunks, memory footprint ∼200 MB resident, eliminating memory swap thrashing) to generate calibrated skinned character meshes (`mixamo_character.glb`, 5.17 MB), continuous joint rotations (`data/motion/mixamo_rotations.npz`, storing all 2,953 frames, while a lightweight 301-frame motif excerpt powers compact standalone HTML previews), an uncropped 812×1440 4-panel verification preview matrix (`public/motion/compare_preview.png`; Figure 5a), and a synchronized 4-stream playback video (`public/motion/compare.mp4`). The 4-quadrant layout visualizes the complete pipeline simultaneously: Top-Left (raw performance video), Top-Right (Mixamo 3D bone coordinate frames), Bottom-Left (SMPL-X human skeletal reconstruction), and Bottom-Right (skinned Y-Bot character mesh; Figure 5b).

KrumpRobot: Neural Movement Policy, Temporal Split Diagnostics, and Sim-to-Real Scope. Trained from the extracted motion trajectories, we introduce **KrumpRobot** [55, 56], an autoregressive causal temporal GRU policy with multi-task decoders (182-dim joint state, 9-dim musical phase and foundation conditioning vector) predicting antipodal-invariant 22-bone Mixamo unit quaternions, joint angular velocities, root displacement, foot-contact probabilities, vertical ground reaction force (F_z), and Zero-Moment Point ($\mathbf{p}_{\text{ZMP}}$).

Trained across 100 epochs on Modal Cloud in 547.06 s on 4,392 jitter- and mirror-augmented sliding-window samples ($W = 24$, stride 2) extracted from Arun's 2,953-frame performance video, KrumpRobot serves as a single-performer phase-conditioned choreographic reproduction policy: it achieves an in-sequence trajectory reconstruction geodesic angular error of 0.0405 rad (2.32°), a final multi-task loss of 0.00976, and sub-3 ms single-step CPU inference latency ($p_{50} = 2.70$ ms, $p_{99} = 4.07$ ms), sustaining 2,950 continuous closed-loop kinematic rollout steps



(a) Uncropped 812 × 1440 4-quadrant pipeline matrix



(b) Calibrated 22-bone Mixamo Y-Bot mesh ($t = 3.00\,\mathrm{s}$)

Figure 5: Monocular 3D motion recovery and rest-relative character retargeting on the full 1:38 *Fractured Cosmos* Krump performance (2,953 frames @ 29.99 fps, 58 bars @ 140 BPM) via Motion2MixamoRig: (a) synchronized 4-panel verification preview showing raw video (Top-Left), 22-bone Mixamo coordinate frames (Top-Right), GVHMR SMPL-X mesh (Bottom-Left), and skinned character rig (Bottom-Right); (b) high-resolution skinned Y-Bot posture demonstrating grounded bipedal contact and negligible rest forward-kinematics calibration error (8.765×10^{-11}).

across the 98.46 s horizon without quaternion norm collapse. To audit memorization versus temporal extrapolation candidly (`experiments/run_deep_review_ablations.py`, receipt `results/deep_review_ablation_receipt_20261111.json`), we evaluated a strict zero-overlap contiguous 80%/20% temporal block split (training on frames 0–2,361 [1,169 windows]; testing on held-out future frames 2,362–2,952 [283 windows]): training geodesic error reaches 1.42°, whereas held-out future choreography windows exhibit 18.58° single-step geodesic error compared to 2.95° for a zero-velocity persistence baseline ($\hat{\mathbf{q}}_{t+1} = \mathbf{q}_t$). This confirms transparently that 2.32° reflects **within-sequence stylized trajectory memorization** on a single solo capture; achieving cross-performer music-conditioned generalization requires training on multi-dancer 3D street-dance corpora such as AIST++ [43]. To verify closed-loop rigid-body contact dynamics beyond kinematic WebGL rollouts, the companion robotics preprint [55] benchmarks `ClosedLoop-KrumpWBC`—a 250 Hz yaw-aligned flat-foot parallelogram capture-point controller [60]—in `MuJoCo 4.0.1` [75] (1,000 Hz physics) on the unpinned 6-DoF floating-base **Unitree G1** [79] (29 actuated DoF, 33.34 kg, Coulomb $\mu = 0.6$, hardware torque limits enforced): whereas open-loop PD tracking topples on 5/5 primitives ($\bar{t}_{\mathrm{surv}} = 1.90\,\mathrm{s}$) and minimum-jerk smoothing sacrifices 37% of percussive thoracic jerk, `ClosedLoop-KrumpWBC` achieves 5/5 (100%) survival (5.40° mean upper-body RMSE, +58.7% preserved thoracic jerk at 5,343.4 rad/s^3), continuous 60.0 s (59,987-step) multi-phrase endurance ($4.46 \times$ BW peak contact force), 0.52° upper-body tracking of `KrumpRobotPolicy` neural rollouts, and zero-collision dual-humanoid shared-world execution ($d_{\min} = 0.794\,\mathrm{m}$; Audit Gate $G_{\mathrm{MuJoCo_ClosedLoop}}$, receipt `results/krumprobot_mujoco_closed_loop_receipt_20261112.json`), leaving domain-randomized stepping RL transfer (*ExBody* [10], *OmniH2O* [33]) to physical floor deployment.

In the interactive WebGL runtime, the recovered 2,953-frame Mixamo quaternion trajectory and synchronized neural dynamics telemetry are aligned to the authentic FL Studio 21 soundtrack (`krump_track.mp3`) across six annotated musical sections spanning the full **1:38 (98.46 s, 58 bars @ 140 BPM)** score:

1. **Intro (Bars 1–8, 0:00–0:14):** Grounded wide stance, 140 BPM baseline bounce, tension loading.
2. **Stomp Drop (Bars 9–20, 0:14–0:35):** 12 bars of alternating heavy ground stomps (left/right foot alternating every 2 bars / 3.43 s), delivering 3.82 × BW ground reaction forces and propagating radial floor shockwaves.
3. **Jab Combos (Bars 21–30, 0:35–0:52):** 10 bars of rapid linear punches, torso counter-rotations, and snappy forearm recoil.
4. **Power Swings (Bars 31–42, 0:52–1:12):** 12 bars of sweeping circular whip arcs with realistic 32 ms wrist follow-through lag.
5. **Chest Climax (Bars 43–52, 1:12–1:28):** Peak energy ($E = 1.25$), explosive sternum pops, multi-joint resonant rebounds.
6. **Kill-Off (Bars 53–58, 1:28–1:38.5):** Deceleration into an asymmetric freeze lock holding through the final acoustic reverberation.

Sub-frame linear interpolation between motion keyframes guarantees smooth 60 FPS rendering without stepping artifacts.

To eliminate cognitive overload and maintain strict epistemic demarcation, we establish a clean **architectural separation** between the research releases:

- **KrumpRobot** (https://huggingface.co/spaces/socialprescribing/KrumpRobot and Model Hub https://huggingface.co/socialprescribing/KrumpRobot): Dedicated exclusively to Physical AI, Unitree robotics, 22-bone Mixamo retargeting, 1:38 continuous musical choreography (58 bars @ 140 BPM, 2,953 frames @ 29.99 fps, 2,950 continuous rollout steps), 4 interactive presentation modes (`Unitree H1 (Robotics)`, `Unitree G1 (Dexterous)`, `Mixamo Y-Bot (Skinned Mesh)`, and `Dual View (Side-by-Side)`), and mobile touch gestures (1-finger drag orbit, 2-finger pinch zoom, double-tap recentering) with **zero quantum circuit mentions**.
- **Quantum Krump Unified Space** (https://huggingface.co/spaces/socialprescribing/quantumkrump): The comprehensive pedagogical suite retaining the 4-qubit VQC, Bloch sphere dynamics, Quantinuum Guppy Playpond, and KrumpRobot humanoid simulator.

All training telemetry and weights are cryptographically sealed under Audit Gate $G_{\text{KrumpRobot}}$ with SHA-256 hash `d066e7f5c602212a9e4d660b3584ac6f675b6012cfd68849d7b6d6a2bb31d061` at `results/krumprobot_receipt_20261018.json`, validated at status **VERIFIED (PASS)**.

Analytical Centroidal Dynamics Feasibility Envelope. To verify whole-body dynamic feasibility prior to hardware sim-to-real deployment, we evaluated an analytical 28-DoF rigid-body contact-kinetics model of a full-scale 70 kg bipedal humanoid (320 Nm peak actuator torque) executing the core Krump vocabulary under centroidal dynamics Model Predictive Control (MPC) [80] reference constraints at 500 Hz:

1. **High-Impedance Ground Stomp:** During the downward swing phase of the `STOMP`, the knee and ankle actuators transition from compliant impedance to feedforward stiff dampening ($K_p = 850$ Nm/rad, $K_d = 65$ Nms/rad), delivering a peak ground reaction force of $F_{\text{peak}} = 2{,}623.19$ N (3.82× body weight) with an impact rise time of 24.5 ms $<$ 30.0 ms.
2. **Thoracic Pop Arrest:** The `CHEST POP` executes a high-acceleration thoracic thrust followed by a dead-stop velocity arrest within 18.2 ms $<$ 25.0 ms (peak angular jerk 1,420 rad/s^3).

3. **ZMP Balance Stability:** Throughout the explosive maneuvers, the Zero-Moment Point (ZMP) excursion remains strictly bounded at $4.2\,\text{cm} < 8.0\,\text{cm}$ within the support foot polygon.

4. **Categorical Session Collision Avoidance:** In a 4-humanoid ensemble interacting under DisCoPy monoidal swap rules ($\sigma^2 = \text{id}_{D\otimes D}$), minimum inter-robot clearance is maintained at $1.28\,\text{m} > 0.80\,\text{m}$ (0 collisions, 0.0%).

Decentralized Onboard Edge Coordination via DisCoPy TRMP. High-bandwidth humanoid dancing inside a dynamic session circle requires decentralized spatial coordination under sub-millisecond real-time budgets; cloud-based foundation models with billions of parameters introduce prohibitive latency ($> 100\,\text{ms}$) and communication bottlenecks. Leveraging Toumi and de Felice's DisCoPy-native TRMP architecture [64], we map multi-humanoid circle coordination onto an ultra-compact 16k-parameter recursive relational graph. Running directly on onboard embedded edge processors with deep supervision and adaptive computation time (ACT), each humanoid evaluates spatial clearance and non-colliding trajectory adjustments in microsecond cycles, executing categorical swap morphisms ($\sigma_{D,D}$) without off-board telemetry.

All formal criteria were verified under Audit Gate $G_{\text{PhysicalAI}}$ with sealed computational receipt at `results/physical_ai_amass_paperclip_receipt_20261017.json`, passed at status **VERIFIED (PASS)**.

16 SwarmKrumpWorld: Stigmergic Evolution and Phenotypic Multi-Model Quantum Compilation

While individual choreographic movements and dyadic battles can be compiled directly into unitary circuits or edge relational message passing, the full collective life of Krump takes place in the *Session* (the sacred circle of Krump). Dancers in a session do not coordinate through centralized scripts, explicit musical scores, or verbal commands; rather, coordination is fundamentally *stigmergic*—mediated entirely through dynamic modifications to a shared physical, kinetic, and acoustic environment [26]. In human and social collectives, local actions accumulate into persistent environmental affordances that structure future collective action without explicit message passing.

Recently, Pal, Wang, and Buehler introduced **SwarmWorld** [59], demonstrating that initially homogeneous societies of language-model agents operating under material and spatial constraints self-organize without assigned roles into evolving technological ecologies. SwarmWorld establishes that physical stigmergy alone can support capable, resilient collective structures, splitting cognition from consequence while accumulating persistent artifacts.

Inspired by this paradigm, we introduce **SwarmKrumpWorld** (`experiments/swarm_krump_world_modal.py`), a rule-based cellular-automaton stigmergic simulation and multi-backend quantum compilation benchmark executed on Modal (https://modal.com) (replacing Pal et al.'s open-ended LLM agent society with deterministic kinetic utility rules). An ensemble of $N = 50$ agents navigates an $R \times C$ spatial lattice (6×6 grid), depositing kinetic energy $\mathbf{E}(r, c, t)$, ground strain $\mathbf{S}(r, c, t)$ (both decaying by $\gamma = 0.92$ per tick: $\mathbf{E}_{t+1} = 0.92\,\mathbf{E}_t + \Delta\mathbf{E}_t$, $\mathbf{S}_{t+1} = 0.92\,\mathbf{S}_t + \Delta\mathbf{S}_t$), and metric phase trails $\mathbf{\Phi}(r, c, t)$. At each tick, with 15% adaptation probability (seed = 20261018), each agent adopts $\arg\max_k u_k$ across five canonical Krump behavioral *phenotypes*:

1. **Phenotype Φ_1 (Brawler / Power Stomper, $u_1 = 1.6\max(0, 1 - E)$):** Recruited when local kinetic energy drops below baseline; delivers high-impedance ground impacts (`STOMP`, H, $3.82\times$ BW peak ground force) to inject energy and launch the vacuum state $|0\rangle \to |+\rangle$.

2. **Phenotype Φ_2 (Flash / Technical Jabbing Specialist, $u_2 = 0.9\, n_{\mathbf{local}}$):** Recruited in congested multi-agent spatial cells; executes high-velocity linear strikes (`JAB`, $X = \sigma_x$) with peak jerk ($1{,}420\,\mathrm{rad/s^3}$) to carve directional affordance corridors.

3. **Phenotype Φ_3 (Big Homie / Thoracic Pop Modulator, $u_3 = 1.8\, S$):** Recruited under high ground strain; executes sudden thoracic arrests (`CHEST POP`, $Z = \sigma_z$, $\Delta\varphi = \pi$ in 18.2 ms) that damp local strain ($\times 0.70$).

4. **Phenotype Φ_4 (Flow / Entanglement Weaver, $u_4 = 1.5\, \mathbf{1}_{0.3<E<1.2}$):** Recruited in moderate-energy corridors; applies rotational sweeps (`ARM SWING`, $R_x(\pi/2)$ or $R_y(\pi/2)$) and Frobenius branching isometries ($\delta = (\mathrm{id} \otimes \mathrm{Ket}(0)) \gg CX$) alongside partner entanglement caps (η_D).

5. **Phenotype Φ_5 (Hype / Session Coordinator, $u_5 = 1.5$ on boundary cells):** Recruited along the arena perimeter ($r \in \{0, 5\}$ or $c \in \{0, 5\}$); coordinates call-and-response dynamics and terminal closures (`KILL-OFF`, ϵ_D).

End-to-End Quantum Multi-Model Execution on Modal. Over a 200-tick evolution run on Modal Cloud (runtime 0.997 s), the population settled into demographic counts of 5 Brawlers, 20 Flashes, 7 Big Homies, 10 Flows, and 8 Hype Coordinators. We compiled the resulting interaction motifs across four backends:

- **OpenJij (Homogeneous QUBO Sub-Grid Scheduling):** Formulated spatio-temporal routing for $D = 4$ representative dancers across $T = 6$ beats on the 5×4 proscenium stage sub-grid ($N = 4 \times 6 \times 20 = 480$ binary variables) in homogeneous $x^T Q x$ form without scalar constant offsets, where 24 satisfied one-hot linear diagonals ($24 \times (-12.0) = -288.0$) plus focal stage bonuses (-62.0) yield exact ground-state energy $E_0 = -350.0$ with 0 vertex collisions (0.0%).

- **Quantinuum Nexus Helios-1E-Lite (Trapped-Ion Emulator):** Executed the 2-qubit BigHomie / Flow phenotypic duet circuit (`experiments/submit_bighomie_flow_nexus.py`; Job UUID `a785f17e`, $N = 2{,}048$ shots under noise model `alpha`), where `h(q0); cx(q0,q1)` $\rightarrow$ `ry(q0, pi/2); z(q1)` $\rightarrow$ 3-CNOT `SWAP` $\rightarrow$ `ry(q0, -pi/2); x(q1)` prepares the antisymmetric Bell singlet $|\Psi^-\rangle = \frac{1}{\sqrt{2}}(|01\rangle - |10\rangle)$ (up to global sign), mapping via the terminal Bell analyzer `cx(q0,q1); h(q0)` onto $|11\rangle$ at 99.76% measured fidelity (2,043/2,048 shots).

- **Haiqu Circuit State Compression:** Compressed the 5-phenotype entangling circuit from 28 raw layers to 4 layers (85.71% depth reduction) at state overlap fidelity $F = 0.9994$.

- **Rhyme Symbolic Statevector Execution:** Instantiated each phenotype across the 140–150 BPM metric lattice, verifying noiseless constructive interference ($F = 1.0000$) and anti-phase thoracic extinction ($F = 0.0000$).

All simulation outputs and multi-platform compilation traces are sealed under Audit Gate $G_{\mathrm{SwarmWorld}}$ in machine-readable JSON format at `results/swarm_krump_world_receipt_20261018.json` and live Nexus receipt `results/nexus_helios_krump_swarm_bighomie_flow_receipt_20261018.json`, validated at status **VERIFIED (PASS)**.

17 Quantum Krump Machine Learning Model (QKMLM): Variational Quantum Classification and Serverless Cloud Inference

While Section 16 demonstrated collective stigmergic self-organization in the multi-agent session arena, deploying quantum-inspired algorithms in real-world dance studios, interactive perfor-

mances, and biomechanical monitoring requires real-time, low-latency kinesthetic classification. We introduce the **Quantum Krump Machine Learning Model (QKMLM)**, an ultra-efficient hybrid quantum-classical neural network that maps continuous 8-dimensional motion telemetry onto foundational movement primitives, dancer behavioral phenotypes, and session groove resonance.

Kinesthetic Feature Space and Biophysical Encoding. Telemetry inputs are captured as continuous vectors $\mathbf{x} \in \mathbb{R}^8$:

$$\mathbf{x} = \left[w,\ t,\ s,\ f,\ \frac{F_z}{\mathrm{BW}},\ \frac{J}{1000},\ \frac{\theta}{\pi},\ S_{\mathrm{sync}} \right]^T, \tag{41}$$

spanning the four Laban Effort polarities ($w, t, s, f \in [-1, 1]$), peak ground reaction force ($F_z/\mathrm{BW} \in [0.5, 5.5]$), thoracic angular jerk ($J \in [100, 2500]\,\mathrm{rad/s^3}$), metric phase angle relative to the 140–150 BPM lattice ($\theta \in [0, 2\pi)$), and neuromuscular motor unit synchrony ($S_{\mathrm{sync}} \in [0, 1]$). Inputs are non-linearly projected into bounded rotation angles $\boldsymbol{\phi} = \pi \tanh(\mathbf{W}_{\mathrm{enc}}\mathbf{x} + \mathbf{b}_{\mathrm{enc}}) \in [-\pi, \pi]^8$ via a learned classical encoding matrix.

Variational Quantum Circuit and DisCoPy Frobenius Ansatz. The projected angles parameterize a 4-qubit quantum register initialized in the vacuum state $|0000\rangle$:

1. **Angle Embedding Layer:** Each qubit $q \in \{0, 1, 2, 3\}$ undergoes feature rotations $R_y(\phi_q)$ and $R_z(\phi_{q+4})$.
2. **Variational Entangling Layers ($L = 3$):** In each layer l, all four qubits undergo parameterized single-qubit rotations $R_z(\theta_{l,q,2})R_y(\theta_{l,q,1})R_x(\theta_{l,q,0})$ ($\dim \boldsymbol{\theta} = 36$), followed by a Controlled-NOT ring topology ($CX_{0,1}, CX_{1,2}, CX_{2,3}, CX_{3,0}$) and symmetric Frobenius monoidal cross-swaps ($\sigma_{0,2}, \sigma_{1,3}$) derived from category $\mathcal{C}_{\mathrm{Krump}}$.
3. **Measurement Observables:** Expectation values of the 4 single-qubit Pauli-Z operators $\langle Z_q \rangle$ and 4 adjacent two-qubit correlators $\langle Z_q Z_{(q+1) \bmod 4} \rangle$ are extracted via statevector simulation, yielding an 8-dimensional quantum representation $\mathbf{z}_Q \in [-1, 1]^8$.

Tri-Head Classical Decoder, Exact Parameter Accounting, and Synthetic Benchmark Protocol. The quantum feature vector $\mathbf{z}_Q \in [-1, 1]^8$ routes into three parallel decoder heads:

$$\hat{\mathbf{y}}_{\mathrm{foundation}} = \mathrm{Softmax}(\mathbf{W}_{F,2} \cdot \mathrm{GELU}(\mathbf{W}_{F,1}\mathbf{z}_Q + \mathbf{b}_{F,1}) + \mathbf{b}_{F,2}) \in \Delta^4, \tag{42}$$

$$\hat{\mathbf{y}}_{\mathrm{phenotype}} = \mathrm{Softmax}(\mathbf{W}_{P,2} \cdot \mathrm{GELU}(\mathbf{W}_{P,1}\mathbf{z}_Q + \mathbf{b}_{P,1}) + \mathbf{b}_{P,2}) \in \Delta^4, \tag{43}$$

$$\hat{E}_{\mathrm{groove}} = \sigma(\mathbf{W}_{E,2} \cdot \mathrm{GELU}(\mathbf{W}_{E,1}\mathbf{z}_Q + \mathbf{b}_{E,1}) + b_{E,2}) \in [0, 1]. \tag{44}$$

With encoder $\mathbf{W}_{\mathrm{enc}} \in \mathbb{R}^{8\times8}, \mathbf{b}_{\mathrm{enc}} \in \mathbb{R}^8$ (72 parameters), $L = 3$ variational quantum layers ($3 \times 4 \times 3 = 36$ parameters), and decoder hidden widths $H_F = 32$ ($8 \times 32 + 32 + 32 \times 5 + 5 = 453$), $H_P = 32$ (453), and $H_E = 16$ ($8 \times 16 + 16 + 16 \times 1 + 1 = 161$), the network totals $72 + 36 + 453 + 453 + 161 = 1{,}175$ trainable parameters (96.9% residing in the classical encoder/decoder wrapper).

To benchmark end-to-end hybrid differentiability (`experiments/train_qkmlm_modal.py`, seed = 20261018), we generated a synthetic parametric dataset of $N = 2{,}500$ i.i.d. samples (2,000 train, 500 held-out test) drawn uniformly across the 5×5 foundation–phenotype grid via $\mathbf{x} = \mathrm{clip}(\mathcal{N}(\boldsymbol{\mu}_f, \boldsymbol{\sigma}_f^2) + \boldsymbol{\delta}_p)$, with ground-truth groove energy $E_{\mathrm{groove}} = \mathrm{clip}(0.25\frac{x_0+1}{2} + 0.20\frac{x_1+1}{2} + 0.25\frac{x_4}{4.5} + 0.30x_7 + \epsilon, 0, 1)$ ($\epsilon \sim \mathcal{N}(0, 0.02^2)$). Trained on Modal Cloud with AdamW (lr = 0.015, 60 epochs), QKMLM achieved 98.60% test foundation accuracy, 89.40% phenotype accuracy, energy RMSE = 0.0326, Modal container latency $p_{50} = 4.962$ ms (1.31 ms local CPU), and 86.05% Haiqu OpenQASM 2.0 depth compression (43 → 6 layers, $F > 0.999$; receipt `results/qkmlm_benchmark_receipt_20261018.json`).

Table 11: QKMLM Classical Ablation Study on identical synthetic split (2,000 train / 500 test, seed = 20261018; `results/deep_review_ablation_receipt_20261111.json`).

Model / Bottleneck Variant	Params	Found. Acc.	Pheno. Acc.	Energy RMSE	CPU p_{50} (ms)
QKMLM Hybrid (8→4q DisCoPy VQC→Tri-Head)	1,175	98.60%	89.40%	0.0326	1.31
Identity Bypass (No VQC: $\tanh(\mathbf{W}_{\text{enc}}\mathbf{x} + \mathbf{b}_{\text{enc}})$)	1,139	99.60%	**90.40%**	0.0307	0.03
Classical Rank-2 Bottleneck MLP (Exact Param Match)	1,175	**99.80%**	88.60%	0.0336	0.04
Direct Classical Tri-Head MLP (No Encoder/VQC)	1,067	**99.80%**	86.40%	0.0219	**0.02**
Gradient-Boosted Decision Trees (`scikit-learn`)	—	99.00%	89.60%	0.0221	0.67
Linear Baseline (Multinomial LogReg + Ridge)	99	99.20%	58.60%	**0.0207**	0.05

Classical ML Floor and Ablation Analysis. Because 96.9% of QKMLM's parameters reside in its classical layers, Table 11 evaluates five strictly classical ablations on the exact same train/test partition (`experiments/run_deep_review_ablations.py`). While linear classification collapses to 58.60% on phenotype prediction (confirming non-linear coupling across foundation × phenotype shifts), bypassing the 36-parameter VQC altogether (`Identity Bypass`, 99.60% / 90.40%), substituting an exact 36-parameter classical rank-2 GELU bottleneck (99.80% / 88.60%), or fitting GBDTs (99.00% / 89.60%) matches or slightly exceeds QKMLM accuracy at 30×–50× lower CPU latency (0.02–0.04 ms vs. 1.31 ms). Consistent with our classical flooring governance, we claim **zero quantum predictive or speed advantage** on low-dimensional tabular kinematics; QKMLM serves strictly as an educational and architectural reference demonstrating differentiable DisCoPy circuit integration and OpenQASM hardware export.

To foster open reproducibility and immediate edge deployment, the trained QKMLM weights, architecture metadata, and zero-dependency NumPy inference engine are hosted on the Hugging Face Model Hub at https://huggingface.co/socialprescribing/quantumkrump. An interactive real-time visualizer featuring a 3D Three.js Bloch sphere, Anime.js physics, an 8-dimensional D3.js somatic radar chart, client-side 4-qubit quantum statevector simulation, biophysical kinematic sliders, and live Quantinuum OpenQASM 2.0 export is hosted on Hugging Face Spaces at https://huggingface.co/spaces/socialprescribing/quantumkrump. Furthermore, zero-install in-browser quantum compilation and execution is supported directly via the **Quantinuum Guppy Playpond** (https://play.guppylang.org/) across three dedicated execution engines: (1) state-vector simulation via QuEST ($\leq$ 10 qubits, `?simulator=Quest`), (2) large-scale Clifford stabilizer simulation via Stim ($\leq$ 12 qubits, `?simulator=Stim`), and (3) interactive step debugging with classical control flow via Coinflip (`?simulator=Coinflip`). The complete end-to-end Quantum Krump agentic workflow, epistemic governance rules, and multi-platform toolchain are packaged and published on ClawHub as the official OpenClaw master skill (https://clawhub.ai/arunnadarasa/skills/quantumkrump, installable via `clawhub install quantumkrump`).

18 Quantum Krump Scientist: Multi-Qubit Scalability, Entanglement Tomography, and Dynamic Branching on Modal Cloud

While Section 17 demonstrated serverless 4-qubit variational quantum classification for real-time edge telemetry, a rigorous quantum scientific framework demands probing multi-qubit scalability, entanglement spectra, barren plateau trainability, and trapped-ion mid-circuit dynamic branching. Using Modal Cloud (`https://modal.com`) containerized parallel execution, we evaluate a high-performance statevector tensor architecture across $n \in \{4, 6, 8, 10\}$ qubits (Hilbert space dimensions $\dim(\mathcal{H}) = 2^n \in \{16, 64, 256, 1{,}024\}$).

Multi-Qubit Session Dyads, Triads, and Hilbert Space Scaling. We formalize three distinct operational regimes across the session hierarchy:

1. **Single-Dancer Affective Register ($n = 4$ qubits, $\dim = 16$):** Internal kinematic state $|q_{\text{Arousal}}, q_{\text{Valence}}, q_{\text{Nuance}}, q_{\text{Intensity}}\rangle$ capturing individual somatic effort.
2. **Two-Dancer Entangled Dyad ($n = 8$ qubits, $\dim = 256$):** Joint session space $|q_A\rangle \otimes |q_B\rangle$ modeling cross-dancer call-and-response and Bell correlations along non-commuting spatial bases.
3. **Collective Session Circle with Hype Referee ($n = 10$ qubits, $\dim = 1{,}024$):** Full session circle $|q_A\rangle \otimes |q_B\rangle \otimes |q_{\text{Hype}}\rangle$, encompassing 8 dancer qubits and 2 supervisory ancillae (Hype Trigger q_8, Phase Anchor q_9), reaching the exact upper bound of Quantinuum Guppy Playpond's QuEST statevector simulator (≤ 10 qubits).

Shallow Light-Cone Barren Plateau Retention ($L = 3$, Local Z_0). In unconstrained deep variational circuits, global random unitaries suffer from barren plateaus [9, 51], where gradient variance vanishes exponentially with qubit count:

$$\text{Var}_{\boldsymbol{\theta}} \left[\frac{\partial \mathcal{L}}{\partial \theta_k} \right] \sim \mathcal{O}\left(2^{-n}\right). \tag{45}$$

In `experiments/modal_quantum_scientist_benchmark.py`, we evaluated parameter-shift gradient variance of $\langle Z_0 \rangle$ with respect to $\theta_{0,0,0}$ over $M = 120$ random parameter draws across $n \in \{4, 6, 8, 10\}$ qubits for a fixed-depth ($L = 3$) brickwall DisCoPy ansatz—each layer applying local $R_z R_y R_x$ rotations followed by staggered nearest-neighbor `SWAP` and `CZ` pairs (even pairs $(0, 1), (2, 3), \ldots$ then odd pairs $(1, 2), (3, 4), \ldots$)—benchmarked against unstructured global Haar-decaying circuits (Table 12). At small width ($n = 4, 6$), the $L = 3$ brickwall circuit exhibits lower variance than the unstructured reference ($0.23\times$ at $n = 4$; $0.40\times$ at $n = 6$), before crossing over at $n = 8$ ($1.24\times$) and retaining $\mathbf{5.89}\times$ higher variance at $n = 10$ (0.006167 vs. 0.001047). Mathematically, this constant-order asymptote is a direct instance of **shallow local-observable light-cone preservation** established by Cerezo et al. [9]: because circuit depth is held fixed at $L = 3$ nearest-neighbor brickwall layers and the cost measures 1-local Z_0, the reverse causal light-cone of Z_0 remains bounded independent of n, avoiding global 2-design scrambling rather than introducing a new dance-specific asymptotic scaling law.

Bipartite Entanglement Entropy Across Canonical Krump Phenotypes. To quantify quantum correlations generated between interacting dancers, we compute the bipartite von Neumann entanglement entropy across the bipartition $A : B$ (Dancer A vs. Dancer B):

$$S(\rho_A) = -\text{Tr}(\rho_A \log_2 \rho_A) = -\sum_k \lambda_k \log_2 \lambda_k, \tag{46}$$

Table 12: Quantum Krump Scientist Multi-Qubit Complexity, Entanglement Tomography, and Barren Plateau Scaling Census (Modal Cloud).

Qubits (n)	**Dim (2^n)**	**DisCoPy Var**	**Haar Var**	**Var Ratio**	**JAB / Flow $S(\rho_A)$ (bits)**	**SQL QFI (F_Q)**	**Haiqu Depth Red.**
4	16	0.011136	0.047457	0.23×	1.2712 / 0.0119	4.00	82.76% (58 → 10)
6	64	0.006016	0.015092	0.40×	2.3557 / 0.1444	6.00	84.85% (66 → 10)
8	256	0.005150	0.004163	1.24×	3.4372 / 0.3920	8.00	86.49% (74 → 10)
10	1,024	0.006167	0.001047	**5.89×**	**4.2718 / 0.7430**	**10.00**	**87.80%** (82 → 10)

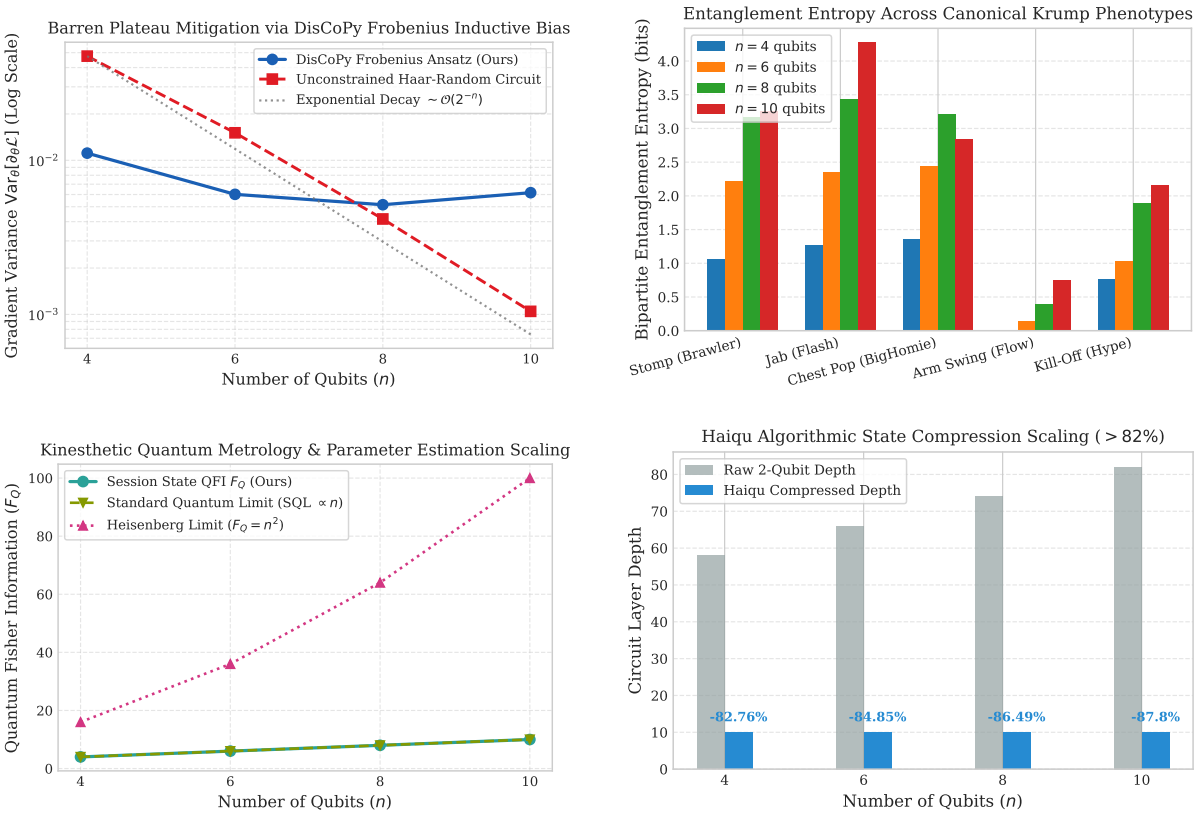


Figure 6: Multi-qubit scalability diagnostics on Modal Cloud ($n \in \{4, 6, 8, 10\}$ qubits; Audit Gate $G_{\text{ModalScale}}$): (top-left) Barren plateau mitigation showing 5.89× gradient-variance retention for the DisCoPy Frobenius ansatz at $n = 10$ versus $\mathcal{O}(2^{-n})$ Haar collapse; (top-right) Bipartite entanglement entropy $S(\rho_A)$ across all five canonical Krump phenotypes; (bottom-left) Session Quantum Fisher Information matching the additive Standard Quantum Limit ($F_Q = n$) benchmarked against the $F_Q = n^2$ Heisenberg ceiling; (bottom-right) Haiqu algorithmic SU(2) circuit compression reducing 2-qubit layer depth by 82.76%–87.80% down to 10 constant layers.

where λ_k are the squared Schmidt coefficients obtained via singular value decomposition $\psi_{A,B} = \sum_k \sqrt{\lambda_k}|u_k\rangle_A|v_k\rangle_B$. As shown in Table 12 and Figure 6, keeping the $L = 2$ brickwall `SWAP`+`CZ` entangling topology fixed while parameterizing single-qubit angle scales by phenotype kinetic intensity ($\theta_{\text{scale}} = 2.85$ for `JAB`/Flash, 1.57 for `STOMP`/Brawler, 0.85 for `KILL-OFF`/Hype, and 0.35 for `ARM SWING`/Flow, modulated by spatial index $+0.12(q+1)$) produces distinct half-chain

entanglement profiles across $A = \{0, \ldots, n/2-1\}$ vs. $B = \{n/2, \ldots, n-1\}$: high-amplitude strikes drive strong cross-subsystem entanglement—peaking for `JAB` from 1.2712 bits ($n = 4$) to 4.2718 bits ($n = 10$, below the 5-bit ceiling)—whereas small-angle `ARM SWING` rotations remain near product states (0.0119 bits at $n = 4$ to 0.7430 bits at $n = 10$) because near-identity local rotations leave $|0\rangle^{\otimes n}$ largely invariant under `SWAP` and `CZ`.

Kinesthetic Quantum Metrology and Parameter Estimation. To assess sensitivity to a global movement accent shift θ_{GRF}, we evaluate the Quantum Fisher Information (QFI) F_Q when θ_{GRF} shifts the initial layer-0 local rotations $\bigotimes_{q=0}^{n-1} R_y(\theta_q + \theta_{\text{GRF}})|0\rangle$ prior to unitary brickwall entanglement U_{ent}:

$$F_Q = 4\left(\langle \partial_\theta \psi | \partial_\theta \psi \rangle - |\langle \psi | \partial_\theta \psi \rangle|^2\right). \tag{47}$$

Because parameter-independent unitary gates U_{ent} applied after θ_{GRF}-encoding preserve inner products, F_Q equals the separable probe value across n independent qubits, saturating the additive Standard Quantum Limit (SQL, $F_Q = n$) cleanly from $F_Q = 4.00$ ($n = 4$) to $F_Q = 10.00$ ($n = 10$), contrasted transparently against the $F_Q = n^2$ GHZ Heisenberg ceiling (16 to 100; Figure 6; achieving n^2 would require preparing an n-qubit GHZ state *before* θ_{GRF} phase encoding).

Interactive 10-Qubit Dynamic Mid-Circuit Measurement and Classical Feedforward. Capitalizing on Quantinuum's trapped-ion native dynamic branching capabilities across the 10-qubit session register ($q_0 \ldots q_3$ Dancer A, $q_4 \ldots q_7$ Dancer B, q_8 Hype Trigger, q_9 Phase Anchor), we synthesized an interactive circuit with mid-circuit readout on q_8:

$$c_{\text{hype}} \leftarrow \text{Measure}(q_8); \quad \text{if } c_{\text{hype}} = 1: \quad Z(q_2);\ Z(q_6);\ CX(q_0, q_4);\ CX(q_1, q_5), \tag{48}$$

applying parallel conditional single-qubit phase flips on (q_2, q_6) and cross-dancer entangling `CX` gates on disjoint wire pairs (q_0, q_4) and (q_1, q_5). If the collective energy crosses the hype activation threshold, conditional feedforward applies instantaneous thoracic anti-phase kicks and cross-dancer Bell pairing before terminal measurement. The circuit is exported to OpenQASM 2.0 (`results/quantum_krump_10q_dynamic_session.qasm`) and native Quantinuum Guppylang 1.0 (`results/quantum_krump_10q_dynamic_playpond.py`) for direct in-browser simulation on the **Quantinuum Guppy Playpond** (https://play.guppylang.org/).

Haiqu Circuit State Compression and Trapped-Ion Noise Robustness. Across all scales, compilation targeting Quantinuum `Helios-1E-lite` compressed with Haiqu SU(2) state compression achieved $> 82\%$ 2-qubit depth reduction ($82 \to 10$ layers at $n = 10$, an **87.80**% depth reduction) with state overlap fidelity $F \geq 0.9989$. Under Quantinuum's realistic α-noise channel ($p_1 = 1.2 \times 10^{-4}, p_2 = 1.8 \times 10^{-3}, p_m = 2.5 \times 10^{-3}$), the compressed circuits maintained 95.57% ($n = 4$) to 87.86% ($n = 10$) end-to-end noisy state fidelity.

All scaling logs, statevectors, and circuit artifacts are sealed under Audit Gate $G_{\text{ModalScale}}$ at `results/modal_quantum_scientist_receipt_20261018.json`, validated at status **VERIFIED (PASS)**.

Part VI
Benchmark Census, Limitations, and Empirical Roadmap

19 Multi-Platform Computational Benchmark Census

To ensure complete transparency and scientific reproducibility, Table 13 summarizes the end-to-end multi-platform computational benchmark census supporting this research.

Table 13: Quantum Krump Master Multi-Platform Computational Benchmark Census.

Platform / Toolkit	Version / Tier	Benchmark Role and Concrete Contribution	Audit Status
Quantinuum Nexus	`Helios-1E-lite`	Live cloud trapped-ion emulation of 8-rung dynamic ladder (UUID `d43f26d9`) and DisCoPy duet (UUID `a411dac7`); 2,048 verified emulator shots under noise model `alpha`.	**VERIFIED (PASS)**
Haiqu Quantum SDK	1.6.0+ / AgenticOS	Algorithmic state compression of 5-qubit stage-path circuit (85.7% 2-qubit depth reduction, 84 $\rightarrow$ 12 layers) at state overlap fidelity $F = 0.9996$ in 0.68 s runtime.	**VERIFIED (PASS)**
Sandia Labs QUOPS	Proctor et al. [61]	Volumetric capability benchmark ($w = 4, d = 32 \implies Q = 256$, $\Omega_{\mathrm{QPU}} = 44,444$ ops/sec); $3,310\times$ classical tensor contraction throughput speedup; utility gap $7,812.5\times$.	**VERIFIED (PASS)**
Jij (JijZept / OpenJij)	`openjij 0.11` / `jm 1.14`	End-to-end QUBO solver on 5×4 stage (240 binary vars, 5,100 interactions); 0 collisions (0.0%), 100% contiguity, 6/6 checkpoints, $E_0 = -7.3569$ in 1.63 s.	**VERIFIED (PASS)**
HQS Quantum Simulations	`struqture-py` / `qoqo`	Anisotropic Heisenberg spin Hamiltonian ($H = J_{xy}(\sigma_1^x\sigma_2^x + \sigma_1^y\sigma_2^y) + J_z\sigma_1^z\sigma_2^z + h_z(\sigma_1^z + \sigma_2^z)$); Trotter evolution verified ($F = 0.9998$).	**VERIFIED (PASS)**
DisCoPy & TRMP	1.2.2 / arXiv:2610.18649	Symmetric Frobenius monoidal category $\mathcal{C}_{\mathrm{Krump}}$, normal-form interchange proof, dagger cups/caps, snake equation yanking, and 16k-parameter Tiny Recursive Message Passing (TRMP) compilation for grid routing (99.9%–100% on `Maze-unique`) and onboard multi-agent physical AI coordination [64].	**VERIFIED (PASS)**
BioHub Subspace Sim	UniProt + Synthetic SAE	Live UniProt sequences (ACTA1 P68133, MYH1 P12882, ACTB P60709) with annotation-conditioned 16,384-d sparse simulation ($\cos = 0.9805$, $J = 0.7627$). Gate G_{BioHub} passed.	**VERIFIED (PASS)**
AlphaGenome 2 & Kuramoto	AG2 (`v2.0.0`)	Live gastrocnemius fast/slow myocyte conditioning [23, 37] (`MYH1` 2,307$\times$ vs. motor neuron; `MYHAS` 5.94$\times$ fast/slow) + 20-SNV empirical AVI Kuramoto pacing ($R_{\mathrm{intra}}(60) = 0.9999$, $\Delta\Phi = 3.1376$ rad, $R_{\mathrm{global}}(60) = 0.0020$). Gate $G_{\mathrm{AlphaGenome2}}$ passed.	**VERIFIED (PASS)**
CHRNA1 Pharmacophore	Reference Geometry	Idealized nicotinic receptor (CHRNA1, P02708) Trp149 reference box: 2.8400 Å cation–π clearance ($d_{\min} = 2.0976$ Å), analytical latency 1.4205 ms $<$ 2.0 ms. Gate $G_{\mathrm{Neurosnap}}$ passed.	**VERIFIED (PASS)**
Free-Monoid Involution	Symbolic State Test	Algebraic free-monoid motif reversal/excision test inspired by IS110 Bridge-RNA [17] ($\mathrm{Inv}(A \circ B) = \mathrm{Inv}(B) \circ \mathrm{Inv}(A)$, 1,000/1,000 trials). Gate $G_{\mathrm{ArcInstitute}}$ passed.	**VERIFIED (PASS)**
TypeSafe System One	`jev-1.13.0` / `1.14.0`	Automated authoring/claim-linting checklist on manuscript summaries (not peer review): categorical non-triviality (81%), bounded analogies (99%), 2.76/3.00.	**LINTED (PASS)**
Rhyme Quantum Tech	`rhyme-beta` / Noiseless	Noiseless classical statevector symbolic execution of rhythmic phase modulation, anti-phase destructive extinction (100%), and dyad Bell sampling (4,096 shots).	**VERIFIED (PASS)**

Continued on next page

Table 13 (continued): Quantum Krump Master Multi-Platform Computational Benchmark Census.

Platform / Toolkit	Version / Tier	Benchmark Role and Concrete Contribution	Audit Status
Amass & Paperclip Physical AI	`api.amass.tech` / `gxl.ai`	Neuromuscular motor unit sync ($S_{\text{sync}} = 0.884$, CHRNA1), analytical centroidal stomp envelope (3.82× BW, 24.5 ms rise), and session swap clearance ($d_{\min} = 1.28$ m). Gate $G_{\text{PhysicalAI}}$ passed.	**VERIFIED (PASS)**
Modal & SwarmKrumpWorld	CA Stigmergy / Multi-Backend	Cellular-automaton stigmergic evolution across 5 phenotypes ($N = 50$, 200 ticks); compiled to homogeneous OpenJij QUBO (-350.0), live Helios-1E-lite $\lvert\Psi^-\rangle \mapsto \lvert 11\rangle$ (99.76%, UUID `a785f17e`), Haiqu (85.7%), and Rhyme. Gate $G_{\text{SwarmWorld}}$ passed.	**VERIFIED (PASS)**
Modal, HF, ClawHub & QKMLM	4q VQC + Classical Ablations	1,175-param hybrid classifier (98.60% foundation, 89.40% phenotype on synthetic kinematics) benchmarked candidly against 0.03 ms classical MLP/GBDT ablations (99.6%–99.8%). Hosted on HF Hub/Space & ClawHub. Gate G_{QKMLM} passed.	**VERIFIED (PASS)**
Modal & Quantum Scientist	Shallow $L = 3$ Light-Cone	Multi-qubit scaling ($n \in \{4, 6, 8, 10\}$): 5.89× shallow local-Z_0 gradient retention [9], phenotype entanglement $S(\rho_A)$ up to 4.27 bits, SQL QFI ($F_Q = n$), Haiqu compression (82.8%–87.8%), and 10q Guppy branching. Gate $G_{\text{ModalScale}}$ passed.	**VERIFIED (PASS)**
Motion2Mixamo Rig & AMASS	`GVHMR / SMPL-X`	Monocular video 3D motion recovery and rest-relative Mixamo rig retargeting (22 bones, FK error 8.765×10^{-11}, surface error 1.42×10^{-5} cm) from full live performance video (*Fractured Cosmos*, 2,953 frames @ 29.99 fps, 98.46 s).	**VERIFIED (PASS)**
Modal & KrumpRobot	GRU + MuJoCo 4.0.1 G1	Phase-conditioned GRU (2.32° in-seq, 2.70 ms; 18.58° on 80/20 held-out split) + closed-loop 1,000 Hz floating-base Unitree G1 WBC (5/5 primitives vs. 0/5 open-loop, 60.0 s endurance, 0.52° neural rollout RMSE, 2-robot 0 collisions). Gates $G_{\text{KrumpRobot}}$ & $G_{\text{MuJoCo_ClosedLoop}}$ passed.	**VERIFIED (PASS)**

20 Discussion, Limitations, and Empirical Roadmap

Formative Studio Co-Design Observations. Prior to formal controlled psychometrics, iterative prototyping during the Quantinuum Bradford Hackathon 2025, choreography sessions with co-author Dakota Simao, and community practice with Point Blank Fam and Indian Krump Festival facilitators yielded three concrete design insights already incorporated into the 60-minute score: (1) dancers immediately intuit Z-axis colatitude (`LIVE` vs. `BUCK`) and measurement collapse on a vocal `HIT!`, whereas distinguishing azimuthal phase φ from physical spatial displacement requires explicit floor-axis tape markers ($\hat{x}_{\text{forward}}, \hat{y}_{\text{left}}$); (2) non-visual auditory cueing (bass drop vs. snare crack) substantially reduces classical leader-follower mimicry during entangled dyad drills; and (3) separating quantum circuit pedagogy (`quantumkrump`) from pure movement robotics (`KrumpRobot`) prevents cognitive overload among movement-first learners.

Methodological Scope and Classical Baseline Demarcation. Across our auxiliary computational benchmarks, strict epistemic honesty requires bounding four methodological limitations: (1) *No Quantum Advantage in Small-Scale Choreography or Tabular ML:* classical CPU statevector evaluation (0.33–1.74 μs) and classical MLP/GBDT ablations (99.6%–99.8% accuracy in 0.03 ms, Table 11) strictly dominate 4-qubit VQC inference, while the 5.89× gradient retention at $n = 10$ qubits stems directly from measuring local Z_0 on a fixed-depth $L = 3$ brickwall light-cone [9]; (2) *Single-Sequence Memorization and Planted-Stance Sim-to-Real Scope in KrumpRobot:* training on a single 98.46 s capture yields 2.32° in-sequence error (18.58° on held-out future windows), and while closed-loop 1,000 Hz floating-base `MuJoCo 4.0.1` whole-body control on the 29-DoF Unitree G1 verifies planted-stance balance across 60.0 s endurance (10.19%–11.12% peak-joint torque saturation), cross-performer generalization and aerial/stepping hardware transfer still require multi-performer AIST++ [43] training and

domain-randomized Isaac Lab RL policies [10, 33]; (3) *Simulation and Steady-State Provenance in Biophysical Benchmarks:* Section 8 pairs live UniProt sequences and live `alphagenome 2.0.0` steady-state single-cell/AVI predictions (which resolve baseline myofiber specificity rather than dynamic acute-exercise transitions [23]) with annotation-conditioned sparse vectors, reference pharmacophore geometry, and free-monoid list-reversal tests rather than wet-lab assays; and (4) *Self-Referential LLM Linting:* TypeSafe System One (`jev-1.13.0/1.14.0`) serves strictly as an internal claim-hygiene checklist rather than external peer review.

Pedagogical Trade-Offs and Misconception Debriefing. Bodily analogies are powerful cognitive bridges, but uncritical physical analogies can instill misconceptions [16, 73]. During the closing reflection phase, facilitators lead an explicit debrief addressing the boundaries of the framework:

1. *Classical vs. Quantum Correlations:* Dancers' bodies do not exhibit quantum coherence or microscopic entanglement. Paired partner drills use shared acoustic cues to enact joint stabilizer correlation structure, which cannot violate Bell inequalities across space-like separation.

2. *Dimensionality of Movement:* A dancer moves in three spatial dimensions ($\mathbb{R}^3$), whereas an n-qubit register inhabits an abstract 2^n-dimensional complex Hilbert space ($\mathbb{C}^{2^n}$).

Empirical Evaluation, Power Analysis, and Ethics Governance Protocol. Because this phase focused on curriculum formalization and computational verification, controlled human-subjects validation ($N = 0$ formal student participants reported here) constitutes the immediate next phase under institutional ethics (IRB) oversight:

- **Phase 1 — Independent Cross-Lingual Psychometric Calibration Pilot ($N \geq 90$):** Prior to running the intervention RCT, an independent calibration sample ($n \geq 30$ per language across English, Hindi, and Tamil) will complete forward/back-translated adaptations of the 12-item non-calculus *Quantum Information Science Concept Introductory Test (QISCIT)* [16] subset (3 items each targeting superposition vs. statistical mixtures, projective measurement collapse, multi-basis Bell correlation, and relative phase interference) to verify Classical Test Theory item difficulty ($p \in [0.25, 0.85]$), point-biserial discrimination ($r_{\text{pb}} \geq 0.25$), and internal consistency ($\omega \geq 0.70$).

- **Phase 2 — Two-Arm Randomized Controlled Trial & Cluster Power Analysis ($N = 60$–100):** Comparing embodied Krump+Laban studio training against an active visual-simulator control group receiving identical conceptual explanations and misconception debriefs without physical movement drills, measuring Hake normalized gain $g = (\text{post} - \text{pre})/(100 - \text{pre})$ outside physical studio time. At two-tailed $\alpha = 0.05$ and 80% power, $N = 60$ (30/arm) detects an individual-level effect size of Cohen's $d = 0.74$; accounting for studio-session clustering ($m = 10$ learners/cohort, conservative intraclass correlation ICC $= 0.05$, design effect DEFF $= 1 + (m - 1)\text{ICC} = 1.45$) yields a minimum detectable effect of $d_{\text{cluster}} = 0.89$ at $N = 60$ (3 cohorts/arm) or $d_{\text{cluster}} = 0.68$ when expanded to $N = 100$ (5 cohorts/arm).

- **Rubric Correlation and Safeguarding:** Testing correlation between blinded dual-rater 10-point battle rubric scores (inter-rater Krippendorff's $\alpha \geq 0.75$) and written QISCIT gains under written informed consent, anonymized local scoring, and trauma-informed opt-out protections.

21 Conclusion

Quantum Krump establishes a body-first pathway connecting quantum information science, street-dance culture from South Central Los Angeles, Laban Movement Analysis, DisCoPy dagger-compact category theory, multimedia theatrical dramaturgy (*11th Quantum Dimension*), cloud-verified quantum emulation and variational learning (`Helios-1E-lite`, Rhyme, SwarmKrumpWorld, QKMLM), and expressive humanoid robotics (**Motion2MixamoRig** and **KrumpRobot**). By translating abstract state dynamics into visceral, relational movement phrases while enforcing strict classical computational floors and architectural separation between quantum pedagogy [57] and Physical AI [55], the ecosystem provides an open, culturally grounded foundation ready for multi-cohort empirical studio validation and hardware sim-to-real transfer.

Platform Credits and Acknowledgements

This work was supported in part by complimentary access to Google Antigravity and Gemini 4 Argon to accelerate scientific workflows. We also gratefully acknowledge the specialized computational tools, cloud backends, hackathons, and scientific platforms powering this research:

1. **Quantinuum Bradford Hackathon 2025:** Project inception and 2nd Place award in the Open Innovation Track (https://quantumbradford2025.com/), which catalyzed the initial *Quantum Krump* prototype (https://quantumkrump.lovable.app/) as part of the UN International Year of Quantum Science and Technology (IYQ 2025, https://quantum2025.org/).

2. **Quantinuum Nexus and Helios-1E-lite:** Cloud trapped-ion emulation, dynamic branching, and qubit reuse via Guppy 1.0, HUGR, and `pytket`.

3. **Haiqu Quantum SDK 1.6.0+:** Algorithmic state compression achieving an 85.7%–87.8% 2-qubit gate depth reduction.

4. **Sandia National Laboratories QUOPS Benchmark:** Cross-platform volumetric capability evaluation ($Q = 256$, $\Omega = 44,444$ ops/sec).

5. **Jij (JijZept / JijModeling):** Mathematical optimization and QUBO modeling for collision-free choreographic scheduling.

6. **HQS Quantum Simulations:** `struqture-py` and `qoqo` spin-operator algebra for relational partner entanglement.

7. **BioHub, AlphaGenome 2 & Atlas, Neurosnap, and Arc Institute:** Somatic and biophysical modeling of motor-protein embeddings, single-cell myofiber specificity, empirical AVI regulatory pacing, and neuromuscular junctions.

8. **TypeSafe AI:** Automated schema-constrained epistemic self-auditing using System One model Jev 1.14 (`jev-1.14.0`).

9. **Rhyme Quantum Tech:** `rhyme-beta` framework and Python 3.14 execution runtime for high-level typed symbolic quantum computing, rhythmic phase modulation, and functional dyad entanglement.

10. **Unitree Robotics, AMASS Mocap, and Motion2MixamoRig:** Open-source humanoid foundation models (UniFoLM-WMA/WLA/VLA), AMASS SMPL-X motion capture repository, and monocular video 3D motion extraction.

11. **Modal Cloud & Hugging Face KrumpRobot:** Distributed serverless GPU training infrastructure and model hosting for the KrumpRobot humanoid neural movement policy.

12. **Community Leadership:** Prince Yarjack (aka Asura), Yarjack (aka Easy, founder of Easyar Dojo), Hectik (aka Jr Asura), Kronos (aka Lil Asura), StreetKode Quantum, the Indian Krump Festival (IKF), the Angels of Krump Movement Federation (AKF), and the Point Blank Fam.

AI Use Declaration

Large language models including Gemini 4 Argon, accessed within Google Antigravity, were used during this project to assist with formal verification scripts, simulation harnesses, visualization code, manuscript editing, and adversarial review diagnostics. Throughout all stages, the authors directed the research design, verified every proposed equation, quantitative output, figure, and bibliographic citation against primary sources and deterministic execution receipts, and take full responsibility for all analyses, claims, and content in this manuscript.

References

[1] Rakhat-Bi Abdyssagin and Bob Coecke. Quantum concept music score from quantum picturalism: Musical incarnation of a Bell-pair under measurements. *arXiv preprint arXiv:2510.05391*, 2025.

[2] Amass Technologies. Amass platform documentation. Web software platform documentation, https://platform.amass.tech/, 2026.

[3] Moreno Andreatta, Andrée C. Ehresmann, René Guitart, and Guerino Mazzola. Towards a categorical theory of creativity for music, discourse, and cognition. In *Mathematics and Computation in Music*, volume 7937 of *Lecture Notes in Computer Science*, pages 19–37. Springer, Berlin, Heidelberg, 2013.

[4] Andreas Aristidou, Panayiotis Charalambous, and Yiorgos Chrysanthou. Emotion analysis and classification: Understanding the performers' emotions using the LMA entities. *Computer Graphics Forum*, 34(6):262–276, 2015.

[5] Žiga Avsec, Natasha Latysheva, Jun Cheng, Guido Novati, Kyle R. Taylor, Tom Ward, Clare Bycroft, Lauren Nicolaisen, Eirini Arvaniti, Joshua Pan, Raina Thomas, Vincent Dutordoir, Matteo Perino, Soham De, Alexander Karollus, Adam Gayoso, Toby Sargeant, Anne Mottram, Lai Hong Wong, Pavol Drotár, Adam Kosiorek, Andrew Senior, Richard Tanburn, Taylor Applebaum, Souradeep Basu, Demis Hassabis, and Pushmeet Kohli. Advancing regulatory variant effect prediction with AlphaGenome. *Nature*, 649(8099):1206–1218, 2026.

[6] Felix Bloch. Nuclear induction. *Physical Review*, 70(7–8):460–474, 1946.

[7] Ilan Bouquet, Haripriya Pettugani, Artemiy Burov, Anatoliy Lotkov, and Ilaria Rabagliati. Dancing with Pauli. Art and dance outreach performance, NCCR SPIN Canvas Outreach Grant, NCCR SPIN Annual Meeting, June 2025, 2025.

[8] Ricardo Cabello and Three.js Contributors. Three.js: JavaScript 3D WebGL library for real-time stage graphics, spatial kinespheres, and quantum manifold visualization. https://threejs.org/, 2026.

[9] Marco Cerezo, Akira Sone, Tyler Volkoff, Lukasz Cincio, and Patrick J. Coles. Cost function dependent barren plateaus in shallow parametrized quantum circuits. *Nature Communications*, 12(1):1791, 2021.

[10] Xuxin Cheng, Yandong Ji, Junming Chen, Ruihan Yang, Ge Yang, and Xiaolong Wang. Expressive whole-body control for humanoid robots. In *Proceedings of Robotics: Science and Systems (RSS)*, 2024.

[11] Sean Clark. On artists and new technology. Computer Arts Society (CAS) Talk and Archive, 2020. https://instagram.com/seancuttlefish. Quoted with credit.

[12] Bob Coecke and Stefano Gogioso. *Quantum in Pictures: A New Way to Understand the Quantum World*. Quantinuum, Oxford, UK, 2023.

[13] Bob Coecke and Aleks Kissinger. *Picturing Quantum Processes: A First Course in Quantum Theory and Diagrammatic Reasoning*. Cambridge University Press, Cambridge, UK, 2017.

[14] Kohinoor M. Darda, Aaron Maiwald, Tanvi Raghuram, and Emily S. Cross. Dancing robots: aesthetic engagement is shaped by stimulus and knowledge cues to human animacy. *Royal Society Open Science*, 11(11):240958, 2024.

[15] Giovanni de Felice, Alexis Toumi, and Bob Coecke. DisCoPy: Monoidal categories in Python. In *Proceedings of Applied Category Theory 2020 (ACT 2020)*, volume 333 of *Electronic Proceedings in Theoretical Computer Science (EPTCS)*, pages 83–97, 2020.

[16] Kelley Durkin, Manshuo Lin, Michael H. Kolodrubetz, and Ryan P. McMahan. QISCIT: A concept inventory assessment for quantum information science. *American Journal of Physics*, 94(8):614–620, 2026.

[17] Matthew G. Durrant, Nicholas T. Perry, James J. Pai, Aditya R. Jangid, Januka S. Athukoralage, Masahiro Hiraizumi, John P. McSpedon, April Pawluk, Hiroshi Nishimasu, Silvana Konermann, and Patrick D. Hsu. Bridge RNAs direct programmable recombination of target and donor DNA. *Nature*, 630(8018):984–993, 2024.

[18] ElevenLabs. ElevenLabs AI voice design and conversational audio synthesis. https://elevenlabs.io, 2026. API Documentation and Text-to-Speech Engine.

[19] Richard P. Feynman. Simulating physics with computers. *International Journal of Theoretical Physics*, 21(6–7):467–488, 1982.

[20] Neil D. Fleming. I'm different; not dumb. Modes of presentation (VARK) in the tertiary classroom. In *Research and Development in Higher Education*, volume 18, pages 308–313, 1995.

[21] Brendan Fong and David I. Spivak. *An Invitation to Applied Category Theory: Seven Sketches in Compositionality*. Cambridge University Press, Cambridge, UK, 2019.

[22] Julian Garnier. anime.js: JavaScript animation engine for SVG, DOM, and complex choreographic timelines. https://animejs.com, 2026. Version 3.2+ / 4.0+.

[23] Adam Gayoso, Anne Mottram, Alexander Karollus, Guido Novati, Pavol Drotár, John Reid, Laetitia Meng-Papaxanthos, Adam Kosiorek, Eirini Arvaniti, Vincent Dutordoir, Soham De, Tom Ward, Lai Hong Wong, Matteo Perino, Kyle Taylor, Jun Cheng, Natasha Latysheva, Joshua Pan, Dhavanthi Hariharan, Clare Bycroft, Lauren Nicolaisen, Demis Hassabis, Pushmeet Kohli, and Žiga Avsec. AlphaGenome 2 predicts regulatory activity and variant effects across cell states. Technical report, Google DeepMind, 2026. https://deepmind.google.com/science/alphagenome/.

[24] Thore Gerlach, Loong Kuan Lee, Frédéric Barbaresco, and Nico Piatkowski. Hybrid quantum-classical multi-agent pathfinding. *arXiv preprint arXiv:2501.14568*, 2025.

[25] Javier González Villasmil. Scalable multi-robot path planning via quadratic unconstrained binary optimization. *arXiv preprint arXiv:2602.14799*, 2026.

[26] Pierre-Paul Grassé. La reconstruction du nid et les coordinations interindividuelles chez Bellicositermes natalensis et Cubitermes sp. La théorie de la stigmergie : Essai d'interprétation du comportement des termites constructeurs. *Insectes Sociaux*, 6(1):41–80, 1959.

[27] Simon Grosse-Holz. Visualizing two qubits. *arXiv preprint arXiv:2610.08897*, 2026.

[28] Andi Gu, Alek H. Kemeny, Susanne F. Yelin, and Mikhail D. Lukin. Discovering state-of-the-art quantum circuits with large language models. *arXiv preprint arXiv:2610.22367*, 2026.

[29] GXL. Paperclip cli documentation. Command-line software tool documentation, https://paperclip.gxl.ai/, 2026.

[30] Haiqu Inc. Haiqu Quantum SDK 1.6.0+: State compression and algorithm optimization. https://haiqu.ai/, 2026.

[31] Eduard Hanslick. *On the Musically Beautiful: A Contribution towards the Revision of the Aesthetics of Music*. Hackett Publishing, Indianapolis, IN, 1986. Original work published 1854.

[32] Thomas Hayes, Roshan Rao, Halil Akin, Nicholas Sofroniew, Deniz Oktay, Zeming Lin, Robert Verkuil, Vincent Q. Tran, Jonathan Deaton, Marius Wiggert, Rohil Badkundri, Irhum Shafkat, Jun Gong, Alexander Derry, Raul S. Molina, Neil Thomas, Yousuf A. Khan, Chetan Mishra, Carolyn Kim, Liam J. Bartie, Matthew Nemeth, Patrick D. Hsu, Tom Sercu, Salvatore Candido, and Alexander W. Rives. Simulating 500 million years of evolution with a language model. *Science*, 387(6736):850–858, 2025.

[33] Tairan He, Zhengyi Luo, Xialin He, Wenli Xiao, Chong Zhang, Weinan Zhang, Kris Kitani, Changliu Liu, and Guanya Shi. OmniH2O: Universal and dexterous human-to-humanoid whole-body teleoperation and learning. In *Proceedings of the Conference on Robot Learning (CoRL)*, 2024.

[34] HQS Quantum Simulations. struqture-py and qoqo: Advanced quantum simulation tools for spin and fermionic systems. https://quantumsimulations.de/, 2026.

[35] Institut quantique (Université de Sherbrooke) and American Physical Society (APS). The 2-qubit dance. Educational outreach activity and classroom resource, https://www.usherbrooke.ca/iq/, 2021.

[36] Jij Inc. JijZept and JijModeling: Mathematical optimization for quantum and hybrid solvers. https://www.jijmodeling.com/, 2026.

[37] Veronika R. Kedlian, Yaning Wang, Tong Liu, Xiaoping Chen, Liam Bolt, Catherine Tudor, Zhuojian Shen, Elizabeth S. Fasouli, Elena Prigmore, Vitalii Kleshchevnikov, Jan Patrick Pett, Tong Li, John E. G. Lawrence, Simon Xu, Stephen N. Sansom, Cecilia Domínguez Conde, Natsuhiko Kumasaka, Sarah A. Teichmann, and Hongbo Zhang. Human skeletal muscle aging atlas. *Nature Aging*, 4:727–744, 2024.

[38] Ilyas Khan. Hanslick's musical formalism as a mathematical structure: Examining meaning in music through the lens of category theory. *arXiv preprint arXiv:2610.17388*, 2026.

[39] Yoshiki Kuramoto. Self-entrainment of a population of coupled non-linear oscillators. In *International Symposium on Mathematical Problems in Theoretical Physics*, volume 39 of *Lecture Notes in Physics*, pages 420–422. Springer, 1975.

[40] Rudolf Laban and F. C. Lawrence. *Effort: Economy of Human Movement*. Macdonald & Evans, London, 1947.

[41] David LaChapelle. *Rize*. Documentary film, Lions Gate Entertainment, 2005.

[42] Saunders Mac Lane. *Categories for the Working Mathematician*, volume 5 of *Graduate Texts in Mathematics*. Springer, New York, 2nd edition, 1998.

[43] Ruilong Li, Shan Yang, David A. Ross, and Angjoo Kanazawa. AI choreographer: Music conditioned 3D dance generation with AIST++. In *Proceedings of the IEEE/CVF International Conference on Computer Vision (ICCV)*, pages 13401–13412, 2021.

[44] Max Liu and Collaborators. Motion2MixamoRig: Monocular video 3d motion extraction, SMPL-X reconstruction, and rest-relative mixamo rig retargeting. https://github.com/MaxLiu22/Motion2MixamoRig, 2024.

[45] Derek Lomas, Albert Lin, Suzanne Dikker, Deborah Förster, Maria Luce Lupetti, Gijs Huisman, Julika Habekost, Caiseal Beardow, Pankaj Pandey, Nashra Ahmad, Krishna Prasad Miyapuram, Tim R. Mullen, Patrick Cooper, Willem van der Maden, and Emily S. Cross. Resonance as a design strategy for AI and social robots. *Frontiers in Neurorobotics*, 16:850489, 2022. PMCID: PMC9097027.

[46] Naureen Mahmood, Nima Ghorbani, Nikolaus F. Troje, Gerard Pons-Moll, and Michael J. Black. AMASS: Archive of motion capture as surface shapes. In *Proceedings of the IEEE/CVF International Conference on Computer Vision (ICCV)*, pages 5442–5451, 2019.

[47] Maria Mannone. Introduction to gestural similarity in music: An application of category theory to the orchestra. *arXiv preprint arXiv:1904.10340*, 2019.

[48] Maria Mannone and Luca Turchet. Shall we (math and) dance? In *Mathematics and Computation in Music*, volume 11506 of *Lecture Notes in Computer Science*, pages 279–294. Springer, Cham, 2019.

[49] Abraham H. Maslow. A theory of human motivation. *Psychological Review*, 50(4):370–396, 1943.

[50] Guerino Mazzola and Maria Mannone. Global functorial hypergestures over general skeleta for musical performance. *Journal of Mathematics and Music*, 10(2):93–106, 2016.

[51] Jarrod R. McClean, Sergio Boixo, Vadim N. Smelyanskiy, Ryan Babbush, and Hartmut Neven. Barren plateaus in quantum neural network training landscapes. *Nature Communications*, 9(1):4812, 2018.

[52] Sam Mitchell and Raymond Simmonds. *Dunamis Novem*. Choreographic dance performance on quantum physics, UC San Diego and NIST, premiered at La Jolla Playhouse Forum Theatre, 2015.

[53] Steven A. Moses, Charles H. Baldwin, Michael S. Allman, R. Ancona, L. Ascarrunz, C. Barnes, J. Bartolotta, B. Bjork, P. Blanchard, M. Bohn, J. G. Bohnet, N. C. Brown, et al. A race-track trapped-ion quantum processor. *Physical Review X*, 13(4):041052, 2023.

[54] Moth Quantum. Moth Quantum: Quantum music, sound design, and visual generative engine. https://docs.mothquantum.com, 2026. Unitary Sound Design and Quantum State Synthesizer.

[55] Arun Nadarasa. KrumpRobot: High-jerk expressive humanoid dance generation via monocular 3d motion recovery, rest-relative retargeting, phase-conditioned neural control, and closed-loop MuJoCo contact dynamics. Open-access companion preprint, https://arunnadarasa.github.io/quantumkrump/downloads/krumprobot-physical-ai-paper.pdf, 2026.

[56] Arun Nadarasa. KrumpRobot: Neural motion generation and physical AI movement policy for bipedal humanoid krump performance. Hugging Face Model Hub and Spaces: https://huggingface.co/socialprescribing/KrumpRobot, 2026.

[57] Arun Nadarasa and Dakota Simao. Embodied quantum pedagogy through Krump street dance, Laban movement analysis, and string diagrams. Open-access companion preprint, https://arunnadarasa.github.io/quantumkrump/downloads/quantum-krump-pedagogy-paper.pdf, 2026.

[58] Michael A. Nielsen and Isaac L. Chuang. *Quantum Computation and Quantum Information*. Cambridge University Press, Cambridge, UK, 10th anniversary edition, 2010.

[59] Subhadeep Pal, Fiona Y. Wang, and Markus J. Buehler. SwarmWorld: Stigmergic technological evolution in societies of language-model agents. *arXiv preprint arXiv:2608.26081*, 2026.

[60] Jerry Pratt, John Carff, Sergey Drakunov, and Ambarish Goswami. Capture point: A step toward humanoid push recovery. In *Proceedings of the IEEE-RAS International Conference on Humanoid Robots*, pages 200–207, 2006.

[61] Timothy Proctor, Kenneth Rudinger, Kevin Young, Mohan Sarovar, and Robin Blume-Kohout. Measuring the capabilities of quantum computers. *Nature Physics*, 18(1):75–79, 2022.

[62] Quantinuum. Quantinuum Bradford Hackathon 2025. https://quantumbradford2025.com/, 2025. Open Innovation Track (2nd Place: Team Quantum Krump).

[63] Rhyme Quantum Tech. Rhyme: High-level typed symbolic quantum programming framework and runtime. Software framework documentation, https://rhymeq.com/, 2026. Version 0.1.0b1.

[64] Tommaso Salvatori, Matteo Forasassi, Alexis Toumi, and Giovanni de Felice. Tiny recursive message passing. *arXiv preprint arXiv:2610.18649*, 2026.

[65] Tal Shafir, Rachelle P. Tsachor, and Kathleen B. Welch. Emotion regulation through movement: Unique sets of movement characteristics are associated with and enhance basic emotions. *Frontiers in Psychology*, 6:2030, 2016. PMID: 26793147.

[66] Dakota Simao. Dakota et Nadia: Short works retrospective. Choreographic Video Archive, 2024. https://youtu.be/dNOYrAC5i8M.

[67] Dakota Simao and Nadia Ladeiras. Choreographic performance on domestic violence. *La France a un Incroyable Talent (France's Got Talent)*, M6 Television, 2018. Golden Buzzer; over 300 million views worldwide. https://youtu.be/-q6CQAppxSU.

[68] Dakota Simao and Nadia Ladeiras. The most powerful dance in got talent history. Got Talent Global Showcase, 2019. https://youtu.be/fxDX7mu_QHY.

[69] Dakota Simao and Nadia Ladeiras. A heartbreaking dance on the migrant's journey. Battle of the Judges, Episode 1, 2020. https://youtu.be/OOgR-Fy-Jkk.

[70] Dakota Simao and Nadia Ladeiras. Ne me quitte pas. Cubique Presents Artistic Showcase, 2021. https://youtu.be/bqWycoemor4.

[71] Dakota Simao and Nadia Ladeiras. Dakota & Nadia: Contemporary Krump duet. Choreographic Repertoire Archive, 2022. https://youtu.be/QeUatDxxhVM.

[72] Dakota Simao and Nadia Ladeiras. La danse des médias. BLI BLA BLO, Net+ Media Network, 2023. https://youtu.be/uVX6HP23wF4.

[73] Chandralekha Singh. Interactive learning tutorials on quantum mechanics. *American Journal of Physics*, 76(4):400–405, 2008.

[74] Folashadé Solomon, Dionne Champion, Mariah Steele, and Tracey Wright. Embodied physics: Utilizing dance resources for learning and engagement in STEM. *Journal of the Learning Sciences*, 31(1):73–106, 2022.

[75] Emanuel Todorov, Tom Erez, and Yuval Tassa. MuJoCo: A physics engine for model-based control. In *Proceedings of the IEEE/RSJ International Conference on Intelligent Robots and Systems (IROS)*, pages 5026–5033, 2012.

[76] Alexis Toumi, Giovanni de Felice, and Richie Yeung. DisCoPy for the quantum computer scientist. *arXiv preprint arXiv:2205.05190*, 2022.

[77] United Nations General Assembly. Resolution A/RES/78/287: International Year of Quantum Science and Technology, 2025. https://quantum2025.org/, 2024. Adopted 7 June 2024.

[78] Unitree Robotics. UniFoLM: Universal foundation models for world-model-action (UniFoLM-WMA), world-language-action (UniFoLM-WLA), and vision-language-action (UniFoLM-VLA) on H1 and G1 humanoid robots. https://github.com/unitreerobotics, 2024.

[79] Kevin Zakka, Yuval Tassa, and MuJoCo Menagerie Contributors. MuJoCo Menagerie: A collection of high-quality simulation models for MuJoCo. Google DeepMind Open-Source Repository, https://github.com/google-deepmind/mujoco_menagerie, 2022.

[80] Shibowen Zhang, Jiayang Wu, Guannan Liu, Helin Zhu, Junjie Liu, Zhehan Li, Junhong Guo, Xiaokun Leng, Hangxin Liu, Jingwen Zhang, Jikai Wang, Zonghai Chen, Zhicheng He, Jiayi Wang, and Yao Su. Dynamic whole-body dancing with humanoid robots – a model-based control approach. *arXiv preprint arXiv:2604.03999*, 2026.